Exploring the Function of Polyphosphate in the Contact Pathway of Blood Clotting and Developing Polyphosphate Probes for Enhanced Specificity

by

Yuqi Wang

A dissertation submitted in partial fulfillment
of the requirements for the degree of
Doctor of Philosophy
(Biological Chemistry)
in the University of Michigan
2021

Doctoral Committee:

Professor James H. Morrissey, Chair
Professor David Ginsburg
Professor Ursula Jakob
Associate Professor Bruce Palfey
Associate Professor Jordan Shavit

Yuqi Wang

yuqiw@umich.edu

ORCID iD: 0000-0003-4980-1514

Dedication

This dissertation is dedicated to my parents, Ms. Yanling Zhou and Mr. Xiaolu Wang, for all their love and support throughout my life.

Acknowledgements

Throughout my thesis I have received immeasurable support and encouragement from my family, friends and co-workers. This acknowledgement section can never fully express my gratitude to these individuals.

I would like to thank my advisor, Dr. Jim Morrissey, for his support and advice throughout my time in his lab. The quality of his scientific knowledge and advice enhanced and enriched my own science and learning during my PhD studies. Working for Jim has helped me to mature from an eager young graduate student to a more focused and independent researcher. It has not always been an easy road but I can honestly say that I would not be who I am today without Jim. I would like to give my sincere thanks to all current Morrissey lab members, especially to Dr. Stephanie A Smith for her guidance, assistance and her enthusiasm for science. Thanks also to the former members from the Morrissey lab that I interacted with, Dr. Yan Wang, Dr. Joshua M Gajsiewicz and Dr. Richard J Travers for their great support.

I would like to thank all of my committee members along with their present and former lab mates as well for their intelligent discussions and help with all aspects of my PhD career so far. I would like to particularly thank Dr. David Ginsburg, for enlightening me with his integrity, intelligence, rigorous scholarship. It has been a great pleasure for me to collaborate with your team. I would like to thank Dr. Laura Haynes, Dr. Audrey C. A. Cleuren and Dr. Andrew Yee and the colleagues from Ginsburg lab for providing support on experimental design and data analysis on the project aiming at polyphosphate probe development. Thanks also to Dr. Jordan Shavit, Dr. Bruce Palfey and Dr. Ursula Jakob. I am so grateful for all the time they spent helping me develop

into a more successful scientist. I would also like to thank my collaborators in the Gailani Lab at Vanderbilt University for providing helpful research suggestions for studying the function of polyphosphate in the contact pathway and sharing the *F12* knockout mice with us and for research support when we were developing the FXII-S545A transgenic mouse model. Together, I am grateful for the help from Dr. Yang Liu form Molecular Innovations for her technical support to help us generate the FXII-S545A transgenic founder mice.

For financial support, I would like to thank the National Heart, Lung, and Blood Institute of the National Institutes of Health, the Program in Biomedical Sciences (PIBS) at Michigan Medicine as well as the American Heart Association.

This research would also not have been possible without the endless support of my family and friends. My parents nurtured and encouraged my love of science since my earliest years. They provided me with all of the opportunities and resources I needed to be successful and taught me through their own actions the value of hard work and dedication in life. I am extremely glad and grateful that they can share in my accomplishments.

Table of Contents

List of Tables

List of Figures

Abstract

The classic coagulation cascade has been well-studied for many years. In the traditional "waterfall" model, both the contact pathway and the tissue factor pathway can trigger blood clotting. The contact pathway is composed of two serine protease zymogens, factor XII and prekallikrein, together with a non-enzymatic co-factor, high-molecular-weight kininogen. Recent discoveries have implicated the contact pathway in thrombosis and inflammation, while it is clearly dispensable for hemostasis. Due to the complexity of the enzymatic reactions and molecular interactions in the contact pathway, the (patho)-physiological mechanisms of contact pathway activation remained unclear. Previous studies suggested several molecules that may modulate the contact pathway, including inorganic polyphosphate. Studying how polyphosphate modulates the contact pathway of coagulation holds promise for developing novel drug targets for treating thrombotic diseases without increasing the risk of bleeding.

Despite being found in all kingdoms of life, polyphosphate polymer lengths are highly variable, with shorter polymers (approximately 60-100 phosphates) secreted from human platelets, and longer polymers (up to thousands of phosphates) in microbes. To reveal the molecular mechanisms of how polyphosphate regulates individual reactions in the contact pathway, we conducted *in vitro* measurements of enzyme kinetics to investigate the ability of varying polyphosphate sizes, together with high-molecular-weight kininogen and Zn^{2+}, to mediate individual proteolytic reactions in the contact pathway and activation of the intrinsic pathway by coagulation factor XII. The results suggested that polyphosphate of different sizes, together with

Zn^{2+} could activate subsets of the contact pathway reactions. The study also raised questions on whether the primary physiological role of coagulation factor XII is to trigger blood clotting.

In addition, a protein engineering study has been conducted to develop a reliable polyphosphate probe with enhanced affinity and specificity. Currently, there is a lack of sensitive and specific method for polyphosphate visualization in mammalian cells and tissues. A recombinant protein from *E. coli* was used and random mutagenesis libraries for displaying on phage surfaces were generated for polyphosphate binding selection assays. Next-generation sequencing was used to detect mutant candidates with desired polyphosphate binding features. These candidates may be used as a functional polyphosphate inhibitor *in vivo*, to prevent its ability of accelerating unwanted coagulation (thrombosis).

To interrogate the role of factor XII-mediated contact pathway *in vivo*, a new transgenic mouse model was generated using CRISPR/Cas knock-in technology, where a precise point mutation was introduced into coagulation factor XII, leading to the loss of enzymatic functions of factor XIIa. Different from currently available factor XII knock-out mice, these new transgenic mice possess intact zymogen factor XII, which should not interfere with neutrophil functions and hence should be a less biased model for coagulation or inflammation studies in the future.

Chapter 1 General Introduction to Blood Coagulation

1.1 Introduction

The hemostatic system has evolved to maintain blood in a fluid state under physiological conditions, but also to react rapidly to vessel injury by sealing defects with fibrin clots through a process called hemostasis.[1] Hemostasis is the physiological process that stops bleeding at the site of an injury while maintaining normal blood flow elsewhere in the circulation. Blood loss is stopped by formation of a hemostatic plug.[2] Working together with platelets, many procoagulant and anticoagulant biomolecules are involved in this process. However, unlike the biologically beneficial clotting process, another type of blood clotting happens when the clotting cascade is triggered inside the lumen of a blood vessel which is termed as thrombosis. This leads to the formation of a thrombus that can impede the flow of blood within an intact vessel. Thrombosis, as the primary cause of heart attacks and strokes, can occur in the arterial or the venous circulation and has a major medical impact.[1,3]

Two coagulation pathways are involved in triggering the blood clotting cascade, the extrinsic pathway (tissue factor pathway) and the intrinsic pathway (contact pathway). The tissue factor pathway is named for a protein called tissue factor (TF) and plays an important role in normal hemostasis and many types of thrombosis. The contact pathway, however, has been shown to be dispensable in normal hemostasis as patients deficient in contact pathway proteins do not show excessive bleeding,[4] but may be involved in some types of thrombosis. Different modulators were found to regulate various parts of the coagulation system. Studying how the coagulation

cascade is regulated holds promises for the discovery of novel drug targets for various clotting disorders.

1.2 Coagulation cascade overview

Blood clotting, or coagulation, is an important process that prevents excessive bleeding when a blood vessel is injured. Platelets and proteins in plasma work together to form a fibrin clot over the site of vessel injury to stop bleeding. Blood clots are healthy and lifesaving when they stop bleeding. But they can also form when they aren't needed and cause a heart attack, stroke, or other serious medical problems.

Waterfall model of coagulation cascade

The formation of a fibrin clot is mediated by a group of well-regulated plasma proteases and cofactors. Although the process of blood clotting has been studied for centuries, the concept of the blood coagulation cascade dates back to the 1960s when Davie, Ratnoff and Macfarlane described the “waterfall” and “cascade” theories outlining the fundamental principle of a cascade of proenzymes leading to activation of downstream enzymes.[5,6] These two independent studies clarified the sequence in which coagulation factors interacted and provided concepts that were readily tested in the laboratory. In both models, an important concept was introduced: the coagulation factors were present in blood in an inactive or precursor form and were converted to active enzymes in a step-by-step manner, starting from coagulation factor XII (FXII).[7] FXIIa, the activated form of FXII, activates factor XI (FXI) to FXIa. Consequently, the downstream coagulation factors including factor IX (FIX), factor X (FX), prothrombin (factor II) and fibrinogen (factor I) are activated one by one to trigger clotting.

The limitations of these classic waterfall models are obvious. The intrinsic pathway originally described by these models does not appear to be essential for *in vivo* hemostasis but may

play a role in pathologic thrombosis. It is now generally accepted that the TF pathway plays the major role in the initiation of blood coagulation following vascular injury and platelet plug formation. These models did not take into account the cellular elements that set the stage for the cell-based model of coagulation.[8] The concept of the coagulation cascade has evolved over the past 60 years. Critical additions and modifications were made in the classic "waterfall cascade model" during the following years to incorporate new discoveries and novel mechanisms. One that was particularly important linked the intrinsic pathway with the extrinsic pathway of blood coagulation at the level of FX, which was known to be the start of the common pathway.[9-11] The other significant change related to coagulation factor VIII (FVIII) and factor V (FV). These two proteins are readily activated by limited proteolysis, particularly by thrombin, but they participate as cofactors rather than enzymes.[12-14]

From a contemporary point of view, there are three stages of normal hemostasis: initiation, amplification and propagation. To initiate blood clotting, the exposure of subendothelial tissue factor leads to the formation of the extrinsic tenase complex, in combination with factor VIIa (FVIIa). The amplification phase involves the conversion from extrinsic to intrinsic thrombin generation. Thrombin generation with fibrin deposition is referred as the propagation phase.[15,16] It is important to notice that although the contact pathway does not participate in hemostatic reactions *in vivo*, there is recent evidence showing the potential association between the contact pathway and thrombosis, which will be discussed in detail later.

Extrinsic pathway

The extrinsic pathway consists of the transmembrane receptor TF and plasma FVII/FVIIa.[17] Disruption of the endothelium of a blood vessel exposes blood to subendothelial cells expressing TF on their surface. The TF:VIIa complex catalyzes the activation of FIX and FX,

leading to thrombin generation and subsequently formation of a fibrin clot.[18] Previous studies have revealed an important role of the extrinsic pathway in both hemostasis and thrombosis. TF knockout mice were found to be non-viable and die early in utero due to severe extravasation of blood cells and abnormal circulation.[19]

TF, also named as coagulation factor III (FIII), is the primary initiator of the extrinsic coagulation cascade.[20] The full length TF is a 47 kDa transmembrane glycoprotein comprising an extracellular domain of 219 amino acids, a transmembrane regions of 23 amino acids, and a cytoplasmic tail of 21 amino acids. The protein structure of TF includes 2 fibronectin type III repeats (termed D1 and D2), 2 disulfide bridges, and 3 glycosylation sites.[21] The full-length TF is found in a wide range of tissues including brain, lung, placenta, heart, testis and kidneys, being constitutively expressed in perivascular cells, such as fibroblasts, pericytes, or epithelial cells.[19,22] Vascular cells, such as smooth muscle cells (SMCs), endothelial cells (ECs) or blood cells, do not express considerable amounts of TF in a quiescent state, but can be induced via different factors.[23] Found in the surrounding subendothelial tissue, one major function of TF is to maintain hemostasis and vessel integrity. TF has also been shown to be involved in angiogenesis, wound healing, apoptosis and proliferation.[24-27]

The main function of FVII is to initiate the process of coagulation in conjunction with TF. FVII is synthesized in the liver and secreted to the blood stream as a glycoprotein with a molecular weight of 50 kDa. FVII, like all the coagulation serine proteases, circulates in the plasma chiefly as an inert zymogen. However, FVII also circulates at low levels in its active enzymatic form, FVIIa. Zymogen FVII is converted to its enzymatic form, FVIIa, by proteolysis of a single peptide bond, resulting in two disulfide-linked polypeptide chains.[28] The protease(s) that is responsible for FVII cleavage *in vivo* is unclear. FXIa, FXa, FXIIa, thrombin, plasmin and TF:VIIa were all shown

to be able to trigger FVII activation *in vitro*.[29-35] Clinically, FVII deficiency results in a rare inherited bleeding disorders.[36]

During vascular injury, FVII/FVIIa binds to TF at a 1:1 ratio on the cell surface and the remaining FVII is rapidly converted to FVIIa.[29] The assembly of TF:VIIa complex on a suitable phospholipid membrane surface greatly enhances the proteolytic activity of VIIa and allows rapid cleavage of its substrates, FX, FIX, and FVII (autoactivation).[37,38] The activation of FX leads to the activation of the common pathway of coagulation, whereas the activation of FIX leads to partial activation of the intrinsic pathway of coagulation.

Intrinsic pathway

Apart from the TF:VIIa triggered coagulation, clotting can also be triggered by the intrinsic pathway. The intrinsic pathway of coagulation is triggered by the activation of the contact pathway. The main components of the contact pathway include FXII, FXI, plasma prekallikrein (PK), and a non-enzymatic cofactor, high-molecular-weight kininogen (HK). Unlike the extrinsic pathway which was shown to play an important role in maintaining hemostasis, the proteins in the contact pathway are dispensable for hemostatic function, since deficiencies of FXII and PK are not associated with excessive bleeding in mice or humans.[39-41] However, recent studies have revealed associations between the contact pathway and thrombosis.[42-45]

The activation of the contact pathway requires interaction with negatively charged surfaces or polymers, which induces a conformational change in zymogen FXII resulting in a small amount of active FXII (FXIIa). FXII is an 80 kDa protease zymogen synthesized in the liver and circulating in the blood stream at a concentration of 375 nM.[46] In human, the *F12* gene encoding FXII is 12 kb in length and is composed of 14 exons.[47] The single-chain FXII zymogen consists of a heavy chain of 353 amino acids and a light chain of 243 amino acids, forming a disulfide bond. The

heavy chain is located at the N-terminus and contains a fibronectin domain type II, an epidermal-growth-factor-like (EGF-like) domain, a fibronectin domain type I, a second EGF-like domain, a kringle domain, and a proline-rich region. The light chain at the C-terminus contains the catalytic domain where the catalytic triad of the serine protease is located.[48] All of the domains are homologous to those found in several other serine proteases, except for the proline-rich region which is unique to FXII. Although the complete crystal structure of FXII has not been solved, biochemical studies have mapped the potential surfaces on the two fibronectin domains.[49-52] Putative artificial surface binding regions were also predicted on the EGF-like domains and the kringle domain.[53,54] Similar to most of the chymotrypsin-like serine proteases, the active site (catalytic triad) of FXII consists of 3 residues, H394, D442, and S544, indicating that *in vivo* the catalytic domain is globular, bringing these three amino acids in close apposition.[48]

FXII can be cleaved by several serine proteases including plasma kallikrein (PKa, the active form of PK)[55], FXIIa (via autoactivation)[56,57], and plasmin[58]. The cleavage of FXII after position R353 yields an activated form α-FXIIa.[59] Unlike the single-chain FXII zymogen, α-FXIIa has two chains (heavy chain and light chain) that are linked by a disulfide bond. The molecular weight of α-FXIIa remains 80 kDa. However, on a reduced protein gel, α-FXIIa migrates as two bands, an ~50 kDa (heavy chain) and ~30 kDa (light chain). α-FXIIa is in turn able to cleave its substrates PK, FXII, FXI, C1 complex[60] and potentially plasminogen[61]. The mutual activation of PK and FXII is known as reciprocal-activation.[62] The cleavage of FXI by α-FXIIa yields FXIa, which in turn cleaves FIX into FIXa and leads to blood clotting.[4] Further cleavage of α-FXIIa at the R334 and R343 positions by PKa yields β-FXIIa, consisting of two polypeptide chains of a 2 kDa heavy chain remnant and a 28 kDa catalytic domain covalently bonded together by the same disulfide bond.[51] The crystal structure of β-FXIIa has been recently resolved with small molecule

inhibitors.[63] Due to the lack of the heavy chain, β-FXIIa is unable to bind to negatively charged surfaces and therefore is inefficient at promoting clotting.[64]

PK is the circulating zymogen of PKa, encoded by the *Klkb1* gene. PK is usually an 85-88 kDa single-chain protein produced in the liver and circulates in the blood, typically bound with a cofactor, HK.[65] Interestingly, PK and FXI are homologous and share 58% amino acid sequence identity with the unique feature of four tandem repeats of 90 amino acid apple domains at the N-termini, which harbor exosites for substrates, cofactors, and receptors.[66] However, Factor XI is a disulfide-linked dimer whereas PK is a monomer.[67,68] A recent study revealed the crystal structure of recombinant full length PKa. In their structure, the catalytic domain is positioned above a disc-shaped assemblage of four apple domains in an active conformation. Contrary to the FXI structure, the intact disc of apple domains in the PKa structure is rotated 180° relative to the catalytic domain.[69]

Like many serine protease zymogens, PK is synthesized as a single-chain inactive precursor. Once cleaved by FXII or other PK activators, PK is activated to PKa. As described above, FXII and PK can activate each other through a mechanism termed reciprocal activation. PKa further liberates kinins (the vasoactive peptides, bradykinin and kallidin) from its substrate, HK, via a double cleavage. The kinins mediate blood coagulation, activate inflammatory response, and regulate blood pressure via vasodilation.[70]

Apart from being the substrate for PKa, HK is an important nonenzymatic cofactor in the contact pathway, since at least 75% of PK circulates bound noncovalently to HK in a 1:1 ratio in plasma.[65,71] Binding with HK enhances the binding of PK and FXI to certain anionic surfaces.[72,73] Although there is lack of evidence showing that FXII circulates bound to HK in plasma, some studies indicated that HK is required in stoichiometric amounts for maximal FXIIa activation of

FXI *in vitro*.[72] Zn^{2+} is also known to be an important cofactor in contact activation as the binding affinities and activities of many proteins in the contact pathway will be enhanced by Zn^{2+}.[56,74,75] Moreover, evidence suggested that Zn^{2+} induces changes in folding of the HK D5 domain and also affects the conformation of the entire HK protein.[76] Considering that the D5 domain of HK is responsible for Zn^{2+} and surface (polymer) binding[77,78], Zn^{2+} and HK concentration dependence of individual reactions in the contact pathway is worth exploring in detail. The biological functions of the contact pathway will be discussed in a later section.

Apart from the described contact pathway components, FXI is also an important zymogen in the intrinsic pathway of blood clotting. In humans, FXI is synthesized mainly in the liver[79] and circulates in plasma at a concentration of ~30 nM (15-45 nM) almost entirely as a non-covalent complex with HK.[80-82] Different from other coagulation factors, FXI presents as a dimer of identical 80 kDa subunits.[68] Similar to PK, FXI monomer also contains four apple domains and a catalytic domain. The apple domain discs are linked to a "saucer" on which the catalytic domain rests. The two monomers interface through the A4 domains.[83] FXI can be converted to FXIa by the enzyme FXIIa[5,6], or FXIa (via autoactivation)[84]. The active protease FXIa subsequently activates FIX to FIXa and eventually leads to the generation of thrombin, which cleaves fibrinogen to fibrin.[85,86] Unlike the contact pathway proteases, deficiency of FXI results in a mild bleeding disorder, suggesting that FXI serves a supportive role in hemostasis.[87] Previous studies also revealed that the downstream protease, thrombin, could also cleave FXI, which may create a positive feedback loop to accelerate thrombin generation.[88,89] These data demonstrated that FXI can support thrombin generation independent of the contact system, can interact with proteases in the contact system, or can serve as an interface of the two systems.[85]

Based on the waterfall model of coagulation, the downstream target of FXIa in the intrinsic pathway of coagulation is FIX.[5,6] FIX is produced as a zymogen and can be cleaved to FIXa by FXIa (intrinsic pathway), or TF:FVIIa (extrinsic pathway).[90,91] FVIII is a nonenzymatic cofactor of FIXa circulating in the bloodstream. The *F8* gene is located on the long arm of the X chromosome and is almost exclusively expressed in endothelial cells.[92,93] When proteolytically activated to FVIIIa, it interacts with FIXa to form a tight noncovalent complex.[94] In the presence of Ca^{2+}, membrane phospholipids, and FVIIIa, the FVIIIa-FIXa complex activates the common pathway by cleaving its downstream substrate FX.[94]

Common pathway

The common pathway begins at FX which is activated to FXa by either the TF:VIIa, or the FVIIIa-FIXa complex in the presence of phospholipid membrane and Ca^{2+}.[95] Once activated to FXa, it goes on to activate prothrombin into thrombin, using FVa as a cofactor. Approximately 80% of blood FV circulates in plasma at a concentration of about 20 nM (7 μg/ml), the remaining 20% being stored in the platelet α-granules (4600–14,000 molecules per platelet).[96] Plasma derived FV is a 330 kDa single-chain protein, which after proteolytic removal of one domain by thrombin or FXa, becomes FVa, consisting of two non-covalently associated chains stabilized by a Ca^{2+} ion.[97,98] FVa and FXa assemble in a Ca^{2+}-dependent complex on phospholipid membranes, which enhances the rate of prothrombin activation by about 300,000-fold.[96] Prothrombin is the zymogen of the allosteric serine protease, thrombin, which is in charge of activating fibrinogen into fibrin.[99] Thrombin can also activate other factors in the intrinsic pathway (i.e., FXI) as well as FV, FVIII and the fibrin stabilizing factor (FXIII).[95] Fibrin subunits crosslink together to form fibrin strands, and FXIII acts on fibrin strands to form a fibrin mesh, which helps to stabilize the platelet plug.[100]

Regulation of the coagulation system & diseases

The coagulation process is finely balanced in our body. A highly complex, integrated and dynamic system has evolved to balance procoagulant, anticoagulant and fibrinolytic forces to enable hemostasis without causing thrombosis.[101] There are many naturally occurring anticoagulant proteins present in the blood stream. Many of them belong to the serpin (serine protease inhibitor) family, which bind specifically to their target enzymes.[102] Tissue factor pathway inhibitor (TFPI) inhibits the TF:VIIa complex and FXa. Activated protein C and protein S, together with thrombin, act by inhibiting the action of the cofactors FVa and FVIIIa. Antithrombin inhibits thrombin, FIXa, FVIIa, FXa, FXIa, and FXIIa. C1 esterase inhibitor (C1-INH), can inhibit FXIIa, PKa, and FXIa of the intrinsic pathway.[103] Apart from inhibiting the proteases in the coagulation cascade, coagulation could also be regulated by dissolving the fibrin clot via a process called fibrinolysis. Plasminogen, tissue plasminogen activator (tPA), and urokinase (uPA) are the main components of the fibrinolysis pathway. Similar to the coagulation cascade, there are many modulators that inhibit the components in the fibrinolysis pathway, including plasmin inhibitors, plasminogen activator inhibitors (PAI) and thrombin activatable fibrinolysis inhibitor (TAFI).[104] Genetic deficiency, or dysregulation of the coagulation proteins or inhibitors may lead to bleeding disorders or thrombotic diseases.

Loss-of-function mutation or deficiency of coagulation factors will lead to many different bleeding disorders, including hemophilia A and B, von Willebrand Disease (VWD), and rare bleeding disorders (RBDs). Hemophilia A and B are rare (1 in 5,000 and 25,000 male births, respectively), X-linked Mendelian bleeding disorders characterized by a lack of one of the proteins involved in blood clotting.[105] Functional copies of FVIII or FIX are missing in individuals with hemophilia A or B, respectively, usually owing to a loss-of-function mutation, deletion or gene

inversion.[101] VWD, the most common inherited bleeding disorder with a prevalence of around 1 in 1000 persons[106], is caused by genetic variances or deficiency of a protein called von Willebrand Factor (VWF), whose primary function is to bind with FVIII and mediate platelet adhesion to wound sites.[107] Nowadays, synthetic drugs or recombinant proteins have been developed to compensate for the deficiency of certain coagulation factors in plasma as treatments of bleeding disorders.[108]

Acute arterial thrombosis is the proximal cause of most cases of myocardial infarction (heart attack) and of about 80% of strokes, collectively the most common cause of death in the developed world. Venous thromboembolism is the third leading cause of cardiovascular-associated death.[3] Mechanistically, thrombi can either obstruct blood flow at the site of formation or detach and embolize to block a distant blood vessel (e.g., pulmonary embolism, embolic stroke). The pathogenic changes that occur in the blood vessel wall and in the blood itself resulting in thrombosis are still unclear. However, studies have provided evidence to show that both intrinsic and extrinsic coagulation pathways[109-111] can contribute to thrombosis, together with cellular responses involving platelets,[112] monocytes,[113] endothelial cells,[114] etc. The current treatments for thrombotic diseases often target thrombin, FXa, or platelets and have side effects including interfering with normal hemostatic function. Since contact pathway activation can lead to thrombus formation via the intrinsic pathway but does not participate in normal hemostasis, understanding the mechanism of contact pathway action in thrombosis is crucial for developing safer and more effective antithrombotic drugs without major bleeding side effects.

1.3 Contact pathway in the biological system

The contact pathway, also known as the plasma kallikrein-kinin system (KKS), is a critical crosstalk mechanism between coagulation and inflammation.[60,115,116] The contact pathway

includes circulating zymogens of the serine proteases FXII and PK, and the non-enzymatic cofactor for PK, HK. In many cases, zymogen FXI and the serpin C1-INH are also included as part of this pathway. Normally, all the zymogens circulate in blood without active enzymatic activity. The presence of C1-INH protects the contact pathway zymogens from slow autoactivation without surfaces.[60,86] The contact pathway gets activated when the zymogens interact with suitable surfaces or polymers, such as polyphosphate[117-122], nucleic acid[123], collagen[124], NETs[125-127], misfolded proteins[128], endothelial cell surfaces[129,130], etc. In the presence of a negatively charged surface, FXII quickly undergoes autoactivation, resulting in a small amount of active enzyme FXIIa.[57,131] It was also reported that PK can undergo autoactivation to form PKa under certain circumstances.[130,132-134] The generated FXIIa then cleaves PK to produce PKa which cleaves more FXII to FXIIa via rapid reciprocal activation reactions to counteract the inhibitory effect of C1-INH.[86]

Contact pathway in coagulation

Once a significant amount of FXII is activated, FXIIa can further activate the downstream substrate of the coagulation cascade, FXI, to produce the protease, FXIa, triggering the intrinsic cascade of coagulation.[135] Previous *in vitro* experiments from our lab demonstrated that this reaction is very slow as compared with other enzymatic reactions in the clotting cascade, even in the presence of polyphosphate.[117] Although the proteolytic cleavage of FXI by FXIIa has been demonstrated *in vitro*, it is unclear whether this reaction happens *in vivo* and plays a role in initiating clotting. In fact, animal studies and clinical data indicated that the contact pathway is completely dispensable for hemostasis, as individuals deficient in either FXII or PK do not show a bleeding tendency.[39-41] This implies that the contact pathway is not required in trauma-induced blood clotting. In contrast, recent studies have shown in experimental animals that FXII deficiency is protective in both arterial[42-44] and venous[45] thrombosis models, suggesting that the contact pathway could be a potential target for

thromboprophylaxis. Further, contact activation by polyP or DNA may play a role in thrombotic diseases including myocardial infarction[136,137] and stroke[138].

Contact pathway in inflammation and immunity

The well-studied, primary physiologic function of the contact pathway is to participate in the inflammation and immunity response. As mentioned before, HK is not only a cofactor for PK, but also a substrate for PKa. PKa cleaves HK to release kallidin, which then is converted to a 9-amino acid peptide chain, bradykinin.[139,140] Bradykinin interacts with G-protein coupled kinin receptors (B1 and B2 receptors) at the cell surface, which elevates vascular permeability and causes vasodilatation of arteries and veins of the gut, aorta, uterus and urethra via different mechanisms.[140] This response is particularly important in allergic reactions and in inflammatory responses. Misregulation of the contact pathway can result in hereditary angioedema (HAE), a disease characterized by recurrent edema attacks and swelling of mucous membranes.[141] Most common types of HAE are caused by reduced levels or dysfunctional C1-INH present in blood, so that FXIIa and PKa cannot be inhibited efficiently, leading to consistent overproduction of bradykinin.[142] The contact pathway also participates in the host-pathogen response in the immune system. Sepsis is an infection-induced systemic inflammatory response syndrome that typically progresses to organ hypoperfusion and death within hours to days when left untreated.[143] Previous studies showed the beneficial effects of FXII inhibition in a baboon model of *E. coli* sepsis.[144] Another study showed that pretreatment with a FXII inhibitor before *E. coli* inoculation led to reduced complement activation, neutrophil degranulation, and levels of tissue plasminogen activator and IL-6 compared to untreated baboons.[145]

Contact pathway in fibrinolysis

The contact pathway components also participate in fibrinolysis, the process of dissolving fibrin clots by the enzyme plasmin. BK has been shown to induce the expression of tPA, an

activator of plasminogen, which cleaves plasminogen to produce plasmin.[86] In addition, FXII itself possesses plasminogen activator activity that can be potentiated by the presence of artificial negatively charged polymer.[61] More recently, it was reported that fibrin-bound polyphosphate polymers amplify this reaction.[146] Conversely, plasmin can also act as a contact pathway activator by directly activating FXII to FXIIa[147], and PK to PKa[148].

1.4 General introduction of polyphosphate (polyP)

While many artificial surfaces are known to activate the contact pathway *in vitro*, the relevant physiologic activator for this system *in vivo* is not yet clear. As mentioned previously, polyP is one of the potential natural substances that have been reported to be able to trigger contact pathway activation.[117-122] As are many other contact activators, polyP is a chain of highly negatively charged polymers, composed of inorganic phosphate. PolyP is an ancient molecule that exists in all kingdoms of life from bacteria to humans.[149] This thesis is mainly focused on the role of polyP in modulating individual reactions of the contact pathway and developing a specific polyP probe and/or inhibitor.

PolyP in prokaryotes and unicellular eukaryotes

The functions of polyP in prokaryotes and unicellular eukaryotes have been well studied over the past several decades. PolyP was first isolated in yeast[150] and then a high concentration of polyP was found in volutin granules, acidocalcisomes, nuclei and mitochondria in yeast, together with divalent metal ions including Ca^{2+}, Mg^{2+}, and Zn^{2+}.[151,152] The length of polyP in microorganisms usually ranges from hundreds to thousands of phosphate units.[149] PolyP is believed to be synthesized by polyP kinase (PPK), a highly conserved enzyme across microorganisms that catalyzes the transfer of terminal phosphate from ATP to the end of a polyP chain. The reaction is reversible, making polyP an important energy reservoir for ATP synthesis in bacteria.[149] Therefore, PolyP is associated with cell viability, proliferation, virulence and stress resistance in prokaryotes and yeast. [152,153]

PolyP in mammals

The function of polyP in mammals has only recently been studied. In 1995, polyP was found in various rodent tissues with various lengths including brain, heart, kidney, liver, and lung.[154] The study also reported that polyP in brain was predominantly about 800 phosphate units in length. In mammalian models, polyP is involved in ion channel activation[155,156], cell signaling pathways[157,158], mitochondrial activities[159], rRNA transcription[160], DNA repair[161], cell apoptosis[162], blood clotting[163], inflammation[120], and bone mineralization[164,165].

In human platelets, polyP was first reported as present in dense granules at a high concentration of approximately 130 mM (0.74 ± 0.08 μmol polyP monomer per 10^{11} platelets).[166] PolyP was also found in mouse RBL-2H3 mast cells.[167] PolyP can be secreted from platelets into the blood stream after activation. Unlike microbial polyP, platelet secreted polyP is smaller and much more homogeneous in size, with polymer lengths of approximately 60 to 100 phosphate units.[120,166] Recent studies demonstrated that membrane-associated polyphosphate in a nanoparticle state was located on the surface of activated platelets.[168] Our lab previously showed that polyP exerted differential effects on blood clotting, depending on its polymer size.[163] Long-chain polyP (ranging from less than a hundred to thousands of phosphate units) accelerates blood clotting at four steps: initiating the contact pathway activation, facilitating FV activation and abrogating TFPI function, accelerating FXI activation by thrombin, and enhancing fibrin polymerization. In contrast, platelet releasate polyP (less than 100 phosphate units) cannot efficiently activate the contact pathway.[149] Further studies revealed that long-chain polyP was in particular required for the FXII autoactivation reaction, but not for other proteolytic reactions in the contact pathway.[169]

Chapter 2 Polyphosphate, Zn^{2+} and High-molecular-weight Kininogen Modulate Individual Reactions of the Contact Pathway of Blood Clotting[a]

2.1 Introduction

The contact pathway of blood clotting—also known as the plasma kallikrein-kinin system—includes the circulating serine protease zymogens, FXII and PK, as well as HK, the non-enzymatic cofactor for PK and a substrate for PKa.[86,170] This pathway, a schematic of which appears in Figure 2.1, is initiated when blood or plasma is exposed to certain charged polymers or suitable surfaces.[131] This interaction is thought to induce a conformational change in FXII that produces small amounts of enzymatically active FXIIa via autoactivation (more precisely, activation of FXII by FXIIa).[57] FXIIa then cleaves PK to PKa, which can reciprocally activate more FXII to FXIIa.[60] PK was also reported to undergo autoactivation to form PKa in the presence of a suitable polymer or surface.[132] Once significant concentrations of FXIIa accumulate, FXIIa activates FXI to FXIa, triggering the intrinsic cascade of coagulation that leads to thrombin generation and fibrin formation.[135] The contact pathway is also a critical connection for crosstalk between coagulation and inflammation.[116,139,170] However, this pathway is completely dispensable for hemostasis, as individuals deficient in either FXII[39,40] or PK[41] have no bleeding tendencies. On the other hand, animal studies have shown that targeting FXII or PK is protective in thrombosis

[a] This chapter has been adapted from a research article published in the Journal of Thrombosis and Haemostasis and used in accordance with the publisher's copyright privileges for publication in a dissertation thesis. Full citation: Wang, Y., Ivanov, I., Smith, S. A., Gailani, D., & Morrissey, J. H. (2019). Polyphosphate, Zn^{2+} and high molecular weight kininogen modulate individual reactions of the contact pathway of blood clotting. *Journal of thrombosis and haemostasis : JTH*, 17(12), 2131–2140. https://doi.org/10.1111/jth.14612

models,[42-45,171] suggesting that the contact pathway could contribute to the development of thrombosis in humans.

While several artificial surfaces and polymers may activate the contact pathway *in vitro*, the relevant (patho)physiologic activators for this system *in vivo* have only recently been suggested.[86] Long-chain polyphosphate (polyP), in particular, has emerged as an especially potent trigger of the contact pathway.[163] In this study, we aimed to investigate the ability of various sizes of polyP, together with two important cofactors, HK and Zn^{2+}, to modulate four proteolytic reactions of the contact pathway: FXII autoactivation, FXII activation by PKa, PK activation by FXIIa, and PK autoactivation.

PolyP is a highly negatively charged polymer of inorganic phosphates that varies in length, depending on biological source. PolyP released from platelets has a fairly narrow size range of approximately 60-100 phosphates long,[166] while unicellular organisms contain heterogeneous polyP that can range up to thousands of phosphates in length.[172] Roles for polyP in prokaryotes and unicellular eukaryotes have been extensively studied[150] but only recently have polyP's functions been explored in multicellular eukaryotes (particularly in mammals). Our previous work demonstrated that polyP acts at multiple stages of the clotting cascade, with pro-hemostatic, pro-thrombotic and pro-inflammatory effects that are highly dependent on polyP chain length.[163,173] In particular, we reported that optimal triggering of plasma clotting via the contact pathway requires very long polyP polymers,[163] although the polymer length-dependence of each individual reaction of the contact pathway was not investigated. In the present study we investigated the details of the requirement for very long-chain polyP to trigger clotting via the contact pathway. Individual enzyme reactions within the contact pathway can contribute to the complement cascade, fibrinolysis, bradykinin generation and inflammation.[86,170] Accordingly, we hypothesized that the

polyP length requirement might not be the same for all four of the individual reactions in Figure 2.1, with platelet-sized polyP possibly supporting subsets of these reactions. We now report that only FXII autoactivation required very long-chain polyP, while the reciprocal enzyme activation reactions (FXII activation by kallikrein, and prekallikrein activation by FXIIa) were accelerated to significant extents by platelet-sized polyP. Furthermore, HK and Zn^{2+} are required only for specific subsets of these reactions.

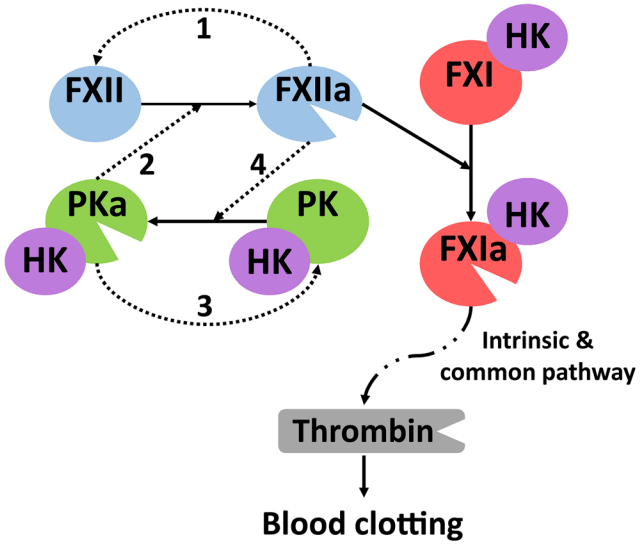

Figure 2.1 Overview of the contact pathway of blood clotting. The following numbered reactions that contribute to initiation of the contact pathway of blood clotting were examined in this study: ***1***, Activation of FXII by FXIIa (FXII autoactivation); ***2***, Activation of FXII by PKa; ***3***, Activation of PK by PKa (PK autoactivation); and ***4***, Activation of PK by FXIIa. Propagation of the clotting cascade happens when FXIIa activates FXI, leading ultimately to thrombin generation.

2.2 Materials and methods

Materials

Polybrene (hexadimethrine bromide), polyethylene glycol and soybean trypsin inhibitor were from Sigma (St. Louis, MO). Human FXII, α-FXIIa, PK, PKa and single-chain HK were from Enzyme Research Laboratories (South Bend, IN). CTI was from Haematologic Technologies (Essex Junction). Polyclonal goat anti-human PK antibody (IgG) was from Affinity Biologicals (Ancaster, Canada). The chromogenic substrate for FXIIa or PKa, H-D-Pro-Phe-Arg-pNA (L-

2120), was from Bachem (Bubendorf, Switzerland). Chelex® 100 Resin was from Bio-Rad Laboratories (Hercules, CA). Ultra-Low Attachment microplates were from Corning Inc (Tewksbury, MA).

Two preparations of heterogeneous, long-chain polyP employed in this study were prepared starting from chemically synthesized, high-molecular-weight polyP (Sigma-Aldrich). One preparation, termed $polyP_{700}$, had a modal length of 700 phosphates (range, 200 to 1300 phosphates) and was solubilized from high-molecular-weight polyP as described.[174] The other, termed $polyP_{1200}$, had a modal length of 1200 phosphates (range, 595 to 1935 phosphates). It was produced from solubilized high-molecular-weight polyP[174] after precipitation with 10 mM NaCl and 25% isopropanol. Narrowly size-fractionated polyP preparations were produced from chemically synthesized polyP by preparative PAGE as previously described,[163,175] and are referred to by their polymer lengths, which were: 28, 42, 65, 68, 79, 110, 143, 211, 315 and 415 phosphates. PolyP concentrations were quantified by measuring inorganic phosphate following hydrolysis in 1 M HCl at 100°C for 10 min.[175] Throughout this study, polyP concentrations are given in terms of molar concentrations of phosphate monomer.

FXII autoactivation

Reactions were performed at 37°C in ultra-low attachment microplate wells with 100 nM FXII in HBSP solution (20 mM *N*-2-hydroxyethylpiperazine-*N'*-2-ethanesulfonic acid (HEPES)-NaOH (pH 7.4), 100 mM NaCl, and 1% w/v polyethylene glycol, 8000 MW). Pilot experiments evaluating the polyP dose dependence included 5 μM $ZnCl_2$ in the presence of 0 to100 μM $polyP_{1200}$ or $polyP_{79}$. Experiments evaluating the polyP size dependence included 5 μM $ZnCl_2$ in the absence or presence of 10 μM narrowly sized-fractionated polyP. Experiments evaluating the impact of $ZnCl_2$ included 10 μM $polyP_{1200}$ and either 2 mM EDTA or 0 to 20 μM $ZnCl_2$.

Experiments evaluating the impact of HK included 10 μM $polyP_{1200}$, 5 μM $ZnCl_2$, and 0 to 900 nM HK. Timed aliquots (10 μL) were removed and quenched in 70 μl ice-cold Quench Buffer I (20 mM HEPES-NaOH (pH 7.4), 5 mM EDTA, and 1 M NaCl). Following quenching, FXIIa amidolytic activities were quantified by measuring A_{405} at 37°C and converting to FXIIa concentrations by reference to a standard curve. Second-order rate constants for FXII autoactivation were calculated according to the method of Tans *et al*.,[132] based on the equation, $d[FXIIa]/dt = k_2[FXII][FXIIa]$.

FXII activation by PKa

These reactions were also conducted in HBSP at 37°C in ultra-low attachment microplate wells. Pilot experiments evaluating the polyP dose dependence contained 100 nM FXII, 100 pM PKa, 100 nM HK, and 10 μM $ZnCl_2$, in the presence of 0 to 100 μM $polyP_{1200}$ or $polyP_{79}$. Experiments evaluating the polyP size-dependence contained 100 nM HK and 10 μM $ZnCl_2$, in the absence or presence of 10 μM narrowly size-fractionated polyP. Experiments evaluating the impact of $ZnCl_2$ included 10 μM $polyP_{1200}$, 100 nM HK, and either 2 mM EDTA or 0 to 20 μM $ZnCl_2$. Experiments evaluating the impact of HK included 10 μM $polyP_{1200}$, 10 μM $ZnCl_2$, and 0 to 900 nM HK. Timed aliquots (10 μL) were removed and quenched in 70 μl ice-cold Quench Buffer II (20 mM HEPES-NaOH pH 7.4, 5 mM EDTA, 50 μg/ml soybean trypsin inhibitor, and 15 μg/ml polybrene). Following quenching, FXIIa amidolytic activities were quantified by measuring A_{405} at 37°C and converting to FXIIa concentrations by reference to a standard curve.

PK activation by FXIIa

These reactions were also conducted in HBSP at 37°C in ultra-low attachment microplate wells. Pilot experiments evaluating the polyP dose dependence contained 100 nM PK, 100 pM FXIIa and 10 μM $ZnCl_2$, in the presence of 0 to 100 μM $polyP_{1200}$ or $polyP_{79}$. Experiments

evaluating polyP size-dependence included 10 μM $ZnCl_2$, in the absence or presence of 10 μM narrowly size-fractionated polyP. For experiments evaluating the impact of $ZnCl_2$, HBSP was pretreated with Chelex® 100 resin (buffered to pH 7.4) to deplete trace divalent metal ions. These assays included 10 μM $polyP_{1200}$ and either 0 to 10 mM EDTA or 0 to 10 μM $ZnCl_2$. Experiments evaluating the impact of HK included 10 μM P_{1200}, 10 μM $ZnCl_2$, and 0-900 nM HK. Timed aliquots (10 μL) were removed and quenched in 70 μl ice-cold Quench Buffer I. Following quenching, amidolytic activities were quantified by measuring A_{405} at 37°C (to prevent temperature-dependent auto-inhibition of PKa).[176] Amidolytic activities were converted to PKa concentrations by reference to a standard curve.

PK autoactivation

Apparent PK autoactivation was evaluated by quantifying PKa after incubating 100 nM PK with 100 nM HK, 10 μM $ZnCl_2$, 10 μM $polyP_{1200}$, and 0 to 2.5 μM CTI in HBSP at 37°C. Timed, 10 μL-aliquots were quenched in 70 μl ice-cold Quench Buffer I. Following quenching, PKa amidolytic activities were quantified by measuring A_{405} at 37°C and converting to PKa concentrations by reference to a standard curve.

Additional experiments employed an inactive mutant form of PK with the active-site serine replaced with alanine (PK-S559A).[121] PK-S559A cDNA[177] was expressed in HEK293 cells using vector pJVCMV under serum-free conditions, and PK-S559A protein was purified by anion-exchange chromatography as described.[121] Enzymatic reactions were then conducted in polypropylene tubes coated with polyethylene glycol (20,000 MW). 200 nM PK-S559A, with or without 70 μM $polyP_{700}$, 200 nM HK, or 25 nM PKa, was incubated at 37°C in HBSP containing 10 μM $ZnCl_2$ and 50 nM of the blocking anti-FXII(a) monoclonal antibody, 1B2.[178] At various time points, aliquots were removed and mixed with reducing SDS sample buffer. Samples were

resolved on SDS-PAGE (12% acrylamide) and transferred to nitrocellulose membranes. Blots were probed with polyclonal IgG to PK. Detection was with a horseradish peroxidase-conjugated secondary antibody and chemiluminescence.

2.3 Results

The four individual enzyme activation reactions that can contribute to activation of plasma clotting via the contact pathway are numbered in Figure 2.1. The goal of the present study was to understand how the polymer length of polyP influences its ability to accelerate these four enzyme reactions individually. Since HK and Zn^{2+} are known modulators of the contact pathway, we also examined their contributions to each reaction, together with polyP. Pilot experiments were performed to determine the optimal concentrations of long-chain and platelet-size polyP to drive individual reactions of the contact pathway (Supplementary figures 2.1, 2.3 & 2.4). For all three reactions, we used 10 μM polyP (in terms of phosphate monomer), which was within the concentration range that gave maximal reaction rates.

PolyP length-requirement for contact pathway reactions

PolyP accelerated FXII autoactivation in a manner that was strongly dependent on polyP polymer length and concentration (Figure 2.2A & Supplementary figure 2.1). Under the experimental conditions tested (100 nM FXII in the presence of 5 μM $ZnCl_2$, examined in a 20-minute endpoint assay), only 0.15 ± 0.03 nM FXIIa was generated in the absence of polyP, whereas 420-fold more FXIIa was generated in the presence of $polyP_{1200}$. Platelet-size polyP (79 phosphates) supported only about fourfold more FXIIa generation than in the absence of polyP. As compared to $polyP_{1200}$, platelet-size polyP did not detectably support this reaction in a 45-minute kinetic assay (Supplementary figure 2.2). Our finding that the amount of FXII autoactivation increased continually with increasing polyP polymer length is highly reminiscent

of the polymer length-dependence by which polyP triggers plasma clotting via the contact pathway.[163] It is also consistent with our previous finding that platelet-size polyP is very weak at triggering clotting via the contact pathway.[163]

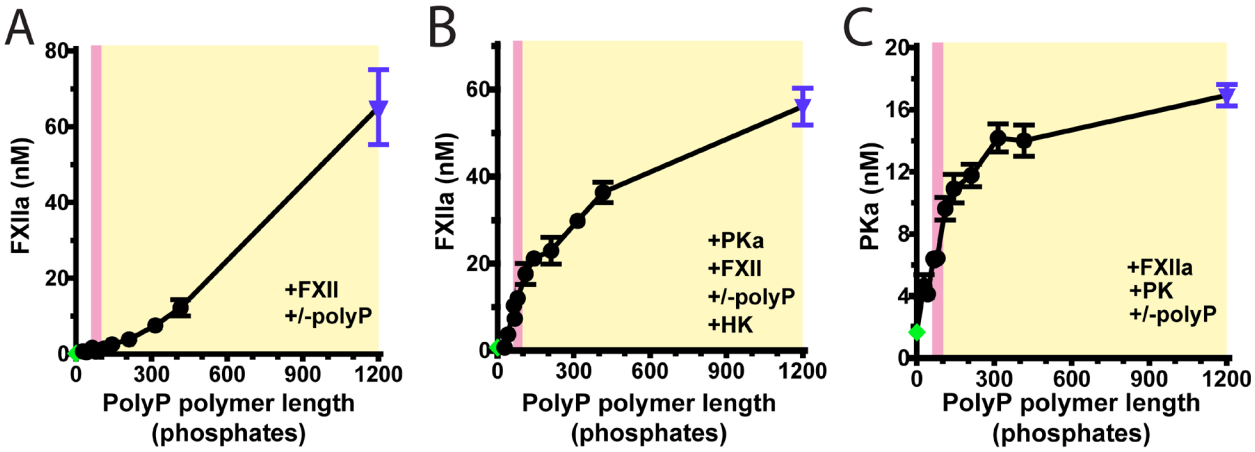

Figure 2.2 The ability of polyP to accelerate the individual reactions of the contact pathway depends on its polymer length. In each *panel*, reactions were conducted without (◆) or with 10 μM polyP (●,▼). *Data points* for size-fractionated polyP preparations (●) are plotted on the *x*-axes according to their polymer lengths, while *data points* for heterogeneous $polyP_{1200}$ (▼) are plotted on the *x*-axes at the modal length of this preparation (1200 phosphate units). In each *panel*, a pink rectangle represents the approximate length range of platelet polyP (60-100 phosphates) [166], and a yellow rectangle indicates the length range of microbial polyP [179]. (A) PolyP length requirement for FXII autoactivation. In an endpoint assay (stopped at 20 min), 100 nM FXII was incubated with 5 μM $ZnCl_2$ without polyP (◆) or with 10 μM polyP (●,▼). HK was not included in this experiment. (B) PolyP length requirement for FXII activation by PKa. In an endpoint assay (stopped at 4 min), 100 nM FXII was incubated with 100 pM PKa, 100 nM HK and 10 μM $ZnCl_2$, without polyP (◆) or with 10 μM polyP (●,▼). (C) PolyP length requirement for PK activation by FXIIa. In an endpoint assay (stopped at 3 min), 100 nM PK was incubated with 100 pM FXIIa and 10 μM $ZnCl_2$, without polyP (◆) or with 10 μM polyP (●,▼). HK was not included in this experiment. Data in all *panels* are mean ± S.E. ($n \geq 3$).

PolyP was required for efficient FXII activation by PKa, in a manner that depended on polyP polymer length and concentration (Figure 2.2B & Supplementary figure 2.3). In a 4-minute endpoint assay (employing 100 nM FXII with 100 pM PKa, 100 nM HK, and 10 μM $ZnCl_2$), only 0.72 ± 1.11 nM FXIIa was generated in the absence of polyP. Inclusion of $polyP_{1200}$ increased FXIIa generation approximately 77-fold. In contrast to FXII autoactivation, however, the effect of polyP polymer length on activation of FXII by PKa showed signs of plateauing at longer polymer lengths. Furthermore, platelet-size polyP (79 phosphates) supported 16-fold more FXIIa

generation than in the absence of polyP. These data demonstrated that platelet-size polyP can accelerate FXII activation by PKa, although the reaction was fastest with long-chain polyP.

PolyP was not absolutely required for PK activation by FXIIa, although the reaction was accelerated by polyP (Figure 2.2C & Supplementary figure 2.4). Under the experimental conditions tested (100 nM PK with 100 pM FXIIa in the presence of 10 μM $ZnCl_2$, examined in a 3-minute endpoint assay), 1.67 ± 0.03 nM PKa was generated in the absence of polyP, whereas 10-fold more PKa was generated in the presence of $polyP_{1200}$. As a function of polyP polymer length, this reaction tended to plateau at even shorter polyP polymer lengths (approximately 315 phosphates) compared with FXII activation by PKa. Platelet-size polyP (79 phosphates) supported approximately 3.8-fold more PKa generation than in the absence of polyP. Thus, as with FXII activation by PKa, these data demonstrated that platelet-size polyP can accelerate FXII activation by PKa, although the reaction was fastest with longer-chain polyP.

Influence of Zn^{2+} on contact pathway reactions

Varying the $ZnCl_2$ concentration (in the absence of HK) demonstrated that Zn^{2+} was required for polyP-mediated FXII autoactivation (Figure 2.3A). FXII autoactivation was essentially undetectable in the presence of 2 mM EDTA in the 20-minute endpoint assay, while the optimal $ZnCl_2$ concentration was approximately 3 to 7.5 μM. Since Zn^{2+} was required for this reaction, 5 μM $ZnCl_2$ was included in FXII autoactivation reactions unless otherwise noted.

FXII activation by PKa in the presence of HK was also Zn^{2+}-dependent, and only minimal amounts of FXIIa (2.74 ± 0.36 nM) were generated in the presence of EDTA in the 4-minute endpoint assay (Figure 2.3B). Optimal $ZnCl_2$ concentrations were 4 μM or higher, resulting in FXIIa generation that was approximately 20-fold higher than in the absence of $ZnCl_2$. Accordingly, 10 μM $ZnCl_2$ was included in reactions of FXII activation by PKa, unless otherwise noted.

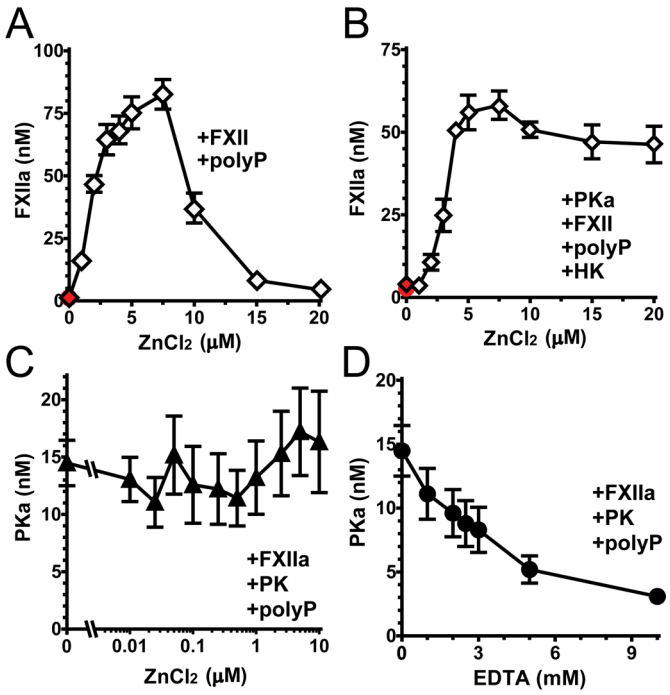

Figure 2.3 Zn^{2+} differentially influences the ability of polyP to accelerate individual reactions of the contact pathway. (A) Zn^{2+} requirement for polyP-mediated FXII autoactivation. In an endpoint assay (stopped at 20 min), 100 nM FXII without HK was incubated with 10 μM $polyP_{1200}$ in the presence of either 2 mM EDTA (●) or varying $ZnCl_2$ concentrations (◇). (B) Zn^{2+} requirement for polyP-mediated FXII activation by PKa. In an endpoint assay (stopped at 4 min), 100 nM FXII and 100 pM PKa were incubated with 100 nM HK and 10 μM $polyP_{1200}$ in the presence of either 2 mM EDTA (●) or varying $ZnCl_2$ concentrations (◇). (C) Zn^{2+} requirement for polyP-mediated PK activation by FXIIa. In an endpoint assay (stopped at 3 min), 100 nM PK and 100 pM FXIIa without HK were incubated with 10 μM $polyP_{1200}$ in divalent metal ion-depleted buffer to which varying $ZnCl_2$ concentrations were added. (D) EDTA inhibits polyP-mediated PK activation by FXIIa in a concentration-dependent manner. In an endpoint assay (stopped at 3 min), 100 nM PK and 100 pM FXIIa without HK were incubated with 10 μM $polyP_{1200}$ in the presence of varying EDTA concentrations. Data in all *panels* are mean ± S.E. ($n \geq 3$).

Activation of PK by FXIIa in the absence of HK was not modulated significantly by added $ZnCl_2$, even when we used solutions that had been pretreated with Chelex beads to deplete trace amounts of divalent metal ions (Figure 2.3C). On the other hand, inclusion of 2 mM EDTA decreased the amount of FXIIa generated by 44% compared to the absence of added $ZnCl_2$ (data not shown). To further investigate this, PK activation by FXIIa was studied in an endpoint assay in the presence of varying EDTA concentrations (Figure 2.3D). We observed that EDTA inhibited this reaction in a concentration-dependent manner over the range of 0 to 10 mM EDTA. We propose that anionic EDTA molecules may compete with polyP for interaction with PK and/or FXIIa, independent of the ability of EDTA to chelate divalent metal ions.

Influence of HK on contact pathway reactions

Although FXII is not thought to circulate bound to HK *in vivo*, we tested if HK could influence rates of polyP-mediated FXII autoactivation (Figure 2.4A). Without HK, polyP$_{1200}$ readily supported FXII autoactivation in the presence of 5 µM $ZnCl_2$. Progress curves for FXII autoactivation were sigmoidal (Supplementary figure 2.2), consistent with models of this process [56,180]. Second-order rate constants for FXII autoactivation were derived from analyses of the reaction data replotted in Figure 2.4B, then given in Figure 2.4C *versus* HK concentration. Although HK was not required for polyP-mediated FXII autoactivation, up to 100 nM HK accelerated the reaction somewhat, while higher concentrations were inhibitory.

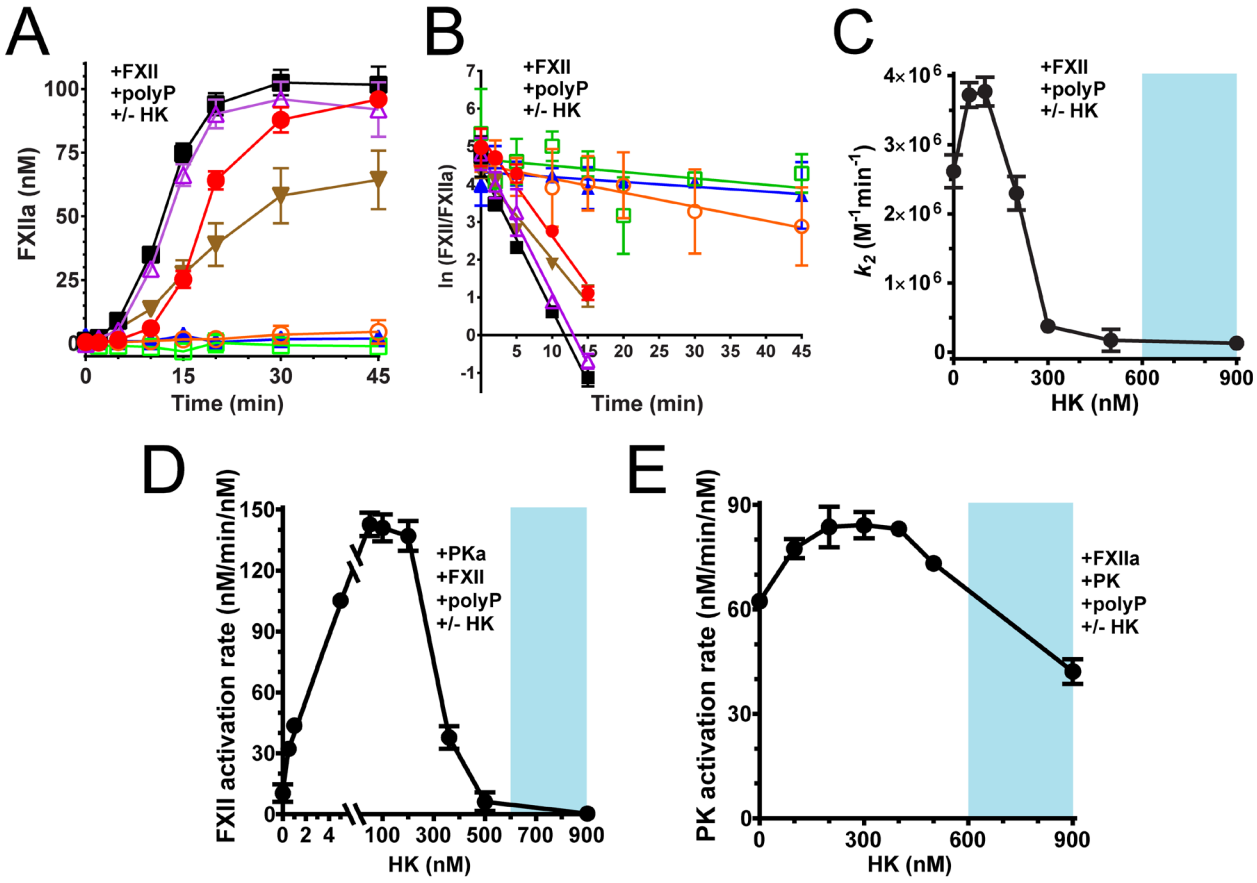

Figure 2.4 HK differentially influences the ability of polyP to accelerate individual reactions of the contact pathway. (A) Influence of HK on polyP-mediated FXII autoactivation. FXIIa levels were measured as a function of time after incubating 100 nM FXII with 10 µM polyP$_{1200}$ in the presence of 5 µM $ZnCl_2$ and 0 (●), 50 (△), 100 (■), 200 (▼), 300 (○), 500 (□), or 900 (▲) nM HK. (B, C) Calculation of second-order rate constants of polyP-mediated FXII autoactivation at various HK concentrations. Data from *panel (A)* (time course of FXII autoactivation) were replotted in *panel (B)* as ln(FXII/FXIIa) values

versus time, to which lines were fitted by linear regression. Second-order rate constants, k_2, were derived from the slopes of these lines as described in *Experimental Procedures*, and plotted in *panel (C)* as a function of HK concentration. (D) Influence of HK on polyP-mediated FXII activation by PKa. FXIIa levels were measured as a function of time after incubating 100 nM FXII and 100 pM PKa with 10 μM $polyP_{1200}$ in the presence of 10 μM $ZnCl_2$ and varying HK concentrations. Initial FXII activation rates are plotted as nM FXII activated per min divided by nM PKa used. (E) Influence of HK on polyP-mediated PK activation by FXIIa. PKa levels were measured as a function of time after incubating 100 nM PK and 100 pM FXIIa with 10 μM $polyP_{1200}$ in the presence of 10 μM $ZnCl_2$ and varying HK concentrations. Initial PK activation rates were plotted as nM PK activated per min divided by nM FXIIa used. Data in all *panels* are mean ± S.E. ($n \geq 3$).

HK substantially increased rates of polyP-mediated FXII activation by PKa (Figure 2.4D). Thus, in the absence of HK, the FXII activation rate was only 10.44 ± 4.36 nM/min/nM, while in the presence of 50-200 nM HK, this rate was accelerated approximately 13.4-fold relative to no HK. As little as 0.5 nM HK supported the reaction to a detectable level (~ 3.2-fold increase over no HK), while HK concentrations of 300 nM and higher reduced the reaction rate. Since the activation of FXII by PKa was readily accelerated by HK, 100 nM HK was generally included in other studies of this reaction.

While HK was not required for polyP-mediated PK activation by FXIIa, the reaction was stimulated by about 34% in the presence of 200 to 400 nM HK (Figure 2.4E). Higher HK concentrations were inhibitory.

PK autoactivation

Autoactivation of PK has been reported to occur in the presence of anionic substances such as dextran sulfate or sulfatides,[132] so it was of interest to examine whether polyP could mediate PK autoactivation. Initial experiments showed that incubating 100 nM PK with 100 nM HK plus 10 μM $polyP_{1200}$ resulted in time-dependent generation of readily detectable PKa (Figure 2.5A). We observed no detectable PKa in the absence of HK (data not shown), indicating that this reaction was highly HK-dependent. We noted, however, that the progress curve for PKa generation was not sigmoidal (Figure 2.5A), as would have been expected for autoactivation kinetics. We therefore considered the possibility that plasma-derived HK might be contaminated with traces of

FXII or FXIIa. If so, we may be observing PK activation by traces of FXIIa, and/or reciprocal activation of PK and contaminating FXII. To test this hypothesis, we examined the effect of including corn trypsin inhibitor (CTI) in this same experiment (Figure 2.5A). CTI inhibits FXIIa activity with minimal effect on the enzymatic activity of PKa.[181,182] Including 0.5 or 2.5 μM CTI in this reaction reduced the amount of PKa generated at 90 min by 38% or 83%, respectively.

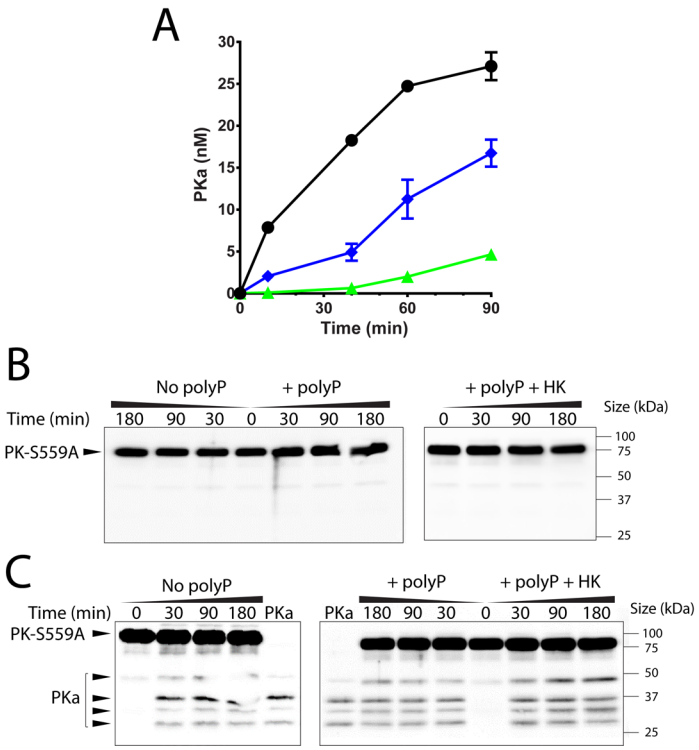

Figure 2.5 The apparent autoactivation of PK in the presence of polyP and HK appears to be due to contamination of HK with traces of FXII(a). (A) Apparent PK autoactivation was inhibited by CTI. PKa levels were measured as a function of time after incubating 100 nM PK with 100 nM HK, 10 μM polyP$_{1200}$ and 10 μM $ZnCl_2$ in presence of 0 (●), 0.5 (◆) or 2.5 (▲) μM CTI. Data are mean ± S.E. ($n \geq 2$). (B) In the presence of an inhibitory FXII antibody, activation of PK-S599A was undetectable by western blot. *Left panel*: 200 nM PK-S599A without HK was incubated with or without 70 μM polyP$_{700}$ in the presence of 10 μM $ZnCl_2$ and 50 nM anti-FXII IgG (1B2). At indicated times, samples were removed into reducing SDS sample buffer. Proteins were resolved by SDS-PAGE, followed by western blot analysis with a polyclonal antibody to human PK. *Right panel*: Parallel time courses of the same reaction conditions as in the *left panel*, but performed in the presence of 200 nM HK. In both panels, t=0 represents the reaction before addition of polyP or HK. (C) In the presence of an inhibitory FXII antibody, cleavage of PK-S599A by added PKa, in the presence or absence of polyP, was undetectable by western blot. *Left panel*: 200 nM PK-S599A and 25 nM purified PKa were incubated without polyP or HK, in the presence of 10 μM $ZnCl_2$ and 50 nM anti-FXII IgG (1B2). Samples were analyzed by western blot with the same polyclonal antibody to human PK as in *panel B*. *Right panel*: Parallel time courses of the reaction performed in the presence of 70 μM long-chain polyP700, with or without 200 nM HK. In both panels, t=0 represents the reaction without HK or polyP before addition of PKa. Purified PKa is included in both panels for comparison purposes.

In further experiments, we employed recombinant PK with the active-site serine mutated to alanine (PK-S559A). In the presence of an antibody that specifically inhibits FXIIa enzymatic

activity (preventing reciprocal PK activation in the presence of FXII), this mutant PK zymogen remained single-chain over a 3-hr period, as visualized on western blot, whether incubated in the presence or absence of polyP or HK (Figure 2.5B). Even when 25 nM PKa was co-incubated with 200 nM PK-S559A (in the presence or absence of polyP or HK), no PK-S559A cleavage was observed over a 3-hr time course (Figure 2.5C). These findings argue against polyP supporting detectable PK activation by PKa, and that contamination with traces of FXII(a) was responsible for the apparent PK autoactivation in the presence of polyP plus HK.

2.4 Discussion

We reported previously that polyP is a novel trigger of plasma clotting via the contact pathway,[183] that polyP is orders of magnitude more potent at triggering clotting than other proposed pathophysiologic contact activators such as nucleic acids,[118] and that the longer the polyP, the greater its ability to activate clotting via the contact pathway.[163] As summarized in Table 2.1 , we now report how the individual enzyme reactions responsible for initiating the contact pathway are influenced by polyP, Zn^{2+} and HK. We found that FXII autoactivation, FXII activation by PKa, and PK activation by FXIIa were all profoundly accelerated by polyP, in a manner that was dependent on polyP polymer length. In contrast, we found no evidence of detectable PK autoactivation in the presence of polyP, with the apparent autoactivation reaction most likely due to trace contamination of FXII(a) in the HK preparation.

Efficient FXII autoactivation required very long polyP polymers, with a dependence on polyP length that was highly reminiscent of the polyP length-dependence for triggering the clotting of plasma via the contact pathway.[163] In contrast, we found that the two reciprocal enzyme activation reactions (FXII activation by PKa, and PK activation by FXIIa) exhibited patterns of polyP length dependence that differed from that of FXII autoactivation. In particular, platelet-size

polyP accelerated both FXII activation by PKa, and PK activation by FXIIa, but had little effect on FXII autoactivation. Our findings suggest that FXII autoactivation is the step in the initiation of the contact pathway that is critically dependent on polyP polymer length, and that it is the inability to readily promote FXII autoactivation that underlies the low plasma clotting activity of platelet-size polyP.[163]

Table 2.1 The influence of polyP size, HK and $ZnCl_2$ on the contact pathway reactions.

Reaction Number on Figure 2.1	Enzyme	Substrate	Optimal Condition		
			PolyP length (phosphates)	**HK (nM)**	**$ZnCl_2$ (μM)**
1	FXIIa	FXII	1200	Not required	3-7.5
2	PKa	FXII	400-1200	50-200	4-20
3	PKa	PK	No reaction	No reaction	No reaction
4	FXIIa	PK	300-1200	Not required	Not required

Although a recent study reported that platelet polyP can potently activate the contact pathway,[168] that study employed silica-based methods for isolating polyP, which we have now shown can result in contamination with highly procoagulant silica particles.[118,174] Furthermore, decades of studies have shown that activated platelets only very weakly activate the contact pathway of clotting.[184]

It has long been assumed that any enzymatic activity of preparations of zymogen FXII derived from plasma were due to contamination of these preparations with traces of FXIIa. However, when Ivanov *et al*. used recombinant FXII proteins that were locked in an uncleavable conformation, they reported weak proteolytic activity of single-chain FXII, which was enhanced by the presence of polyP.[121] In the present study, we observed polyP-mediated conversion of FXII to FXIIa, as quantified by quenching the reactions to displace bound polyP. The polyP-mediated

autoactivation we observed could be initiated by the weak proteolytic activity of single-chain FXII bound to polyP, traces of FXIIa in the FXII preparation, or both.

One may wonder why maximal rates of FXII autoactivation required such long polyP polymers. The molecular mass of FXII(a) is about 80 kDa, with an estimated diameter of 5-6 nm, assuming a spherical shape.[185] A polyP polymer of 1200 phosphates would have a fully extended length of about 240 nm,[186] which is some fortyfold longer than the diameter of FXII. A possible explanation is that efficient FXII autoactivation may require assembly of many FXII and FXIIa molecules together on the same polyP scaffold. Another possibility is that Zn^{2+} binding to polyP alters its structure such that it does not exist in a fully extended conformation. A parallel finding from a previous study is that hairpin-forming RNA oligomers are more procoagulant than linear RNA, and in particular, structure-forming RNA aptamers were much better at mediating PK autoactivation.[187] There are at least 4 putative Zn^{2+} binding sites on the heavy chain of FXII,[48] so interactions between Zn^{2+}, polyP and FXII(a) could be quite complex.

Zn^{2+} enhances the binding affinities and proteolytic activities of many of the proteins in the contact pathway.[56,74,75] Zn^{2+} induces conformational changes in HK,[76] and a binding site for Zn^{2+} has been described in the D5 domain of HK, which also contains the binding site for anionic polymers.[77,78] As summarized in Table 2.1, we found that micromolar concentrations of $ZnCl_2$ greatly enhanced both of the enzymatic reactions in which FXII was the substrate (i.e., polyP-mediated FXII autoactivation and activation of FXII by PKa), but $ZnCl_2$ had little effect on the enzymatic reaction in which PK was the substrate (i.e., polyP-mediated activation of PK by FXIIa). Interestingly, although we found no requirement for $ZnCl_2$ in supporting polyP-mediated PK activation by FXIIa, this reaction was inhibited by EDTA in a concentration-dependent manner (Fig. 3D). EDTA chelates divalent metal ions, but it also contains 4 anionic carboxylate groups.

We suspect that millimolar concentrations of anionic EDTA might compete with anionic polyP for binding to PK, FXIIa or both. Indeed, higher $polyP_{1200}$ concentrations progressively reduced the inhibitory effect of EDTA (Supplementary figure 2.5).

In the present study, HK played different roles in each reaction in the contact pathway (Table 2.1). In fact, the only reaction strongly requiring HK was the one in which PKa served as the enzyme (i.e., polyP-mediated activation of FXII by PKa). This is consistent with our previous finding that at physiologic salt concentrations, PKa did not bind appreciably to polyP unless HK was present [117]. HK was not required in reactions in which FXIIa was the active enzyme (i.e., polyP-mediated FXII autoactivation and FXIIa activation of PK), although HK did modulate these reactions to some degree. In all three reactions investigated in this study, higher HK concentrations ($\geq$ 500 nM) were inhibitory. HK circulates at a plasma concentration of about 650-900 nM [188], which falls in the range that inhibited polyP-driven contact pathway reactions. However, one should note that in plasma, much of the HK circulates bound to FXI and PK (and possibly other partners), so the free HK concentration is not known with certainty. In this study, the concentrations of HK and $ZnCl_2$ were chosen to optimize the biochemical assays and not necessarily mimic physiologic concentrations. The negative effect of HK on FXII autoactivation at high concentrations might be particularly surprising, since binding interactions between HK and FXII(a) have not been shown. However, one could rationalize the effect of HK on FXII autoactivation by postulating that HK competes with FXII(a) for binding to polyP, so that high HK concentrations would alter the effective concentration of polyP available to interact with FXII. This might also explain the mildly stimulatory and inhibitory effects of HK on polyP-mediated PK activation by FXIIa, depending on HK concentration. Exploring this further would require systematically varying both the polyP and HK concentrations. Reaction rates reported here are

maximal rates under fixed conditions and rates in vivo may vary. In particular, the apparent ability of high HK concentrations to inhibit reactions such as FXII autoactivation is likely to be reversed at higher polyP concentrations, although it was not practical to explore all possible combinations of reactant concentrations in the present study.

In summary, this study shows that three of the four possible enzyme activation reactions involved in triggering the contact pathway of clotting were greatly accelerated by polyP, in a manner that depended strongly on polyP polymer length. Of these three polyP-mediated reactions, Zn^{2+} was only required when FXII was the substrate, while HK was only required when PKa was the enzyme. PolyP polymer lengths are known to vary substantially depending on the biological source, with shorter polyP chains (60 to 100 phosphates long) secreted from activated platelets, mast cells and basophils.[166,189] On the other hand, microbial polyP polymers can range in length up to thousands of phosphates,[172] and mammalian brain is also reported to contain long-chain polyP (approximately 800 phosphates long).[154] Furthermore, platelets secrete Zn^{2+}, such that the local concentration of this metal ion in the vicinity of platelet aggregates could greatly exceed that of normal plasma.[75,190]

Our findings therefore identify conditions under which these three polyP-mediated reactions (FXII autoactivation, FXII activation by PKa, and PK activation by FXIIa) may be differentially regulated via secretion of shorter-chain polyP and Zn^{2+}. Thus, platelets, mast cells and basophils may be able to orchestrate subsets of the contact pathway reactions that could lead, for example, to bradykinin generation without activation of the final common pathway of the clotting cascade. Mechanisms for activating subsets of these enzyme reactions without necessarily triggering plasma clotting could have implications for inflammatory reactions and diseases such as HAE, which are driven by highly dysregulated bradykinin formation via the contact pathway,

but without thrombosis.[86,170,191] Other precedents for this exist. For example, previous studies have reported that endothelial cell prolyl carboxypeptidase can activate PK independent of FXIIa.[192,193] On the other hand, elaboration of long-chain polyP from microbes may be capable of activating the contact pathway to participate in both inflammatory reactions and the full plasma clotting system as part of the innate immune response.

2.5 Supplementary figures

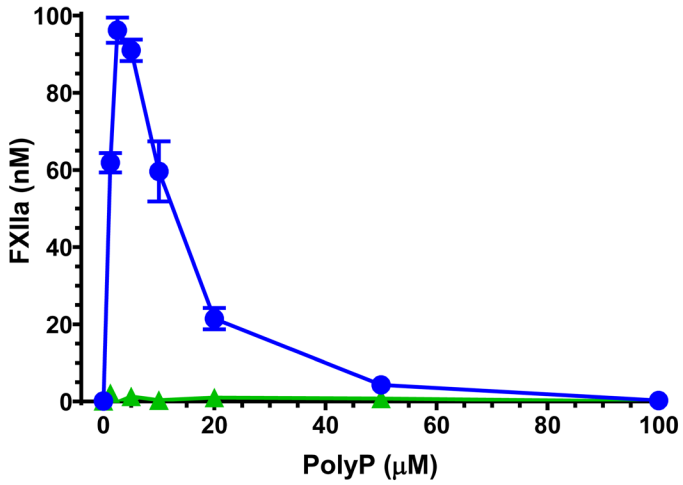

Supplementary figure 2.1 The dose dependence of polyP to accelerate FXII autoactivation. In an endpoint assay (stopped at 20 min), 100 nM FXII without HK was incubated with varying concentrations of polyP$_{1200}$ (●) or polyP$_{79}$ (▲) in the presence of 5 μM $ZnCl_2$. Timed aliquots (10 μL) were removed and quenched in 70 μl ice-cold Quench Buffer I Data in all *panels* are mean ± S.E. ($n \geq 3$).

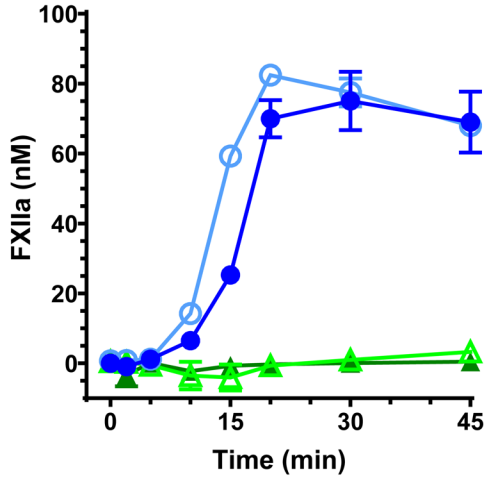

Supplementary figure 2.2 The progress curve of polyP-mediated FXII autoactivation. FXIIa levels were measured as a function of time after incubating 100 nM FXII without HK but with 2.5 (○), 10 (●) μM polyP$_{1200}$, 10 (△) or 100 (▲) μM polyP$_{79}$ in the presence of 5 μM $ZnCl_2$. Data in all *panels* are mean ± S.E. ($n \geq 3$).

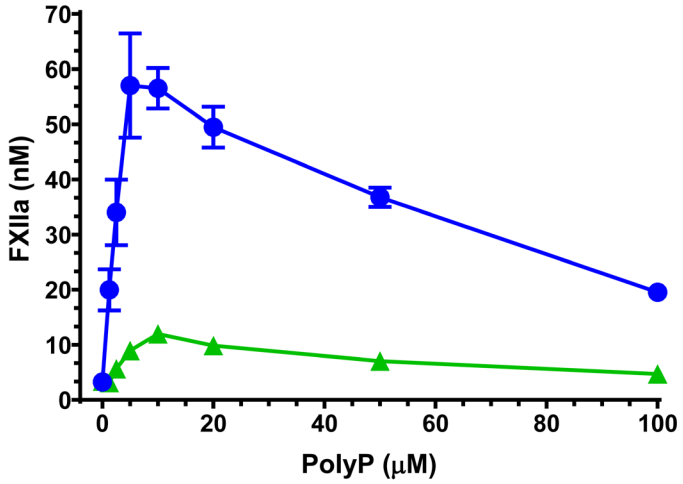

Supplementary figure 2.3 The ability of long-chain and platelet-size polyP to accelerate FXII activation by PKa depends on polyP concentration. In an endpoint assay (stopped at 4 min), 100 nM FXII and 100 pM PKa were incubated with 100 nM HK and with varying concentrations of $polyP_{1200}$ (●) or $polyP_{79}$ (▲) in the presence of 10 μM $ZnCl_2$. Data in all *panels* are mean ± S.E. ($n \geq 3$).

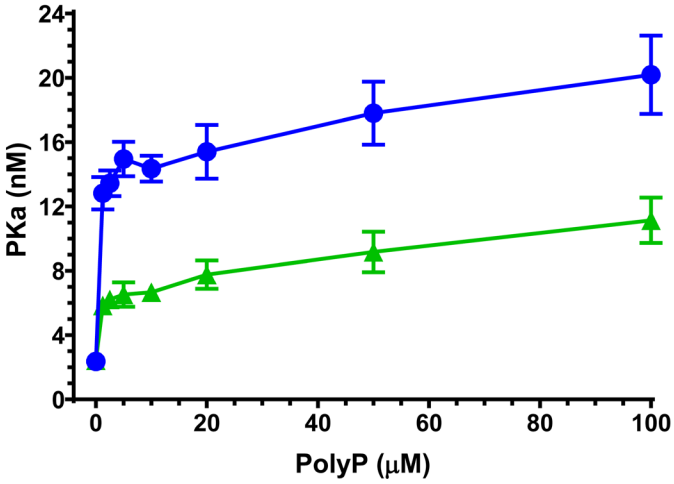

Supplementary figure 2.4 The ability of long-chain and platelet-size polyP to accelerate FXII activation by PKa depends on polyP concentration. In an endpoint assay (stopped at 3 min), 100 nM PK and 100 pM FXIIa without HK were incubated with varying concentrations of $polyP_{1200}$ (●) or $polyP_{79}$ (▲) in the presence of 10 μM $ZnCl_2$. Data in all *panels* are mean ± S.E. ($n \geq 3$).

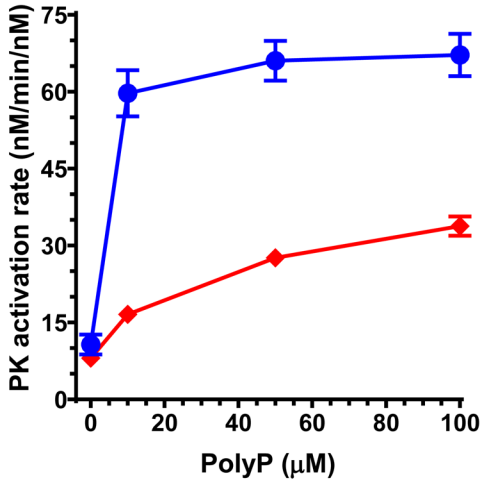

Supplementary figure 2.5 Influence of EDTA on polyP-mediated PK activation by FXIIa. PKa levels were measured as a function of time after incubating 100 nM PK and 100 pM FXIIa and varying concentrations of $polyP_{1200}$ without HK in the presence of 0 (●) or 5 (◆) mM EDTA. Initial PK activation rates were plotted as nM PK activated per min divided by nM FXIIa used. Data in all *panels* are mean ± S.E. ($n \geq 3$).

Chapter 3 Factor XI Activation by Factor XIIa is Modulated by Polyphosphate and Zn^{2+}

3.1 Introduction

FXII is an 80 kDa protease zymogen synthesized in the liver that circulates at a concentration of 375 nM.[194] It is a key component in the contact pathway of blood clotting, which includes the circulating serine protease zymogens, FXII and PK, as well as a non-enzymatic cofactor for PKa, HK.[86,170] The contact pathway can be triggered when plasma contacts certain (typically, anionic) polymers or surfaces,[131] thereby inducing a conformational change in FXII that leads to the generation of a small amount of FXIIa via autoactivation.[57] FXIIa then cleaves PK to generate initial amounts of PKa.[60] FXII(a) and PK(a) undergo reciprocal activation to generate a burst of active enzymes. Once significant FXIIa accumulates, it cleaves the downstream substrate, FXI, leading ultimately to thrombin generation and fibrin formation.[135] The contact pathway is a crosstalk between coagulation and inflammation and is also known as the plasma kallikrein-kinin system.[116,139,170] In particular, PKa can proteolyze HK to release the vasoactive peptide, bradykinin, an important inflammation mediator.[140]

For a long time, FXII was not thought to play an essential role in blood clotting, since its deficiency is not associated with bleeding.[39-41] More recently, animal studies and clinical data indicate that the contact pathway is dispensable for hemostasis, as individual deficient in either FXII or PK do not show a bleeding tendency,[116,139,170] implying that FXII-mediated activation of FXI is not required in trauma-induced blood clotting. However, recent studies have shown in experimental animal models that FXII deficiency is protective in both arterial[42-44] and venous[45]

thrombosis models, suggesting that the activation of FXI by FXIIa could be a potential target for thromboprophylaxis. Although the proteolytic cleavage of FXI by FXIIa has been demonstrated *in vitro*, it is unclear how fast this reaction happens with the presence of its physiological activators and whether it plays a role in initiating clotting *in vivo*.

While several artificial surfaces and polymers may activate the contact pathway *in vitro*, the relevant (patho)physiologic activators for this system *in vivo* have only recently been suggested.[86] PolyP is a highly negatively charged polymer of inorganic phosphates that varies in length, depending on biological source.[149,154] PolyP released from platelets has a fairly narrow size range of approximately 60-100 phosphates long,[166] while unicellular organisms contain heterogeneous polyP that can range up to thousands of phosphates in length.[172] Our previous work demonstrated that polyP acts at multiple stages of the clotting cascade, with pro-hemostatic, pro-thrombotic and pro-inflammatory effects that are highly dependent on polyP chain length.[149,163] Long-chain polyphosphate (polyP), in particular, has emerged as an especially potent trigger of contact pathway activation[163] and the activation of FXI by thrombin.[195] In this study, we aimed to investigate the ability of various concentrations and sizes of polyP, together with two important cofactors, HK and Zn^{2+}, to modulate the activation of FXI by FXIIa. We also aimed to compare the ability of FXIIa on FXI activation with two other proteases, human α-thrombin and trypsin. We now report that FXI activation by FXIIa was accelerated by polyP in a size-dependent manner. Zn^{2+} was also an important modulator of this reaction. However, FXIIa was not a very efficient enzyme for FXI activation, even with the presence of optimal dose of polyP, which implies that the primary role of FXIIa may not be triggering blood clotting.

3.2 Materials and methods

Materials

Polybrene (hexadimethrine bromide) and polyethylene glycol were from Sigma (St. Louis, MO). Human FXI, FXIa, α-FXIIa, and single-chain HK were from Enzyme Research Laboratories (South Bend, IN). Human α-thrombin and corn trypsin inhibitor were from Haematologic Technologies (Essex Junction, VT). Trypsin (treated with N-tosyl-L-phenylalanine chloromethyl ketone) was from Worthington Biochemical Corporation (Lakewood, NJ). The chromogenic substrate for FXIa, Pyr-Pro-Arg-pNA (L-2145), was from Bachem (Bubendorf, Switzerland). Ultra-Low Attachment microplates were from Corning Inc (Tewksbury, MA).

A heterogeneous, long-chain polyP preparation ($polyP_{1200}$) was prepared as described.[169] It ranged in polymer length from about 595 to 1935 phosphates, with a modal length of 1200 phosphates. Narrowly size-fractionated polyP preparations were produced from chemically synthesized polyP by preparative PAGE as described,[163,175] and are referred to by their polymer lengths, which were: 28, 42, 68, 79, 110, 143, 211, 315 and 415 phosphates. PolyP concentrations were quantified by measuring inorganic phosphate after complete hydrolysis, as described.[175] Throughout this study, polyP concentrations are given in terms of molar concentrations of phosphate monomer.

FXI activation assays

Reactions were performed at 37°C in ultra-low attachment microplate wells in HBSP solution (20 mM *N*-2-hydroxyethylpiperazine-*N'*-2-ethanesulfonic acid (HEPES)-NaOH (pH 7.4), 100 mM NaCl, and 1% w/v polyethylene glycol, 8000 MW). Experiments evaluating the polyP dose dependence included 1 nM FXIIa, 100 nM FXI, and 10 μM $ZnCl_2$ in the presence of 0 to100 μM $polyP_{1200}$. Experiments evaluating the polyP size dependence included 1 nM FXIIa, 100 nM

FXI, and 10 μM $ZnCl_2$ in the absence or presence of 10 μM narrowly sized-fractionated polyP or $polyP_{1200}$. Experiments evaluating the impact of $ZnCl_2$ included 1 nM FXIIa, 100 nM FXI, 10 μM $polyP_{1200}$ and either 2 mM EDTA or 0 to 20 μM $ZnCl_2$. Experiments evaluating the impact of HK included 1 nM FXIIa, 100 nM FXI,10 μM polyP ($polyP_{79}$, $polyP_{211}$ or $polyP_{1200}$), 10 μM $ZnCl_2$, and 0 to 200 nM HK. Timed aliquots (10 μL) were removed and quenched in 70 μL ice-cold Quench Buffer I (20 mM HEPES-NaOH (pH 7.4), 5 mM EDTA, and 1 M NaCl).

Experiments comparing the ability of FXIIa, trypsin and α-thrombin to activate FXI included 1 nM activator (FXIIa, trypsin or α-thrombin), 100 nM FXI, 10 μM $ZnCl_2$, 0 or 10 μM $polyP_{1200}$, and 0 or 100 nM HK. Timed aliquots (10 μL) were removed and quenched in 70 μL ice-cold Quench Buffer II (20 mM HEPES-NaOH (pH 7.4), 5 mM EDTA, 500 nM corn trypsin inhibitor, and 15 μg/mL polybrene). Following quenching, FXIa enzymatic activities were evaluated by measuring A_{405} in a microplate reader at room temperature after adding Pyr-Pro-Arg-pNA substrate, and converting the initial rates to FXIa concentrations by reference to a standard curve.

3.3 Results

Long-chain polyP is a potent trigger of plasma clotting via the contact pathway,[183] so we wanted to understand how polyP modulates the individual reactions of this pathway. In our recent study in Chapter 2,[169] we reported how polyP, together with Zn^{2+} and HK, accelerates the three reactions in the triggering phase of the contact pathway: FXII autoactivation, activation of PK by FXIIa, and activation of FXII by PKa. In the classical view of the clotting cascade, the connection between the contact pathway and the final common pathway of blood clotting is through FXI activation by FXIIa. Accordingly, in the present study, we now examine how polyP, Zn^{2+} and HK modulate FXI activation by FXIIa.

PolyP concentration-requirement for FXI activation by FXIIa

We first examined whether long-chain polyP modulated FXI activation by FXIIa. We found that although polyP was not absolutely required for this reaction, long-chain polyP accelerated FXI activation by FXIIa in a manner that was highly dependent on $polyP_{1200}$ concentration (Figure 3.1 & Supplementary figure 3.1). Under the experimental conditions tested (an endpoint assay in which 100 nM FXI was activated by 1 nM FXIIa in the presence of 10 μM $ZnCl_2$), the reaction was optimal at 10 to 20 μM $polyP_{1200}$, which resulted in approximately tenfold more FXIa product formed than in the absence of polyP. We therefore chose to employ 10 μM polyP in the rest of our experiments, unless otherwise noted.

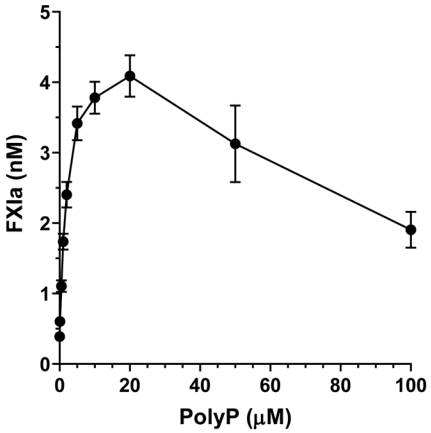

Figure 3.1 The dose dependence of polyP to accelerate FXI activation by FXIIa. In an endpoint assay (stopped at 10 min), 100 nM FXI and 1 nM FXIIa without HK were incubated with varying concentrations of $polyP_{1200}$ (●) in the presence of 10 μM $ZnCl_2$. Timed aliquots (10 μL) were removed and quenched in 70 μl ice-cold Quench Buffer I. Data are mean ± S.E. ($n \geq 3$).

PolyP length-requirement for FXI activation by FXIIa

Given that the polymer size of polyP varies considerably depending on biological source,[149] we were interested to see how polyP polymer length affects its ability to support FXI activation by FXIIa. We therefore quantified initial rates of FXIIa-dependent FXI activation in the presence of 10 μM polyP of varying sizes, all in the presence of 10 μM $ZnCl_2$. We found that rates of FXI

activation increased with polyP polymer length (Figure 3.2 & Supplementary figure 3.2). PolyP polymers of the size range secreted by platelets (~60 to 100 phosphates long) enhanced the rate of FXIa generation approximately six-fold compared to no polyP, while long-chain polyP ($polyP_{1200}$) enhanced this rate approximately 14-fold relative to no polyP. These data show that even platelet-size polyP could accelerate FXI activation by FXIIa, although the reaction was fastest with long-chain polyP.

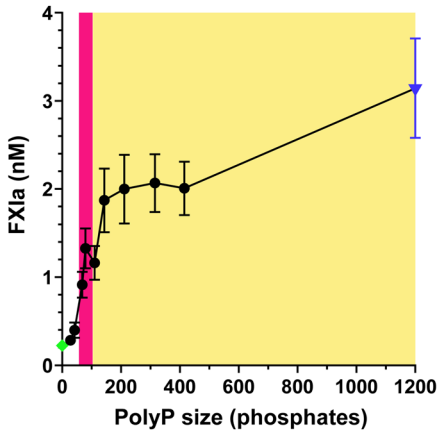

Figure 3.2 The ability of polyP to accelerate FXI activation by FXIIa depends on its size. In an endpoint assay (stopped at 10 min), 100 nM FXI was incubated with 1 nM FXIIa and 10 µM $ZnCl_2$ without polyP (◆) or with 10 µM polyP (●,▼). HK was not included in this experiment. *Data points* for size-fractionated polyP preparations (●) are plotted on the *x*-axis according to their polymer lengths, while *data point* for heterogeneous $polyP_{1200}$ (▼) is plotted on the *x*-axis at the modal length of this preparation (1200 phosphate units). The pink rectangle represents the approximate length range of platelet polyP (60-100 phosphates), and the yellow rectangle indicates the length range of microbial polyP. Data are mean ± S.E. ($n \geq 3$).

Influence of Zn^{2+} on FXI activation by FXIIa

Zn^{2+} is well known to modulate the contact pathway, and in our previous study (Chapter 2) on the effect of polyP on the individual reactions in the triggering phase of the contact pathway we reported that Zn^{2+} was required in reactions in which FXII was the substrate.[169] In the present study, we found that Zn^{2+} was not absolutely required to support FXI activation by FXIIa in the presence of polyP, and in fact we found measurable rates of FXI activation even in the presence of EDTA (Figure 3.3 & Supplementary figure 3.3). Nonetheless, micromolar concentrations of

Zn^{2+} substantially accelerated FXI activation by FXIIa, with an optimal Zn^{2+} concentration of 10 μM. This optimal Zn^{2+} concentration resulted in a 15.6-fold higher rate of FXI activation by FXIIa (in the presence of 10 μM $polyP_{1200}$) compared to the rate in the absence of $ZnCl_2$. Since Zn^{2+} greatly accelerated FXI activation by FXIIa, 10 μM $ZnCl_2$ was included in all FXI activation reactions unless otherwise noted.

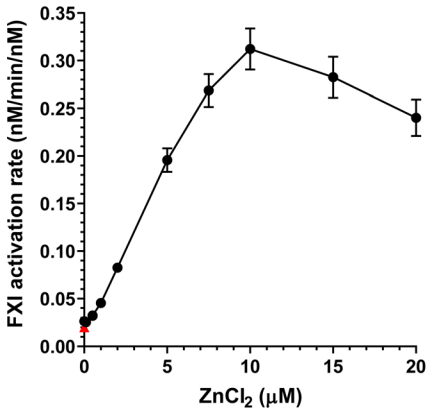

Figure 3.3 Zn^{2+} influences the ability of polyP to accelerate FXI activation by FXIIa. FXIa levels were measured as a function of time after incubating 100 nM FXI and 1 nM FXIIa with 10 μM $polyP_{1200}$ in the presence of 2 mM EDTA (▲) or various concentrations of $ZnCl_2$ (●). Initial FXI activation rates were plotted as nM FXI activated per min divided by nM FXIIa used. Data are mean ± S.E. ($n \geq 3$).

Influence of HK on FXI activation by FXIIa

Because FXI largely circulates bound to HK *in vivo*, we tested if HK could influence the rate of polyP-mediated FXI activation by FXIIa using three different sizes of polyP (Figure 3.4 & Supplementary figure 3.4). Although HK was not required for this reaction, it moderately stimulated FXI activation by FXIIa in the presence of 10 μM $ZnCl_2$. Thus, with the inclusion of 100 nM HK, the amount of FXIa generated in 10 minutes was increased by about 150%, 72.5% or 18% in the presence of $polyP_{79}$, $polyP_{211}$ or $polyP_{1200}$, respectively (Figure 3.4).

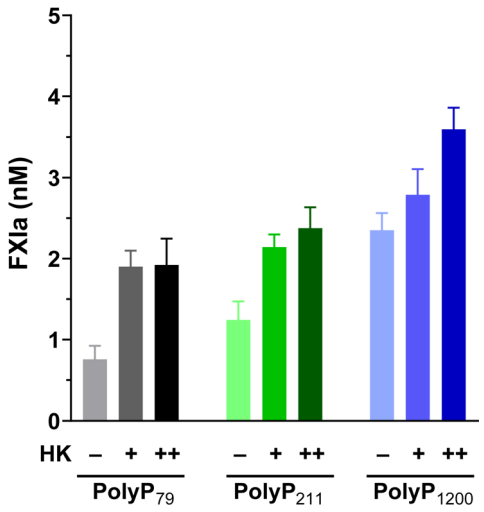

Figure 3.4 HK influences the ability of polyP to accelerate FXI activation by FXIIa. In the presence of 10 μM $ZnCl_2$, 100 nM FXI and 1 nM FXIIa were incubated with 10 μM $polyP_{79}$, $polyP_{211}$, or $polyP_{1200}$ without HK (left) or with 100 nM (middle) or 200 nM HK (right). Timed aliquots (10 μL) were removed and quenched in 70 μl ice-cold Quench Buffer I at 10 min. Data are mean ± S.E. ($n \geq 3$).

Ability of FXIIa versus α-thrombin and trypsin to activate FXI

In our previous study of the ability of polyP to support the individual reactions in the triggering phase of the contact pathway, we used comparable substrate concentrations (100 nM) as in the present study, and similar concentrations of polyP and Zn^{2+}. However, we observed far higher rates of enzyme activation than we observed in this study of the activation of FXI by FXIIa.[169] Thus, in our previous study, the optimal rate of polyP-mediated FXII activation by PKa was approximately 140 nM/min/nM. Similarly, the optimal rate of polyP-mediated PK activation by FXIIa in our previous study was approximately 80 nM/min/nM. In sharp contrast, even under optimal conditions, the fastest rate of FXI activation by FXIIa we observed in this study was about 0.3 nM/min/nM (Figures 3.2 & 3.3). Strikingly, this rate is hundreds of times slower than the rates of the reciprocal activation reactions involving FXII and PK. The relatively weak ability of FXII to activate FXI may help explain why it is necessary, in a typical aPTT clotting test, to preincubate citrated plasma with the aPTT reagent for 2 or 3 minutes before recalcifying. Presumably, this

relatively long preincubation time is necessary to generate enough FXIIa so that the FXIIa-mediated FXI activation reaction can still yield measurable clotting times.

These results made us consider how FXIIa compared to other potential activators of FXI. Accordingly, we performed a side-by-side comparison between the ability of 1 nM FXIIa, α-thrombin and trypsin to activate 100 nM FXI in a 10-minute-long endpoint assay, with or without polyP or Zn^{2+} (Figure 3.5 & Supplementary figure 3.5). Without polyP, thrombin resulted in no detectable FXIa generation while trypsin resulted in 2.15 ± 0.102 nM FXIa and FXIIa resulted in 0.13 ± 0.01 nM FXIa. Inclusion of 10 μM $polyP_{1200}$ resulted in readily measurable FXIa generation by thrombin, consistent with our previous studies showing that polyP accelerates this reaction some 3000-fold.[195,196]

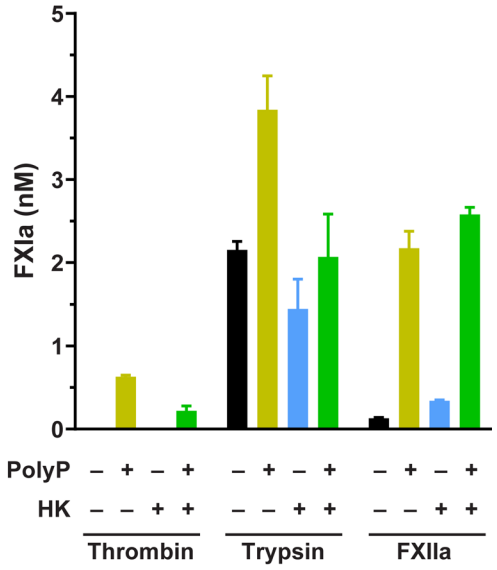

Figure 3.5 The ability of polyP to accelerate FXI activation by various proteases. In the presence of 10 μM $ZnCl_2$, 100 nM FXI and 1 nM thrombin, trypsin, or FXIIa were incubated with no polyP or HK (black), 10 μM $polyP_{1200}$ (yellow), 100 nM HK (blue) or with both polyP and HK (green). Timed aliquots (10 μL) were removed and quenched in 70 μl ice-cold Quench Buffer II at 10 min. Data are mean ± S.E. ($n \geq 3$).

3.4 Discussion

We reported previously that polyP is an important modulator of plasma clotting via the contact pathway in a size dependent manner[183] and it is much more potent at triggering clotting

than other pathophysiologic activators such as nucleic acids.[118] In this study, we report that FXI activation by FXIIa, the reaction linking the contact pathway and blood clotting, is influenced greatly by polyP, Zn^{2+} and moderately by HK. Platelet-size polyP can trigger the reaction although long-chain polyP is more potent. $ZnCl_2$ greatly accelerated this reaction by as much as 15-fold. We also found that compared with two other proteases, trypsin and α-thrombin, FXIIa did not have an overwhelming advantage in activating FXI, even at its optimal reaction condition.

In the reaction where FXI, FXIIa and polyP were incubated together, there were in fact four different reactions going on: FXI autoactivation, FXI activation by FXIIa, FXIIa autolysis and FXIa autolysis. Demonstrated in our previous study, polyP accelerates all four reactions in a size and dose-dependent manner.[117,195] Due to technical reasons in a microplate-based assay setting, it was inevitable to have FXI autoactivation, FXIIa and FXIa autolysis going on while FXIIa is activating FXI. Because of the complicated nature of these serine proteases, we did not report second-order rate constants for this reaction. A more quantitative measurement may be achieved by generating an inactive mutant version of FXI with the active site serine being to alanine. However, this should not prevent the potential FXIIa autolysis while the reaction is going on. We believe that this could explain why some of the reaction progress curves were in convex shape while some were in linear shape (Supplementary figure 3.1), as with lower concentration of polyP, FXIa autolysis might be dominant and mask out FXI activation.

The same effect on reaction progress curves has also been seen with the inclusion of HK (Supplementary figures 3.4 & 3.5). HK moderately enhanced the activation of FXI but also seemingly enhanced FXIa autolysis. This is probably due to the "template effect" of polyP. HK contains the binding site for anionic polymers such as polyP on its light chain[77,197], which implies

that the presence of HK will change the effective polyP concentration to bind with FXI and FXIIa in the solution.

Zn^{2+} enhances the binding affinities and proteolytic activities of many of the proteins in the contact pathway.[56,74,75] Although there are at least four putative Zn^{2+} binding sites on FXII(a),[48] our previous study showed that $ZnCl_2$ had little effect on the activation of PK by FXIIa.[169] The structure of FXI and PK are similar, so we did not expect the activation of FXI by FXIIa to be Zn^{2+} dependent. Intriguingly, $ZnCl_2$ greatly enhanced the reaction rate of FXI activation by FXIIa. This is probably due to the complicated interaction between FXI, polyP, HK and Zn^{2+} as HK is required for optimal FXI binding to activated platelets in the presence of Zn^{2+}.[68] The interaction with Zn^{2+} induces conformational changes in HK,[76] and the D5 domain of HK also contains a putative binding site for Zn^{2+}.[77,78]

3.5 Supplementary figures

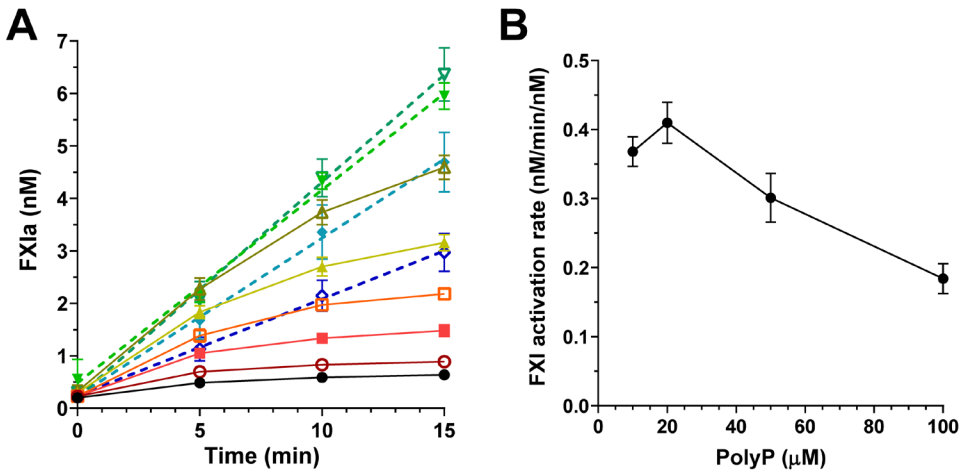

Supplementary figure 3.1Dose dependence of polyP to accelerate FXI activation by FXIIa. (A) FXIa levels were measured as a function of time after incubating 100 nM FXI and 1 nM FXIIa with 0 (●), 0.1 (○), 0.5 (■), 1 (□), 2 (▲), 5 (△), 10 (▼), 20 (▽), 50 (◆) or 100 (◇) μM polyP$_{1200}$ in the presence of 10 μM $ZnCl_2$ without HK. Data points were either connected (solid lines) or fitted by linear regression (dashed lines). (B) For those progress curves fitted with linear regression, the initial FXI activation rates were plotted as nM FXI activated per minute divided by nM FXIIa used. Data are mean ± S.E. ($n \geq 3$).

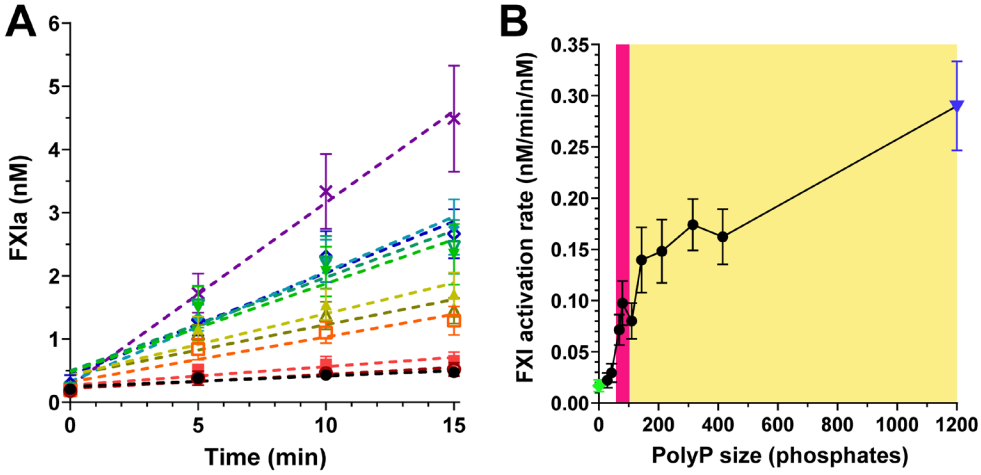

Supplementary figure 3.2 The size dependence of polyP to accelerate FXI activation by FXIIa. (A) FXIa levels were measured as a function of time after incubating 100 nM FXI and 1 nM FXIIa without polyP (●) or with 10 μM polyP$_{28}$ (○), polyP$_{42}$ (■), polyP$_{68}$ (□), polyP$_{79}$ (▲), polyP$_{110}$ (△), polyP$_{143}$ (▼), polyP$_{211}$ (▽), polyP$_{315}$ (◆), polyP$_{415}$ (◇) or polyP$_{1200}$ (×) in the presence of 10 μM $ZnCl_2$ without HK. Data points were fitted by linear regression (dashed lines). (B) Initial FXI activation rates were plotted as nM FXI activated per minute divided by nM FXIIa used. *Data points* for no polyP (◆) or size-fractionated polyP preparations (●) were plotted on the *x*-axis according to their polymer lengths, while *data point* for heterogeneous polyP$_{1200}$ (▼) was plotted on the *x*-axis at the modal length of this preparation (1200 phosphate units). The pink rectangle represents the approximate length range of platelet polyP (60-100 phosphates), and the yellow rectangle indicates the length range of microbial polyP. Data are mean ± S.E. ($n \geq 3$).

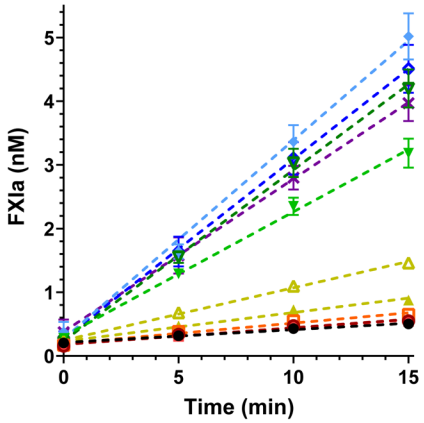

Supplementary figure 3.3 Zn^{2+} differentially influences the ability of polyP to accelerate FXI activation by FXIIa. FXIa levels were measured as a function of time after incubating 100 nM FXI and 1 nM FXIIa with 10 μM $polyP_{1200}$ in the presence of 2 mM EDTA (●) or 0 (○), 0.1 (■), 0.5 (□), 1 (▲), 2 (△), 5 (▼), 7.5 (▽), 10 (◆), 15 (◇), 20 (×) μM $ZnCl_2$. Data points were fitted by linear regression (dashed lines). Data are mean ± S.E. ($n \geq 3$).

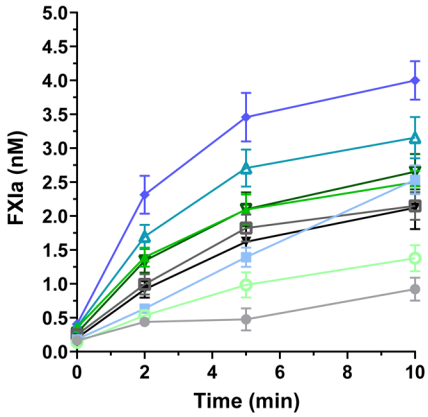

Supplementary figure 3.4 HK moderately influences the ability of polyP to accelerate FXI activation by FXIIa. FXIa levels were measured as a function of time after incubating 100 nM FXI and 1 nM FXIIa with 10 μM $polyP_{79}$ (supplemented with 0 (●), 100 (□), or 200 (▼) nM HK), $polyP_{211}$ (supplemented with 0 (○), 100 (▲), or 200 (▽) nM HK), or $polyP_{1200}$ (supplemented with 0 (■), 100 (△), or 200 (◆) nM HK) in the presence of 10 μM $ZnCl_2$. Data points were connected to show the progress curves. Data are mean ± S.E. ($n \geq 3$).

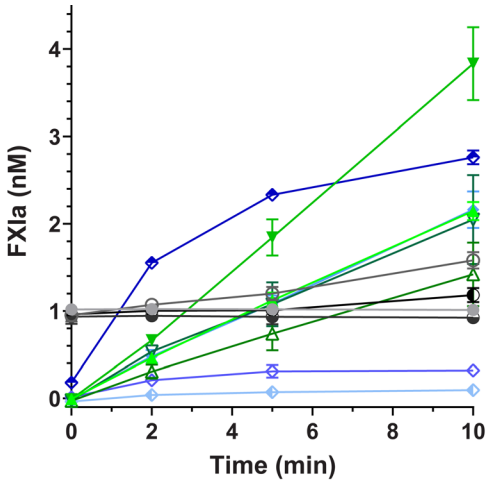

Supplementary figure 3.5 The ability of polyP to support FXI activation by various proteases. FXIa levels were measured as a function of time after incubating 100 nM FXI and 1 nM thrombin (with no polyP or HK (●), 10 μM polyP$_{1200}$ (○), 100 nM HK (◒) or both (◐)), trypsin (with no polyP or HK (▲), 10 μM polyP$_{1200}$ (▼), 100 nM HK (△) or both (▽)), or FXIIa (with no polyP or HK (◈), 10 μM polyP$_{1200}$ (◆), 100 nM HK (◇) or both (◓)) in the presence of 10 μM $ZnCl_2$. Data points were connected to show the progress curves. Data are mean ± S.E. ($n \geq 3$).

Chapter 4 Directed Evolution of the *E. coli* Exopolyphosphatase Polyphosphate Binding Domain Using Phage Display and Next-generation Sequencing

4.1 Introduction

PolyP is a polymer of inorganic phosphate residues linked by high-energy phosphoanhydride bonds. It exists in all kingdoms of life and has been found to play important roles in different organisms depending on its location and size. In bacteria and yeast, polyphosphate kinases are responsible for reversibly synthesizing polyP from ATP[172] under specific conditions, implying that polyP may serve as an energy reservoir for the synthesis of ATP in these organisms.[152] PolyP can also be degraded by polyphosphatases.[198,199] PolyP has been shown to be important for cell proliferation,[157,200] apoptosis,[162,201] stress responses[165,202] and virulence.[153,203] In higher eukaryotes, polyP has been shown to be present in the human brain[154], granulocytes,[204] fibroblasts,[205] platelets,[166,168] rat liver nuclei[206] and mitochondria,[207] with various sizes and abundance levels[154]; however, until recently the functions of polyP in mammals remained unclear. Apart from its functions in cell survival, proliferation and apoptosis [153,203], polyP in mammalian cells was also demonstrated to modulate inflammation,[208] blood clotting,[163] angiogenesis,[209] calcification,[210] bone mineralization,[211] amyloid fibril formation[212] and tumor metastasis.[213] Targeting polyP may hold promises for the treatment of thrombotic diseases, infectious diseases, neurodegenerative diseases and cancer.

Given polyP's known and potential functions in the mammalian system, there is an urgent need for better methods to inhibit or probe polyP *in vivo*. Current polyP probes are limited to synthetic small molecules that bind to polyP, or recombinant polyP binding proteins, both of which

are known to have drawbacks. One of the most widely used polyP probes, 4',6-diamidino-2-phenylindole (DAPI)[214-220], undergoes a shift of its fluorescent emission spectra when bound to polyP.[219] However, this staining method for polyP has been recently called into question, as both RNA[221] and inositol phosphates[222] cause a similar fluorescence shift bound to DAPI. Other polyP probes, including toluidine blue (TBO)[223] and synthetic fluorescent molecules[224] have similar non-specific binding issues. Additionally, it is unknown if these small molecule polyP binders inhibit the (patho)physiological functions of polyP.

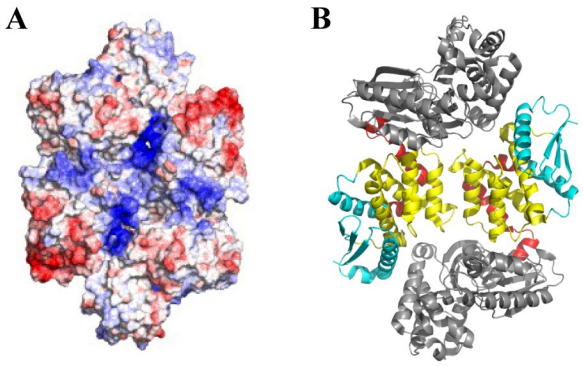

Figure 4.1 Structure illustration of *E. coli* PPX. (A) Image was adapted from Rangarajan *et al*. where electrostatic potential of *E. coli* PPX (PDB $_2$FLO) was calculated and mapped to the molecular surface, showing regions of positive potential (blue) within the putative polyP binding cleft.[225] **(B)** Amplicon 1 and 3-5 were highlighted on the crystal structure of *E. coli* PPX dimer (PDB $_2$FLO). The catalytic domains were shown in gray, amplicon 1 regions of PPXbd were shown in red, whereas amplicon 3-5 were highlighted in yellow.

Several recombinant proteins have also been developed for polyP labeling, including the conserved histidine α-helical domain (CHAD)[226] at the C-terminus of the bacterial triphosphate tunnel metalloenzyme ygiF,[227] and the recombinant polyphosphate binding domain (PPXbd)[228-231] of *E. coli* exopolyphosphatase (PPX) that catalyzes polyP degradation.[198,232] PPXbd is a 24.5 kDa domain from the PPX enzyme that has been used for both polyP visualization[167,228-230] and inhibition.[231,233-236] *E. coli* PPX is a 58 kDa exopolyphosphatase, that forms dimers in solution, and catalyzes polyP degradation.[198,232] Limited proteolysis of *E. coli* PPX indicated two functional domains, an N-terminal catalytic domain (structural domain I and II), and the C-terminal polyP

binding domain PPXbd (structural domain III and IV).[232] The binding of polyP to PPXbd is driven by charge-charge interactions.[225] A crystallographic study revealed a deep S-shaped canyon extending along the dimer interface and lined with basic residues, suggesting the possible polyP binding site (Figure 4.1A).[225,237] Computational models have also proposed a similar polyP binding scheme on PPX.[238] Like small molecule probes, the significant challenge of using these naturally occurring polyP binding protein domains is nonspecific binding. Both CHAD[226] and PPXbd were shown to bind with heparin, a heavily negatively charged glycosaminoglycan (GAG) molecule that is enriched in basophils[239] and mast cells[240,241] in all mammals.

In this study, we coupled phage display assisted directed evolution with next-generation sequencing (NGS) to engineer PPXbd with enhanced polyP affinity and specificity. PPXbd mutational libraries were displayed as a fusion protein on the surface of M13 filamentous phage. Enriched mutants in phage libraries after polyP binding selection were determined by NGS and their characteristics confirmed using recombinantly expressed PPXbd variants (Figure 4.2).

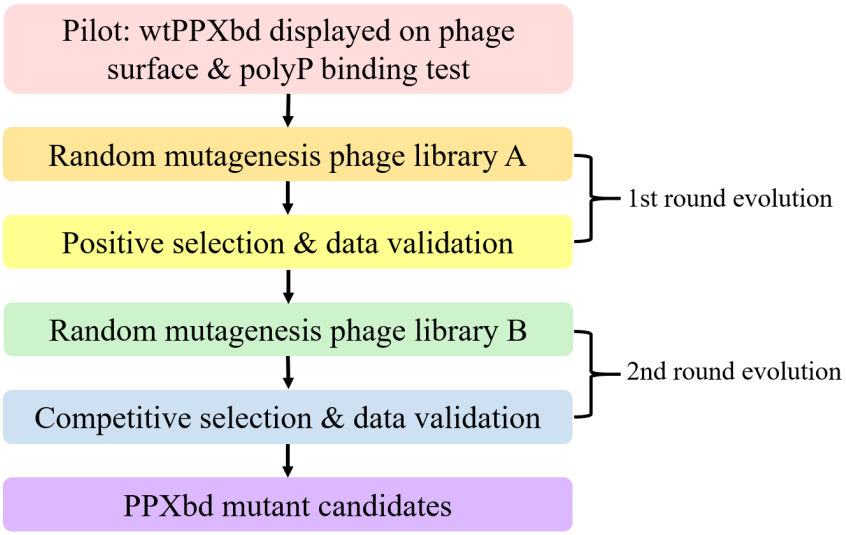

Figure 4.2 General workflow of PPXbd directed evolution. We aimed to screen for PPXbd mutants with enhanced polyP affinity in the first round evolution and screen for mutants with enhanced specificity in the second round evolution. Since the interaction between polyP and PPXbd is known to be charge dependent, a PPXbd mutation enhanced interaction with polyP might also increase affinity towards other negatively charged molecules such as heparin. Similarly, mutations on PPXbd leading to decreased binding to other negatively charged targets might also inevitably affect its affinity towards polyP. There was a fine balance between affinity and specificity. To prevent dramatic decreases of polyP affinity when we were screening for PPXbd mutants using common,

negatively charged molecules as competitors, we constructed a new library (phage library B) starting from mutants that were known to have an improved polyP affinity compared with wtPPXbd.

4.2 Materials and methods

Materials

Phagemid pAYE-FE (Genbank #MW464120)[242,243] was constructed based on previously described method.[244] Helper phage M13KO7 was from GE Life Sciences (Chicago, IL). SlickSeal™ microcentrifuge tubes were from VWR (Radnor, PA).The QIAquick PCR Purification Kit, QIAquick Gel Extraction Kit, Plasmid Maxi Kit and Plasmid Mini Kit were from Qiagen (Hilden, Germany). Primers were from Integrated DNA Technologies IDT (Newark, NJ). Q5 High-Fidelity DNA polymerase, Proteinase K, Amylose Resin, BL21(DE3) Competent *E. coli*, NEB 5-alpha Competent *E. coli*, NEBNext® Ultra™ End Repair/dA-Tailing Module, NEBNext® Ultra™ II Ligation Module, AMPure XP beads, enterokinase light chain, NotI-HF® and AscI restriction enzymes were from New England Biolabs (Ipswich, MA). XL1-Blue cells, XL1-Blue Supercompetent Cells, XL1-Blue Electroporation-Competent Cells, GeneMorph II Random Mutagenesis Kit, Herculase II Fusion DNA Polymerase and Bioanalyzer DNA 1000 Kit were from Agilent (Santa Clara, CA). T4 DNA Ligase, QuantiFlour® dsDNA System and GoTaq® Green Master Mix were from Promega Corporation (Madison, WI). Streptavidin, Pierce™ streptavidin-HRP, Dynabeads™ MyOne™ Streptavidin T1, B-per™ Complete Bacterial Protein Extraction Reagent, 1-step™ Ultra TMB-ELISA Substrate and monoclonal anti-Maltose Binding Protein (MBP) antibody conjugated with horseradish peroxidase (HRP) were from Thermo Fisher Scientific (Waltham, MA). MiSeq Reagent Kit was from Illumina (San Diego, CA). GlycoBlue™ Coprecipitant was from Invitrogen (Carlsbad, CA). NEXTFLEX® DNA Barcodes was from PerkinElmer (Waltham, MA). Heparin sodium was from APP Pharmaceuticals, LLC (Schaumburg, IL). Anti-M13 antibody [B62-FE2] (HRP) was from Abcam (Cambridge, UK).

Anti-fd Bacteriophage antibody, mouse Genomic DNA, heparan sulfate, chondroitin sulfate, hyaluronic acid and cOmplete™ EDTA-free Protease Inhibitor Cocktail Tablets were from Millipore Sigma (Burlington, MA). Biacore™ consumables, Sensor Chip SA and Sensor Chip CM4 were from Cytiva (Marlborough, MA). High Bind Stripwell™ Microplate and Black Round Bottom Plate were from Corning Inc. (Corning, NY).

The biotinylated polyP was prepared starting from chemically synthesized, high-molecular-weight polyP (Sigma-Aldrich). Termed as bitoin-polyP$_{560}$, the narrowly size-fractionated polyP had a modal length of 560 phosphates (range, 475 to 695 phosphates). It was solubilized from high-molecular-weight polyP using base hydrolysis followed by isopropanol precipitation,[174] followed by a preparative PAGE as previously described,[163,175] and was then biotinylated in the presence of EDAC and amine-PEG$_2$-biotin.[245] PolyP concentrations were quantified by measuring inorganic phosphate following hydrolysis in 1 M HCl at 100°C for 10 min.[175] Throughout this study, polyP concentrations are given in terms of molar concentrations of phosphate monomer.

Phage display vector and library construction

E. coli PPXbd (wild-type) cDNA sequence was previously codon optimized and synthesized byGenScript Corporation (Piscataway, NJ) and subcloned into a pACYCT2 plasmid from Addgene (Watertown, MA) (Supplementary table 4.1). To display the wtPPXbd on the surface of filamentous phage M13, the wtPPXbd was then cloned into the pAY-FE vector at restriction sites AscI-NotI, using standard PCR and subcloning techniques (Figure 4.3A). In this case, the N-terminal wtPPXbd was fused to a FLAG tag and E tag followed by the C-terminus of the pIII coat protein at the C-terminus. To increase the expression of PPXbd on the phage surface, the original amber stop at the N-terminus of the fusion protein was replace by Gln. As control, a

ΔPPXbd phagemid was constructed with most of the wtPPXbd sequence deleted, leaving only 12 residues fused from each end (MEGRF from the N-terminal end and STPEIAA from the C-terminal end). The ligation mixes were transformed into XL1-Blue Supercompetent Cells.

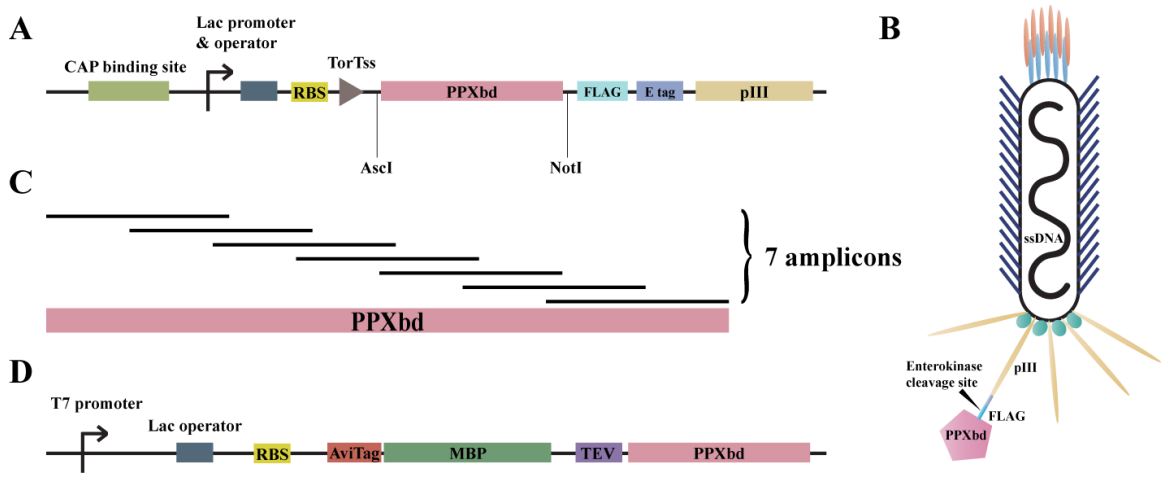

Figure 4.3 Construction of phagemid, plasmid and expression of M13 phage vector. (A) Expression of cloned wtPPXbd or PPXbd mutagenesis libraries in pAYE-FE phagemid was driven by the lac promoter. An amber stop which was initially placed between the TorTss and the insert gene in the pAYE-FE phagemid was mutated into Gln. The cloned wtPPXbd or PPXbd libraries were C-terminally fused to a FLAG tag and an E tag and a tandem, truncated M13 pIII coat protein composed of a glycine-serine rich linker and the pIII anchor domain. (B) PPXbd-FLAG-pIII fusion protein was expressed on the surface of an M13 filamentous phage. The FLAG tag was susceptible for enterokinase cleavage. Expression of the pAYE phagemid bearing wtPPXbd or PPXbd libraries on the surface of M13 phage required the infection of XL-1 blue cells by helper phage M13KO7 (not included in the figure), which induced proper phage packaging and phage secretion. (C) Due to the size limit of the NGS platform chosen in this study, the PPXbd gene was divided into 7 overlapping amplicons, each with 150 bp, while preparing for NGS sequencing. (D) Expression of selected PPXbd mutants selected from NGS data analysis was driven by the T7 promoter. The cloned wtPPXbd or PPXbd mutants was N-terminally fused to an AviTag, MBP for purification, and a TEV cleavage sequence.

To construct phage library A to be used in the first round of directed evolution (positive selection), wtPPXbd fusion protein was randomly mutagenized using GeneMorph II Random Mutagenesis Kit. Primers used for library construction are listed in Supplementary table 4.2. The PPXbd library was then subcloned into pAYE-FE phagemid (containing an ampicillin resistance cassette) at the AscI and NotI restriction sites. The ligation mix was electroporated into XL1-Blue Ultracompetent Cells.[246]

To construct phage library B to be used in the second round of directed evolution (competitive selection), site directed mutagenesis was performed on wtPPXbd phagemid to

generate three mutants (Q95R, A176E and E187K). Random mutagenesis was performed on individual PPXbd mutant phagemids. The ligation mixes were pooled together and transformed into Ultracompetent XL1-Blue cells.

The depth of both libraries was determined by quantifying the number of ampicillin resistant colonies. Mutation frequencies were estimated by Sanger sequencing of the PPXbd inserts from randomly selected individual colonies (n = 22 for library A and n = 49 for library B) and represented as number of nucleotide mutations per clone.

Expression, purification and titer of phage

Phage were prepared as previously described.[244] Briefly, *E. coli* harboring wtPPXbd or ΔPPXbd phagemid were grown in LB Broth supplemented with 2% glucose and ampicillin (100 μg/mL) at 37°C. During mid-log phase (OD 600 0.3-0.4), bacteria were infected with M13KO7 helper phage at a multiplicity of infection of ~100, followed by growth for an additional 1 h at 37°C. Cells were pelleted by centrifugation (4250 × *g* for 10 minutes at 4 ºC), resuspended in 2xYT media (16 g/L tryptone, 10 g/L yeast extract, 5 g/L NaCl) supplemented with ampicillin (100 μg/mL), kanamycin (30 μg/mL) and IPTG (0.4 mM) to induce expression of PPXbd fusion protein, and grown for 16 hours at 37°C. Phage were precipitated by the double precipitation method,[247] with polyethylene glycol-8000 (2.5% w/v) and NaCl (0.5 M) at 4°C. The phage pellets were resuspended with filtered TBS solution (50 mM Tris-HCl (pH 7.4), 150 mM NaCl).

Expression and purification of phage libraries followed a similar protocol, except that 2 mL of XL-1 blue glycerol stock was directly added into a 100 mL culture, and the phage expression process shortened from 16 hours to 4 hours to minimize biased enrichment due to growth advantages. Phage titer was determined using XL-1 blue cells following standard procedures.[247]

Verification that wtPPXbd pIII fusion protein retains polyP binding

An ELISA was performed to ensure that wtPPXbd displayed on phage surface had polyP binding ability. Anti-phage antibody was diluted in 50 mM carbonate buffer (pH 9.6) and added into a high bind microplate. Wells were washed 3 times in wash buffer I (20 mM 20 mM *N*-2-hydroxyethylpiperazine-*N'*-2-ethanesulfonic acid (HEPES) (pH 7.4), 100 mM NaCl, 0.05% v/v TWEEN® 20). After a blocking step, M13KO7 helper phage, ΔPPXbd phage or wtPPXbd phage (all possess an amber stop before the PPXbd region) were diluted in blocking buffer I (20 mM Hepes (pH 7.4), 5% BSA, 0.05% Tween® 20) and added into corresponding wells. In the experiment to test the binding between anti-phage antibody and phage, anti-phage antibody conjugated with HRP was diluted 200-fold and added into the wells. In parallel experiments, biotin-polyP$_{560}$ was diluted to 50 μM, preincubated with 1 μg/mL streptavidin-HRP, and added to the wells. TMB substrate was used to quantify the amount of PPXbd bound to each well and 2 M sulfuric acid was added to stop the reaction before A_{450} values were measured in a microplate reader.

Bio-panning

For wtPPXbd displayed on the phage surface, 25 μL Dynabeads per tube were suspended in SlickSeal™ microcentrifuge tubes and washed 3 times in balancing buffer (50 mM Tris-HCl (pH 7.4), 1 M LiCl, 1 mM EDTA). 0.5 mL of 250 μM biotin-polyP$_{560}$ was added to the tube and mixed with the beads on a rotor at room temperature for 1 hour. The beads were then washed 3 times in wash buffer I. Approximately, 4 x 10^{10} wtPPXbd phage or ΔPPXbd phage were diluted in 1 mL phage buffer I (wash buffer I supplemented with 1% w/v bovine serum albumin (BSA)) and added to each tube. After incubation with rotation at room temperature for 2 hours, the beads were washed 3 times in wash buffer I and the bound phage were cleaved overnight at 4°C by 40

μL diluted enterokinase in enterokinase buffer I (20 mM Tris-HCl (pH 7.4), 50 mM NaCl, 2 mM $CaCl_2$). Cleavage by enterokinase at the FLAG tag should only release the phage body bound through PPXbd (Figure 4.3B). Phage bodies were eluted with an extra 60 μL of TBST solution (TBS with 0.05% TWEEN 20). The selected phage titers were quantified and reported as cfu/mL.

For round one positive selection (library A, n = 2), the bio-panning was conducted in a buffer with 140 mM NaCl and 5 mM KCl, similar to the salt conditions in plasma. 50 μL Dynabeads per tube were suspended in SlickSeal™ tubes and washed 3 times in balancing buffer. Vehicle or 250 μM biotin-$polyP_{560}$ was added to corresponding tubes at a volume of 0.5 mL and mixed with the beads on a rotor at room temperature for 1 hour. After washing, 0.5 mL block buffer II (20 mM HEPES-NaOH (pH 7.4), 140 mM NaCl, 5% BSA) was applied for 1 hour to minimize non-specific binding. Phage library A was diluted in phage buffer II (20 mM HEPES-NaOH (pH 7.4), 140 mM NaCl, 5 mM KCl, 0.05% TWEEN® 20, 5% BSA) and added to each tube, aiming at a total number of 5 x 10^9 clones. The binding reactions were incubated at room temperature for 2 hours followed by 3 washes using phage buffer II. Enterokinase was diluted to 400 units/mL in enterokinase buffer II (enterokinase buffer I with 5% BSA). The enzyme cleavage, phage elution and titer steps were performed.

The round two competitive selection (library B, n = 3) was performed similarly with the following modifications. In this experiment, 30 μL per tube Dynabeads and 25 μM biotin-$polyP_{560}$ were used. Phage library B was added to each tube together with various competitors (25 or 50 U/mL heparin, 10 ng/μL mouse genomic DNA, 2 μg/mL heparan sulfate, 25 μg/mL hyaluronic acid, or 25 μg/mL chondroitin sulfate).

NGS library preparation

The ssDNA was extracted from the input and selected phage libraries using phenol-chloroform and precipitated with isopropanol. 15 µL of phage were mixed with 85 µL TE buffer (20 mM Tris-HCl (pH 7.4), 1 mM EDTA) and 5 µL diluted Proteinase K, incubating at 55°C for at least 3 hours. 100 µL phenol-chloroform-alcohol (v/v 25:24:1) was added into the mixture followed by vigorous vortex for 1 minute. The liquid mixture was then centrifuged at 20,000 x g for 10 minutes at room temperature. 75 µL of aqueous upper layer was collected and added into 7.5 µL 3M Na-Acetate solution (pH 5.0). GlycoBlue (1 µL) solution was added into the tube together with 85 µL isopropanol. DNA was extracted and precipitated overnight at -70°C. Precipitated DNA was collected by centrifugation at 20,000 x g for 20 minutes at 4°C, washed by 1 mL 70% pre-cold ethanol, followed by another round of centrifugation. After removing all the ethanol, the DNA pellet was resuspended in 10 µL H_2O.

Due to the read length limitations of the NGS platform used in this study, the PPXbd region in the phage libraries was divided into 7 overlapping amplicons (150 bp each) which were then PCR amplified using nested PCR and barcoded for NGS (Figure 4.3C). Mutation frequency PCR primers and Q5 polymerase were mixed with used 100 ng extracted phage DNA to amplify the PPXbd region. After 30 cycles, the PCR product was purified, quantified and used as template for amplicon PCR. During the amplicon PCR, 10 ng purified nested PCR product was added into the PCR reaction mix with Q5 polymerase and individual primer pairs (Supplementary table 4.3). To prevent laddered products, 18 cycles of nested PCR were performed. PCR amplicon products were gel purified and prepared using NEBNext DNA Library Prep Master Mix Kit. NextFlex sequencing adapters containing barcodes were ligated for indexing and sequencing as previously described.[246] Sample purity and length were verified by the Bioanalyzer 2100 before NGS using

the Illumina MiSeq at the University of Michigan or the Illumina HiSeq platform at MedGenome, Inc. (Foster City, CA). HTS data were analyzed using DESeq2.[248]

Recombinant protein production

To validate the NGS data, selected PPXbd mutants were expressed as a soluble fusion protein AviTag-MBP-PPXbd in *E. coli* (Figure 4.3D). A synthetic peptide containing the AviTag biotin acceptor peptide (GLNDIFEAQKIEWHE) was cloned into a wtPPXbd containing plasmid[229] at NcoI and XbaI (performed by Epoch Life Sciences). Site-directed mutagenesis was performed to create specific single mutations in PPXbd. Plasmids containing wtPPXbd or PPXbd mutants were then transformed into BL21-DE3 cells for expression. *E. coli* colonies bearing each plasmid were inoculated into 5 mL of LB media supplemented with kanamycin (30 μg/mL). The overnight starter culture was added to 1 L of NZY media (14 g NZ-Amine A, 7.5 g yeast extract, 5 g NaCl, pH 7.5) and protein expression was induced by adding 0.4 mM IPTG at an OD_{600} of 0.4-0.6. After overnight expression at 15°C, the bacteria were then pelleted at > 5,000 × g and lysed by B-per reagent supplemented with protease inhibitor tablet. The fusion PPXbd proteins were purified on amylose resin at 4°C according to the manufacturer's instructions and quantified based on the absorption at 280 nm.

Surface plasmon resonance

The binding of recombinant PPXbd (wild type and variants) to polyP was quantified by surface plasmon resonance (SPR) using a Biacore™ 3000 instrument (GE healthcare). Biotin-$polyP_{560}$ was immobilized on the experimental flow cell of a SA sensor chip or a CM4 chip coated with streptavidin. Excess biotin was added to block extra biotin binding sites on streptavidin. PPXbd was diluted into various concentrations (0-200 nM) in the Biacore buffer (20 mM HEPES (pH 7.4), 140 mM NaCl, 5 mM KCl, 1 mM EDTA, 0.005% v/v Surfactant P20) and added to both

experimental and reference flow cell (without biotin-polyP$_{560}$). After each cycle, the chip was regenerated by regeneration buffer (1 M NaCl, 1 mM EDTA) to ensure the removal of PPXbd from polyP. Maximal RU values at steady state equilibrium from the experimental flow cell were subtracted by the values from the reference cell and data were exported into Graphpad Prism 8 for further analysis. Background measurements (baseline levels) were subtracted before determining dissociation constants (K_d) by applying one-site total binding equation ($Total\ binding = B_{max} \times PPXbd_{conc} \div (K_d + PPXbd_{conc}) + NS \times PPXbd_{conc} + Background$), in which nonspecific binding (NS) was assumed to be proportional to PPXbd concentration. Average K_d values (n ≥ 3) were reported for each PPXbd variant.

NGS Data analysis

Statistics for NGS data were performed using DESeq2 in the R environment.[248] The enrichment or depletion of PPXbd variants was represented by $\log_2$ fold enrichment scores, which estimated the $\log_2$ fold change of read counts before and after selection. Statistical significance of specific variants was determined by both the q-value and base mean count. For MiSeq data, variants with a q-value of $<10^{-5}$ and a base mean count > 25 were considered significant. For HiSeq data, variants with a q-value of $<10^{-5}$ and a base mean count > 40 were considered significant. Data were plotted either in the form of heat map, MA plot or volcano plot.

4.3 Results

wtPPXbd displayed on the phage surface binds to polyP

In order to test if wtPPXbd displayed on the phage surface still maintained its ability to bind with polyP, an indirect ELISA was performed with immobilized phage. M13KO7 helper phage and ΔPPXbd phage were included in the ELISA as negative controls as they do not have intact wtPPXbd displayed on the surface. All three types of phage bound specifically to an anti-

phage antibody (Supplementary figure 4.1A, *left panel*). In the presence of biotin-polyP$_{560}$, wtPPXbd phage bound 62% more polyP as compared with ΔPPXbd phage, and 120% more polyP as compared with the M13KO7 helper phage (Supplementary figure 4.1A, *right panel*). To amplify the difference between wtPPXbd phage and control, the amber stop codon before the PPXbd region was replaced by Gln and new phage were tested in ELISA. Without polyP, there was minimal background signal detected. In the presence of 20 μM polyP, wtPPXbd phage without the amber stop demonstrated more than 3-fold increased binding to polyP as compared to ΔPPXbd phage (Supplementary figure 4.1B). The pAYE-FE phagemid without the amber stop was used in all subsequent experiments unless otherwise specified. Biotin-polyP$_{560}$ was immobilized on streptavidin coated magnetic beads and either wtPPXbd phage or ΔPPXbd phage were added. Bound phage were cleaved by enterokinase to ensure only phage bound via wtPPXbd or ΔPPXbd were eluted, whereas those that nonspecifically "stuck" to the polyP-coated beads would not be eluted. 5.7 x 10^7 wtPPXbd phage were eluted, following enterokinase treatment, and showed more than 100-fold greater binding efficiency compared to ΔPPXbd phage (Figure 4.4). These experiments demonstrate that wtPPXbd displayed on the phage surface binds polyP, and suggests that our bio-panning approach will be an effective method when applied to our phage library.

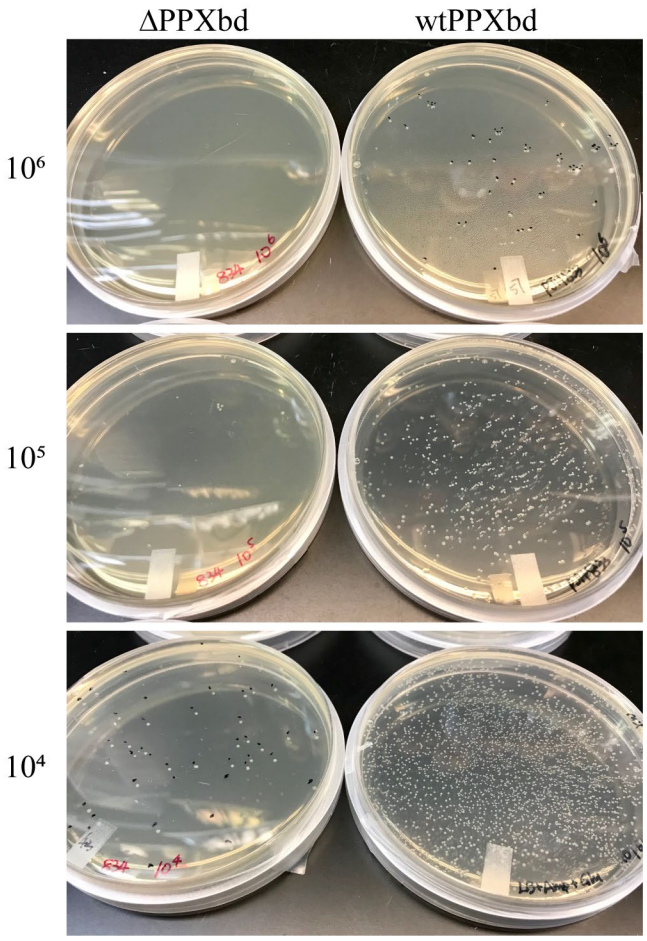

Figure 4.4 wtPPXbd expressed on phage surface binds with polyP. Both ΔPPXbd phagemid and wtPPXbd phagemid were expressed on the phage surface. 0.5 mL of 250 µM biotin-polyP$_{560}$ was added to each tube containing 25 µL of streptavidin coated Dynabeads. 4 x 10^{10} phages were diluted in phage buffer I (see Method) and added into each tube. After 2-hour incubation, the unbound phages were washed off. The bound phages were cleaved overnight by enterokinase and eluted. To quantify the number of bound phages, eluted phages from each group were added to XL-1 blue MRF' cells for infection. The phage titer result was demonstrated as colony forming plaques from each group.

Bio-panning for the selection of PPXbd mutants with enhanced polyP affinity (library A)

Phage library A had a depth of 3.96 x 10^7 clones and ~36% were wtPPXbd without mutation. For the remaining 64% of PPXbd mutants, the average mutation frequency was roughly 2.3 bp per clone. Following DESeq2 analysis of the NGS data, the enrichment or depletion of individual missense and nonsense mutations were determined (Figure 4.5A). Enriched mutations are associated with improved affinity for PPXbd, whereas depleted variants imply a loss of ability to bind polyP efficiently. The relative fold of enrichment of each PPXbd variant, including wild-

type amplicons, and statistical significance (*q*-value) are shown as a volcano plot in Figure 4.5B. To identify target PPXbd variants for further directed evolution, the largest significant ($q \leq 5x10^{-5}$) log_2 fold enrichment scores were identified (Table 4.1). To further narrow down the pool of potential candidates for biochemical characterization, a combination of criteria was considered. Due to the known charge-charge interaction properties between polyP and PPXbd, those variants that contained changes in electronic charges resulting in a mutation to a basic residue, or the neutralization of an acidic residue (i.e., E187K & D89N) were selected. At some amino acid positions, multiple missense mutations were enriched (i.e., Q95R, Q95H & Q95K; A176E & A176S), implying a potential significance to these residues. Finally, the variant, S81I exhibited more than 2-fold significant enrichment following selection and was also subjected to further characterization. In total, the 8 variants mentioned above were selected for further *in vitro* characterization.

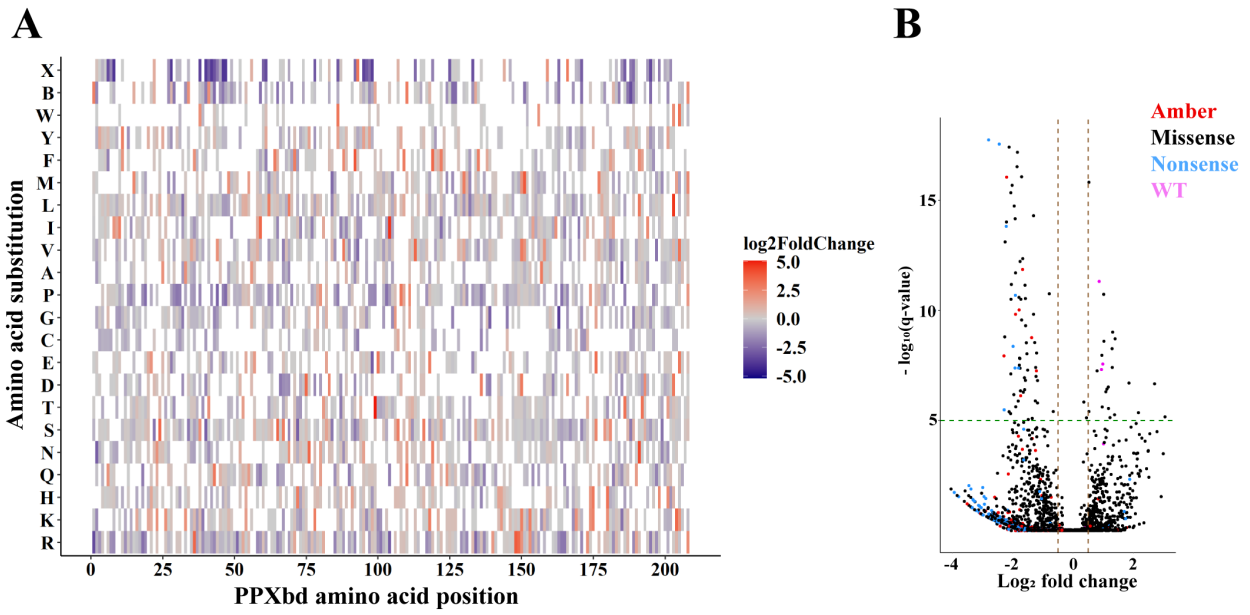

Figure 4.5 Positive selection for polyP binding was performed using phage library A. 0.5 mL of 250 µM biotin-polyP$_{560}$ was added to each tube containing 50 µL of streptavidin coated Dynabeads. A negative control was also conducted by adding no biotin-polyP$_{560}$ to the beads (not shown on the figure). 5 x 10^9 phages were diluted in phage buffer II (see Method) and added into each tube. After 2-hour incubation, the unbound phages were washed off. The bound phages were cleaved overnight by enterokinase and eluted. DNA was extracted from eluted phages and the input library. The prepared amplicon sequencing library was submitted for MiSeq. The positive selection NGS data was shown as heat map (A) and volcano plot (B). (A) Heat map indicating average

Log_2 fold enrichment scores for PPXbd mutants selected for polyP binding. PPXbd amino acid positions were plotted on *x-axis* and the amino acid substitutions (X for ochre or opal stop whereas B for amber stop) were plotted on *y-axis*. Enriched mutations (log_2 fold change > 0) were indicated in red, while depleted mutations (log_2 fold change < 0) were indicated in blue. White indicates amino acid substitutions that were not present in the mutational library. (B) PPXbd wild type amplicon (●), mutant amplicon with missense (●), nonsense (●), or amber stop (●) mutation was plotted as individual dot on each panel, where the log_2 fold change values of the polyP selected *versus* input library were plotted on the *x-axis* and the $-log_{10}$(q-value) of the positive selection were plotted on *y-axis*.

Table 4.1 PPXbd mutants with more enrichment than wtPPXbd after positive selection.

Mutant	Log_2 fold change normalized to wtPPXbd
A57E	0.840
D89N	0.185
N71S	0.190
S75R	0.410
D89N	0.182
Q95R	0.351
Q95H	0.372
Q95K	0.436
S81I	1.23
R119H	0.0891
L122M	0.159
D116N	0.0997
N143K	0.221
L122Q	0.437
L131M	0.360
D160N	0.357
A208V	0.160
A209T	0.080
A208T	0.163
E187K	0.650
A176S	2.33
A176E	2.68

Selection of PPXbd mutations that enhanced polyP binding affinity

The polyP binding affinities of purified mutant PPXbd and wtPPXbd were tested by SPR (Supplementary figure 4.2). wtPPXbd demonstrated a steady-state binding affinity of K_d = 28.1 ± 6.09 nM. In contrast, the S81I mutant demonstrated no detectable binding to polyP, which was surprising as this variant showed a greater than 2-fold enrichment during phage display selection. This might be an example of different behaviors of phage-displayed proteins and soluble proteins. An alternative possibility was that S81I needed to work *in cis* with other mutations in order to enhance the binding between PPXbd and polyP. Several tested mutants exhibited reduced K_d levels compared to WT, including D89N, Q95K, Q95R, A176E, A176S and E187K (with K_d values reduced by 50.8%, 44.9%, 62.8%, 3.2%, 13.5% and 75.1%, respectively (Figure 4.6)). Q95R (K_d = 10.4 ± 3.01) and E187K (K_d = 7.01 ± 1.71) exhibited the tightest binding affinities. Of note, both

mutations substitute a positively charged residue. Combining some of these mutants did not seem to result in an additive effect for their affinity towards polyP (Figure 4.6).

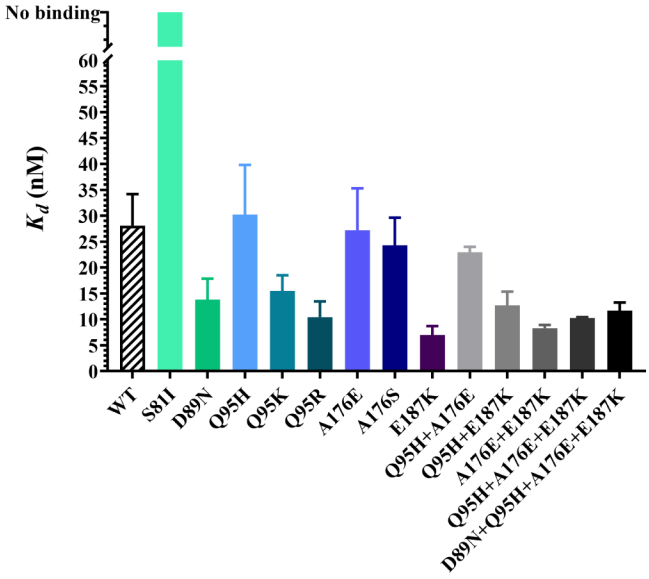

Figure 4.6 Selected PPXbd mutants had higher binding affinity towards polyP. Biotin-polyP$_{560}$ was immobilized on the experimental flow cell of a SA sensor chip or a CM4 sensor chip coated with streptavidin. Each fusion protein AviTag-MBP-PPXbd containing mutations on PPXbd was diluted to various concentrations (1-100 nM) in the Biacore buffer (see Method) and flowed through both reference and experimental flow cell. Maximal RU values at steady state from the experimental flow cell were subtracted from the values from reference cell (Supplementary figure 4.2). Baseline levels were removed before the binding levels were plotted versus PPXbd concentration to obtain binding curves. Data points were fitted using the one-site ligand binding equation to obtain dissociation constants (K_d). Data are mean ± S.E. ($n \geq 3$).

Specificity test of wtPPXbd binding to polyP with the presence of different competitors

Heparin binding to wtPPXbd would be expected to result in nonspecific signals when using wtPPXbd as a probe for polyP in mammalian cells or tissues. To test whether other negatively charged biological polymers could contribute to PPXbd nonspecific binding, the specificity of phage displaying wtPPXbd was tested in the presence of genomic DNA, heparan sulfate, hyaluronic acid or chondroitin sulfate as competitor. As expected, heparin effectively competed wtPPXbd phage binding to polyP (Supplementary figure 4.3A) in a dose-dependent manner (Supplementary figure 4.3B). In the presence of biotin-polyP$_{560}$, the addition of 25 U/mL heparin decreased the number of bound phage by 87.4%. Increasing the concentration of heparin to 50

U/mL decreased the number of eluted phage by 93.6%, bringing down the level of bound phage close to the background level (no polyP) (Supplementary figure 4.3B). This suggested that with enough heparin, all wtPPXbd phage would be competed off polyP. Mouse genomic DNA or hyaluronic acid did not effectively compete with wtPPXbd phage binding to polyP (Supplementary figure 4.3C & E), while heparan sulfate and chondroitin sulfate moderately decreased the number of bound phage, but not in a dose-dependent manner (Supplementary figure 4.3D & F).

Bio-panning for the selection of PPXbd mutants with enhanced polyP specificity (library B)

Due to the charge-charge interaction property between PPXbd and polyP, PPXbd mutants with enhanced specificity (less likely to bind with heparin) would most likely lower affinity for polyP. To prevent dramatic loss of polyP affinity in the second round selection, Q95R and E187K mutants, with the highest binding affinities for polyP (Figure 4.6) were employed as DNA templates for constructing phage library B. Although A176E did not demonstrate a significantly lower K_d, it was also included as the template DNA for random mutagenesis, in case all variants based on Q95R or E187K mutations possessed tight binding ability to both polyP and heparin.

Phage library B had a depth of 6.36×10^7 clones and ~40% were PPXbd Q95R, A176E or E187K without any additional mutations. For the remaining 60% of library B, the average random mutation frequency was ~2.3 bp per clone in addition to the underlying Q95R, A176E, and/or E187K mutation. Following positive selection to polyP coated beads, ~24% of phage were eluted from polyP beads, whereas <0.8% of phage were eluted in the absence of polyP (background binding). The number of phage bound to polyP decreased in the presence of heparin in a dose-dependent manner, as compared with the positive selection. No significant competition with PPXbd phage binding to polyP beads was observed with mouse genomic DNA and other GAG

molecules (Figure 4.7). These results are consistent with data obtained from using phage displayed wtPPXbd (Supplementary figure 4.3).

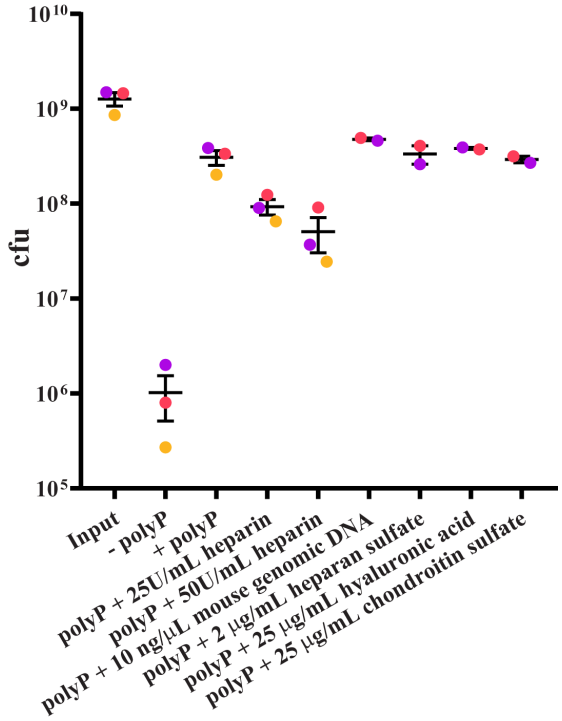

Figure 4.7 Competitive selection of library B showed heparin as a good polyP competitor. 0.5 mL of 25 μM biotin-polyP$_{560}$ was added to each tube containing 30 μL of streptavidin coated Dynabeads. A negative control was also conducted by adding no biotin-polyP$_{560}$ to the beads (Supplementary figure 4.6). 5 x 10^9 phages mixed with 0 or 25 U/mL heparin, 10 ng/μL mouse genomic DNA, 2 μg/mL heparan sulfate, 25 μg/mL hyaluronic acid, or 25 μg/mL chondroitin sulfate were diluted in phage buffer II (see Method) and added into each tube. After 2-hour incubation, the unbound phages were washed off. The bound phages were cleaved overnight by enterokinase and eluted. Phage concentrations were plotted as the number of colony forming plaques (cfu). For each experimental group, biological duplicates or triplicates were plotted as individual data point.

The enrichment or depletion of polyP binding for missense mutations in PPXbd in the absence of competitors is shown in Supplementary figure 4.4. The enrichment or depletion of substitutions in the presence of different doses of heparin are shown in Figure 4.8A & Supplementary figure 4.5A, with fold enrichment and statistical significance (q-value) displayed in a volcano plot in Figure 4.8B & Supplementary figure 4.5B. The substitutions exhibiting the most significant enrichment in polyP binding are listed in Tables 4.2, 4.3 & 4.4. As negative

control when no polyP was used in the bio-panning, no mutants were significantly enriched after selection (Supplementary figure 4.6).

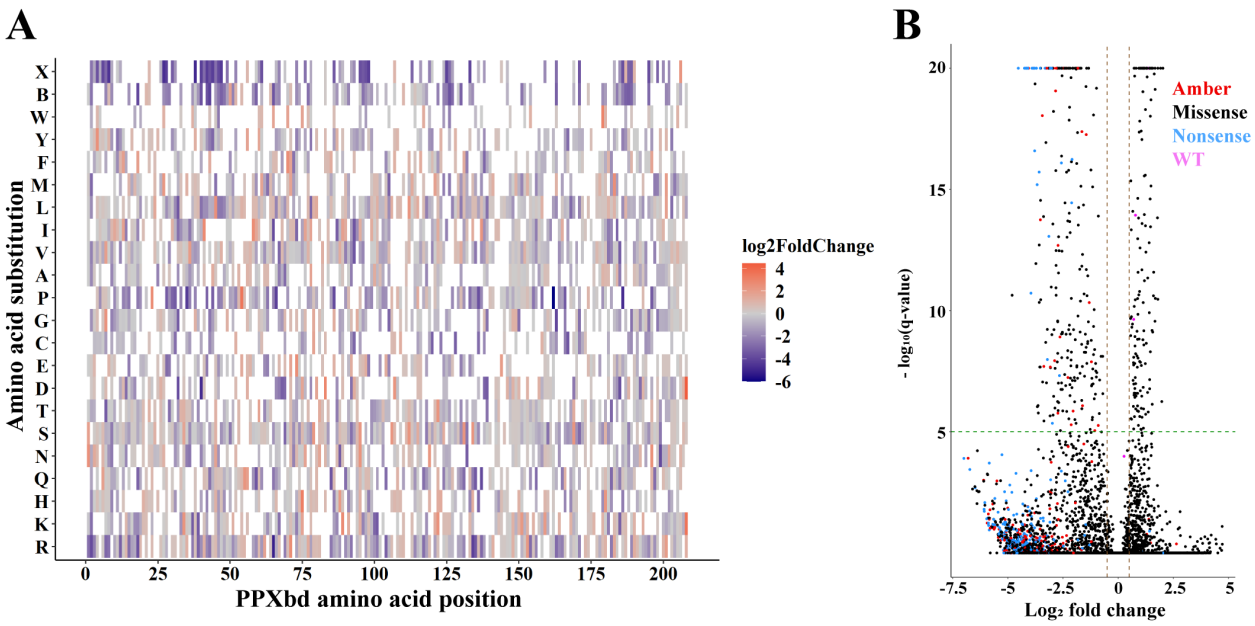

Figure 4.8 Competitive selection against heparin was performed using phage library B. 0.5 mL of 25 µM biotin-polyP$_{560}$ was added to each tube containing 30 µL of streptavidin coated Dynabeads. 5 x 10^9 phages mixed with 25 U/mL heparin were diluted in phage buffer II (see Method) and added into each tube. After 2-hour incubation, the unbound phages were washed off. The bound phages were cleaved overnight by enterokinase and eluted. DNA was extracted from eluted phages and the input library. The prepared amplicon sequencing library was submitted for HiSeq. The competitive selection NGS data was shown as heat map (A) and volcano plot (B). (A) Heat map indicating average Log_2 fold enrichment scores for PPXbd mutants selected for polyP binding with the competitions of 25 U/mL heparin. PPXbd amino acid positions were plotted on *x-axis* and the amino acid substitutions (X for ochre or opal stop whereas B for amber stop) were plotted on *y-axis*. Enriched mutations (log_2 fold change > 0) were indicated in red, while depleted mutations (log_2 fold change < 0) were indicated in blue. White indicates amino acid substitutions that were not present in the mutational library. (B) PPXbd wild type amplicon (●), mutant amplicon with missense (●), nonsense (●), or amber stop (●) mutation was plotted as individual dot on each panel, where the log_2 fold change values of the heparin competitive selection *versus* input library were plotted on the *x-axis* and the $-log_{10}$(q-value) of the positive selection were plotted on *y-axis*.

Table 4.2 PPXbd mutants with more enrichment than wtPPXbd after competitive selection with 25 U/mL heparin.

Mutant	Log_2 fold change normalized to wtPPXbd
R13H	0.310
G3D	0.327
A15V	0.296
R6H	0.337
R4H	0.395
R6S	0.615
Q8E	0.815
L33M	0.152
M39L	0.297
L33Q	0.116
Q38R	0.114
E41D	0.0110
A57S	0.0151
E27D	0.0977
Q47H	0.0919
Q38L	0.138
A57E	0.676
V68I	0.0221
S81G	0.0939
Q86E	0.115
N87Y	0.191
L90M	0.113
L77R	0.628
F93L	0.107
E96G	0.0628
N94S	0.130
L77V	0.240
Q54R	0.0364
A111T	0.113
M101L	0.441
M101V	0.129
Q95H	0.315
N94S	0.0915
D116E	0.110
Q97E	0.320
Q86E	0.425
L90M	0.0711
A111S	0.310
Q95K	0.325

N87Y	0.441
R119H	0.405
L122M	0.140
D116E	0.0345
Q133R	0.0161
N143K	0.863
L131M	0.141
L122Q	0.346
F128Y	0.257
L134M	0.0281
F123Y	0.364
F128I	0.0224
L122V	0.0193

L129M	0.0277
Q133K	0.178
N143H	0.472
T150I	0.0199
T149I	0.0220
V178M	0.236
D160N	0.181
D159N	0.321
F172L	0.152
D159E	0.0193
T150A	0.0709
L177P	0.372
L177M	0.196

D170G	0.152
S173R	0.267
D160G	0.366
L177Q	0.525
L177R	0.906
D159H	0.896
E187K	0.986
E187R	0.967

Table 4.3 PPXbd mutants with more enrichment than wtPPXbd after competitive selection with 50 U/mL heparin.

Mutant	Log_2 fold change normalized to wtPPXbd
R13H	0.409
G3D	0.445
A15V	0.347
R6H	0.423
R4H	0.391
R6P	0.406
R6S	0.788
Q8E	0.853
L33M	0.170
M39L	0.240
E41K	0.0391
L33Q	0.123
Q38R	0.0503
E27D	0.127
Q28H	0.0114
Q47H	0.184
Q38L	0.163
A57E	0.630
V68I	0.0120
S81G	0.0921
N71S	0.0832
Q86E	0.200
N87Y	0.369
L90M	0.0182
L77R	0.776

F93L	0.00299
E96G	0.00733
D89H	0.00382
L77V	0.555
Q54R	0.290
M101I	0.0422
A111T	0.0243
M101L	0.461
M101V	0.175
Q95H	0.382
N94S	0.133
D116E	0.0703
Q97E	0.544
Q86E	0.542
A111S	0.314
Q95K	0.513
N87Y	0.364
R119H	0.456
L122M	0.136
D116E	0.0706
Q133R	0.0933
N143K	0.920
L131M	0.226
L122Q	0.394
F128Y	0.228
L134M	0.0264
F123Y	0.336
F128I	0.0112

L122R	0.0891
Q133K	0.313
N143H	0.577
T150I	0.0193
T149I	0.0837
V178M	0.215
S173N	0.0163
D160N	0.246
D170N	0.174
Q174H	0.0186
D159N	0.349
F172L	0.0790
T150A	0.128
L177P	0.289
L177M	0.158
D170G	0.156
S173R	0.156
D160G	0.467
L177Q	0.560
S161R	0.0741
T149N	0.420
L177R	0.924
D159H	0.731
E187K	1.05
E187R	1.00
E190K	1.33

Table 4.4 PPXbd double mutants with more enrichment than wtPPXbd after competitive selection.

+ polyP (no heparin)		25 U/mL heparin + polyP		50 U/mL heparin + polyP	
Mutant	Log_2 fold change normalized to wtPPXbd	Mutant	Log_2 fold change normalized to wtPPXbd	Mutant	Log_2 fold change normalized to wtPPXbd
Q95R-D89N	0.397	Q95R-Q97E	0.619	Q95R-Q97E	0.671
		E187K-R196H	0.979	E187K-R196H	1.08
		E187K-E183K	1.40	E187K-G191S	1.14
		E187K-E190K	1.50	E187K-E183K	1.61
				E187K-E190K	1.75

Characterization of polyP affinity of selected PPXbd mutants

Selected mutations were expressed in the PPXbd fusion protein construct with the E187K mutation and polyP binding affinities characterized by SPR (Figure 4.9). Combined with the E187K mutation, very few double mutants showed a dramatically improved K_d as compared with E187K single mutant, consistent with the hypothesis that those substitutions enriched after competitive selection with heparin may have reduced polyP affinity. Out of the PPXbd variants built on E187K, E187K-N143H and E187K-L177Q mutants had the lowest average K_d values. The K_d values for the rest of the double mutants were between 8-16 nM. Not surprisingly, most of the selected substitutions exhibited higher polyP affinity than wtPPXbd (Figure 4.9). This was likely because of the presence of E187K, which may "rescue" the polyP affinity to some degree. Table 4.5 summarized the average K_d values from all mutants that were tested to date.

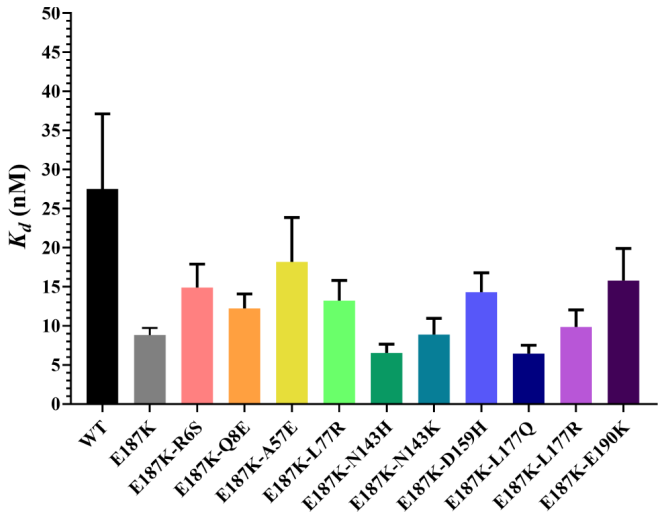

Figure 4.9 Selected PPXbd mutants had improved binding affinity towards polyP. The polyP affinity of each mutant were tested via SPR, and then compared with wtPPXbd. Biotin-polyP$_{560}$ was immobilized on the experimental flow cell of a SA sensor chip coated with streptavidin. Each fusion protein AviTag-MBP-PPXbd containing mutations on PPXbd was diluted into various concentrations (1-150 nM) in the Biacore buffer (see Method) and flow through both reference and experimental flow cell. Maximal RU values at steady state equilibrium from the experimental flow cell was subtracted by the values from reference cell. Baseline levels were removed before the binding levels were plotted versus PPXbd concentration to obtain binding curves. Data points were fitted using the one-site total binding equation to obtain dissociation constants (K_d). Data are mean ± S.E. ($n \geq 3$).

Table 4.5 Summary of average K_d values of all PPXbd mutants binding with polyP.

Mutant	Average K_d value (nM) ± SEM	Source figure
WT	27.9 ± 5.00	4.6 & 4.9
S81I	No binding	4.6
D89N	13.8 ± 4.03	4.6
Q95H	30.2 ± 9.56	4.6
Q95K	15.5 ± 3.02	4.6
Q95R	10.4 ± 3.01	4.6
A176E	27.2 ± 8.08	4.6
A176S	24.3 ± 5.31	4.6
E187K	7.6 ± 1.17	4.6 & 4.9
Q95H-A176E	23.0 ± 1.02	4.6
Q95H-E187K	12.7 ± 2.63	4.6
A176E-E187K	8.30 ± 0.623	4.6
Q95H-A176E-E187K	10.3 ± 0.170	4.6
D89N-Q95H-A176E-E187K	11.7 ± 1.58	4.6
E187K-R6S	14.9 ± 3.01	4.9
E187K-Q8E	12.2 ± 1.86	4.9
E187K-A57E	18.2 ± 5.65	4.9
E187K-L77R	13.2 ± 2.58	4.9
E187K-N143H	6.52 ± 1.14	4.9
E187K-N143K	8.89 ± 2.06	4.9
E187K-D159H	14.3 ± 2.48	4.9
E187K-L177Q	6.45 ± 1.06	4.9
E187K-L177R	9.84 ± 2.20	4.9
E187K-E190K	15.8 ± 4.11	4.9

4.4 Discussion

As the region of *E. coli* PPX that binds polyP, PPXbd holds promise as a potential polyP probe or inhibitor *in vivo*. However, previous studies have indicated that PPXbd also binds to other negatively charged molecules, especially heparin that is found in mammalian basophils[239] and mast cells[240,241]. In this study, we performed directed evolution of PPXbd that led to an increase of its polyP binding affinity and specificity. After the first round of evolution, we found several point mutations that resulted in enhanced polyP affinity, including Q95R and E187K. Starting from these mutant PPXbd, the second round evolution allowed us to find a pool of mutant candidates that bound more specifically to polyP than to heparin.

Directed evolution is an artificial, yet powerful tool to engineer proteins with unachievable functions during natural evolution. Being an enzyme with high processivity, the PPX enzyme dimer contains an aqueduct that provides a physical basis for polyP to passing through along during catalysis.[198,232,237] In addition, PPX is generally well conserved across bacterial strains.[225] This implies that naturally occurring polyP related enzymes may not have the optimal structure to achieve tight and specific polyP binding function as their polyP binding sites need to possess flexible structures to allow polyP chains to move along during catalysis. For instance, one of the most conserved residues is E491, which corresponds to E187 on PPXbd.[225] Mutations such as E187K, which substitutes an acidic residue for a basic residue, resulting in tighter polyP binding, is less likely to be appreciated in natural selection as it destroys the flexibility of the enzyme. However, these mutations which lead to enhanced polyP binding ability, were artificially evolved by phage display, and efficiently identified by NGS.

We found that for both wtPPXbd displayed on phage and PPXbd phage library B, only heparin could effectively compete off phage from binding to polyP beads, in a concentration-

dependent manner. Mouse genomic DNA, heparan sulfate, chondroitin sulfate or hyaluronic acid were not effective competitors, which was consistent with our previous studies with soluble wtPPXbd. This result was consistent with the fact that heparin has the highest negative charge density of any known biomolecule.[249,250] Our lab has previously reported that artificial RNA molecules (polyG and polyI) could bind to proteins (i.e., FXII) that are known to interact with polyP.[117] We suspect that there may be certain nucleic acid sequences forming particular secondary structures such as G-quadruplex in DNA or RNA that may preferably interact with polyP binding proteins, including PPXbd. In this study, we only used up to 10 μg/mL mouse genomic DNA and did not observe any evidence for binding to PPXbd, whereas the concentration of DNA within the nucleus could range up to 10 mg/mL.[251] To further investigate if nucleic acids could interfere with polyP staining by PPXbd, future studies could examine whether highly concentrated nucleic acids extracted from mammalian cell culture can compete with PPXbd for PolyP binding.

Principal component analysis (PCA) was performed to analyze the NGS data and the PCA plot after the second round of evolution implied that there were some regions of PPXbd that may better distinguish polyP from heparin (Supplementary figure 4.7). For all 7 amplicons, the input libraries were well separated with selected libraries, with or without heparin as competitor, on the *x-axes*. Therefore, the first principal component was suspected to be associated with the ability of binding to polyP. Similarly, we propose that the second principal component was associated with heparin interaction. Surprisingly some, but not all amplicons showed a clear separation between positive selection group (with only polyP) with competitive selection groups (with heparin and polyP) along the *y-axis*, such as amplicon 3, 4, 5 and possibly amplicon 1 (Figure 4.1B). This interesting result suggests that there might be particular regions of PPXbd that are able to distinguish polyP and heparin, whereas other regions may be mainly responsible for binding with

negatively charged residues in general. To test this hypothesis, future experiments may be performed by generating random fragmentation libraries for competitive selection, instead of using random mutagenesis libraries. However, creating a truncated version of PPXbd may sacrifice its high affinity towards polyP, as there are multiple basic residues spreading over all domains on PPXbd that are suspected to interact with polyP.[225,237]

In fact, it is evident from previous studies that *E. coli* PPX is a highly processive enzyme with the ability to recognize polyP of specific lengths, as the polyP gel showed that inclusion of PPX produced discrete P_{50}, P_{14} and P_2 intermediates. In our preliminary studies when we immobilize biotin-polyP at the bottom of a microplate well, PPXbd fused with MBP could only bind to polyP with a chain length of over 100. This limited out ability to develop probes against the short chain polyP that are predominant forms in mammals. To achieve this goal, generating truncated versions of PPXbd by random fragmentation may offer an alternative approach. Some other smaller size polyP binding proteins such as CHAD could also be used as an evolution target. We propose that similar method could be widely adapted to many different proteins to acquire or enhance multiple functions.

Combining phage display with NGS greatly improved the efficiency of directed evolution and saves time on the labor-intensive bio-panning process. However, one drawback of this method is that it will be very hard to detect multiple mutations acting in *cis*, in contrary to the traditional phage display followed by Sanger sequencing. Since the maximum read lengths for the current Illumina Miseq or Hiseq platform is ~150 bp, the entire PPXbd gene (627 bp) was divided into 7 amplicons before sequencing. This high throughput sequencing method will not be able to detect if there were two or more mutations on different amplicons that work together to increase polyP binding characteristics. One could also choose novel sequencing platforms such as single-molecule

real-time (SMRT) sequencing or nanopore sequencing that allow longer reads, although they may result in fewer number of total reads, potentially lower consensus accuracy and higher cost.[252] However, we did find several enriched double mutants on amplicon 7 that may enhance polyP binding specificity, most of them containing E187K, which was used as one of the template when constructing the random mutagenesis phage library B (Table 4.4). Based on this result, it is reasonable to suspect that some of the single mutants that appeared to be enriched after selection may have synergic effects with the appearance of E187K. Thus, we decided to express selected mutations using the PPXbd fusion protein construct with E187K mutation. Due to time limitations, the characterization of the mutant PPXbd specificity will be measured using microplate based ELISA in the future.

In this study, we adapted phage display in combination with NGS to perform a proof-of-concept protein engineering project, where a domain of naturally occurring polyP degrading enzyme was evolved to acquire high polyP affinity and specificity after two rounds of evolution. We propose that similar method could be adapted to generate powerful protein tools with new properties or improved existing functions in different fields of studies.

4.5 Supplementary figures and tables

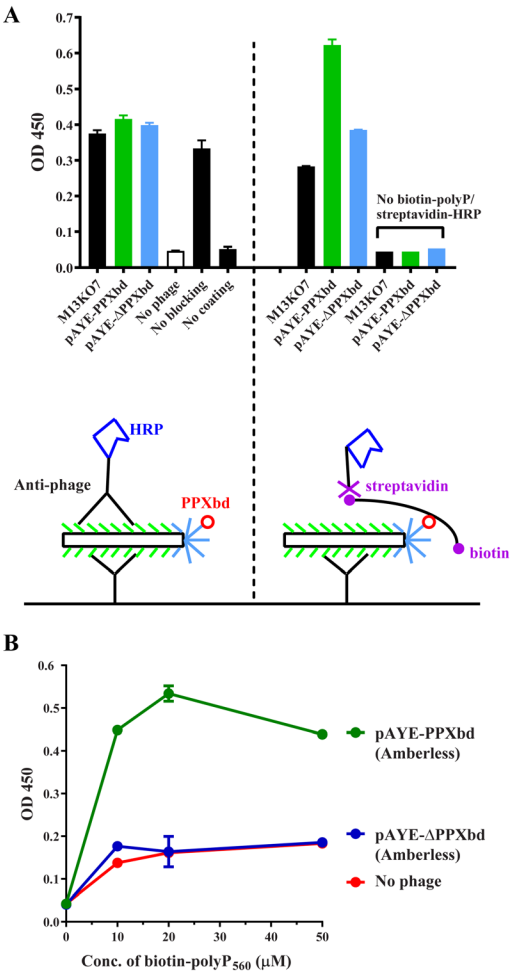

Supplementary figure 4.1 wtPPXbd expressed on phage surface binds with polyP. Sandwich ELISA was performed to test if wtPPXbd cloned into original pAYE phagemid and expressed on the phage surface can bind with polyP. Anti-phage antibody was diluted in 50 mM carbonate buffer (pH 9.6) and added into high bind microplate. A blocking step was performed using 20 mM HEPES (pH 7.4), 5% BSA and 0.05% TWEEN® 20. (A) About 10^9 M13KO7 helper phage (●), ΔPPXbd-pAYE phage with amber stop (●) and wtPPXbd-pAYE phage with amber stop (●) were added into corresponding wells. On the *left panel*, anti-phage antibody conjugated with HRP was added to the wells. On the *right panel*, 50 μM biotin-polyP$_{560}$ was preincubated with 1 μg/mL streptavidin-HRP was added to the wells. All wells were developed using TMB substrate and stopped by sulfuric acid before A450 was read. (B) M13KO7 helper phage (●), ΔPPXbd-pAYE phage without amber stop (●) and wtPPXbd-pAYE phage without amber stop (●) were added into corresponding wells. 0, 10, 20 or 40 μM biotin-polyP$_{560}$ was preincubated with 1 μg/mL streptavidin-HRP was added to the wells. All wells were developed using TMB substrate and stopped by sulfuric acid before A450 was read.

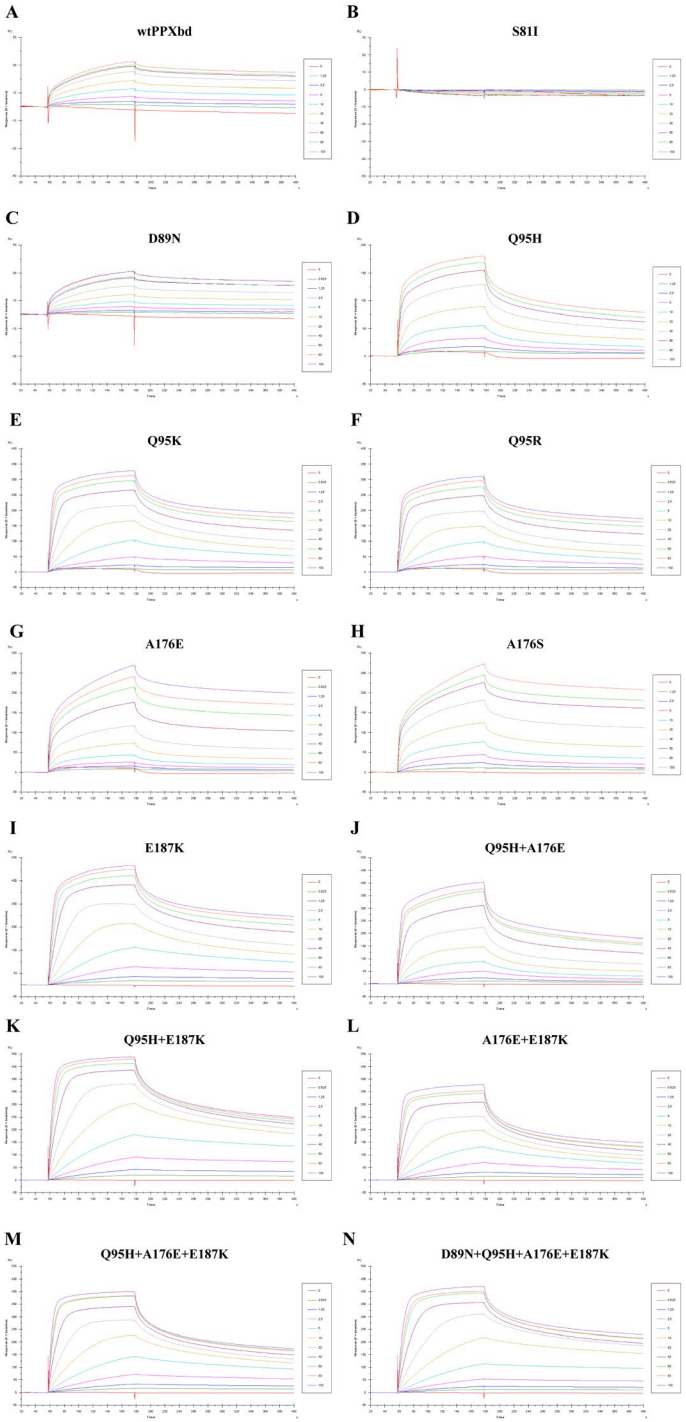

Supplementary figure 4.2 Selected PPXbd mutants had higher binding affinity towards polyP as compared with wtPPXbd. Biotin-polyP$_{560}$ was immobilized on the experimental flow cell of a SA sensor chip or a CM4 sensor chip coated with streptavidin. Each fusion protein AviTag-MBP-PPXbd containing mutations on PPXbd was diluted into various concentrations (1-100 nM) in the Biacore buffer (see Method) and flow through both reference and experimental flow cell. Maximal RU values at steady state equilibrium from the experimental flow cell was subtracted by the values from reference cell. Above were representative sensorgrams for each recombinant PPXbd mutant after reference subtraction and baseline normalization. Baseline levels were removed before the binding levels were plotted versus PPXbd concentration to obtain binding curves. Data points were fitted using the one-site ligand binding equation to obtain dissociation constants (K_d).

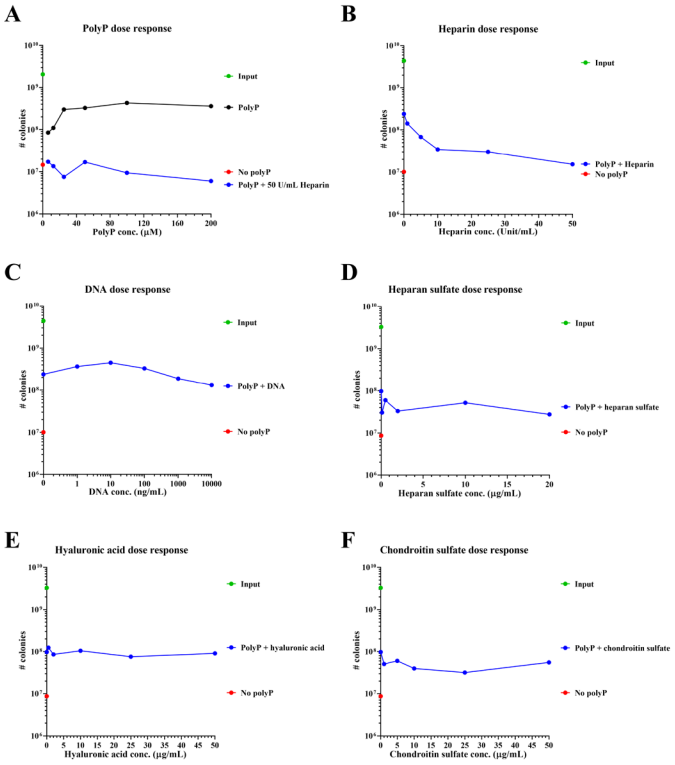

Supplementary figure 4.3 Competitors screening using wtPPXbd phage. (A) To optimize the dose of biotin-polyP$_{560}$ used for competitive selection, 0.5 mL of 0, 6.25, 12.5, 25, or 50 μM biotin-polyP$_{560}$ was added to each tube containing 30 μL of streptavidin coated Dynabeads. A negative control was also conducted by adding no biotin-polyP$_{560}$ to the beads (●). 5 x 10^9 phages mixed with 0 (black) or 50 U/mL (●) heparin were diluted in phage buffer II (see Method) and added into each tube. After 2-hour incubation, the unbound phages were washed off. The input (●) and selected phages were cleaved overnight by enterokinase and eluted. Eluted phages were tittered and plotted as the number of colony forming plaques. (B-F) 0.5 mL of 25 μM biotin-polyP$_{560}$ was added to each tube containing 30 μL of streptavidin coated Dynabeads. A negative control was also conducted by adding no biotin-polyP$_{560}$ to the beads (red). 5 x 10^9 phages were mixed with 0, 1, 5, 10, 25 or 50 U/mL heparin (B); 0, 1, 10, 100, 1000 or 10000 ng/μL mouse genomic DNA (C); 0, 0.1, 0.5, 2, 10 or 20 μg/mL heparan sulfate (D); 0, 0.5, 2, 10, 25 or 50 μg/mL hyaluronic acid (E); 0, 1, 5, 10, 25 or 50 μg/mL chondroitin sulfate (F) in phage buffer II (see Method) and added into each tube. Bound phages were prepared and tittered as described in (A).

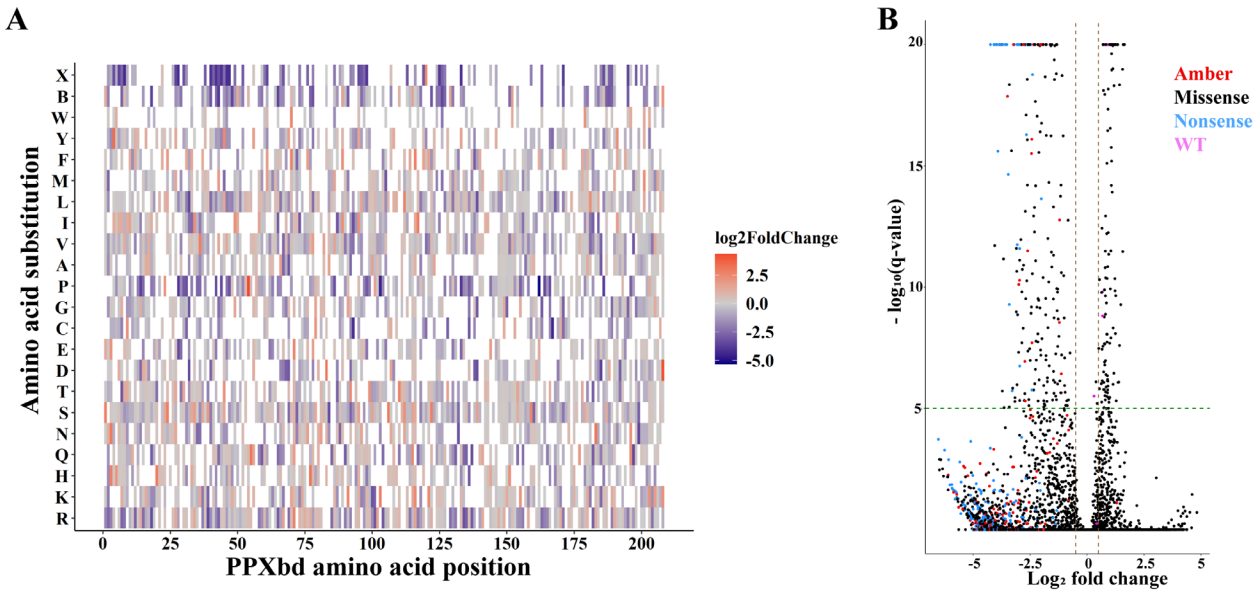

Supplementary figure 4.4 Positive selection without heparin was performed using library B. 0.5 mL of 25 µM biotin-polyP$_{560}$ was added to each tube containing 30 µL of streptavidin coated Dynabeads. 5 x 10^9 phages without any competitors were diluted in phage buffer II (see Method) and added into each tube. After 2-hour incubation, the unbound phages were washed off. The bound phages were cleaved overnight by enterokinase and eluted. DNA was extracted from eluted phages and the input library. The prepared amplicon sequencing library was submitted for HiSeq. The competitive selection NGS data was shown as heat map (A) and volcano plot (B). (A) Heat map indicating average Log_2 fold enrichment scores for PPXbd mutants selected for polyP binding without any competitors. PPXbd amino acid positions were plotted on *x-axis* and the amino acid substitutions (X for ochre or opal stop whereas B for amber stop) were plotted on *y-axis*. Enriched mutations (log_2 fold change > 0) were indicated in red, while depleted mutations (log_2 fold change < 0) were indicated in blue. White indicates amino acid substitutions that were not present in the mutational library. (B) PPXbd wild type amplicon (●), mutant amplicon with missense (●), nonsense (●), or amber stop (●) mutation was plotted as individual dot on each panel, where the log_2 fold change values of the heparin competitive selection *versus* input library were plotted on the *x-axis* and the $-log_{10}$(q-value) of the positive selection were plotted on *y-axis*.

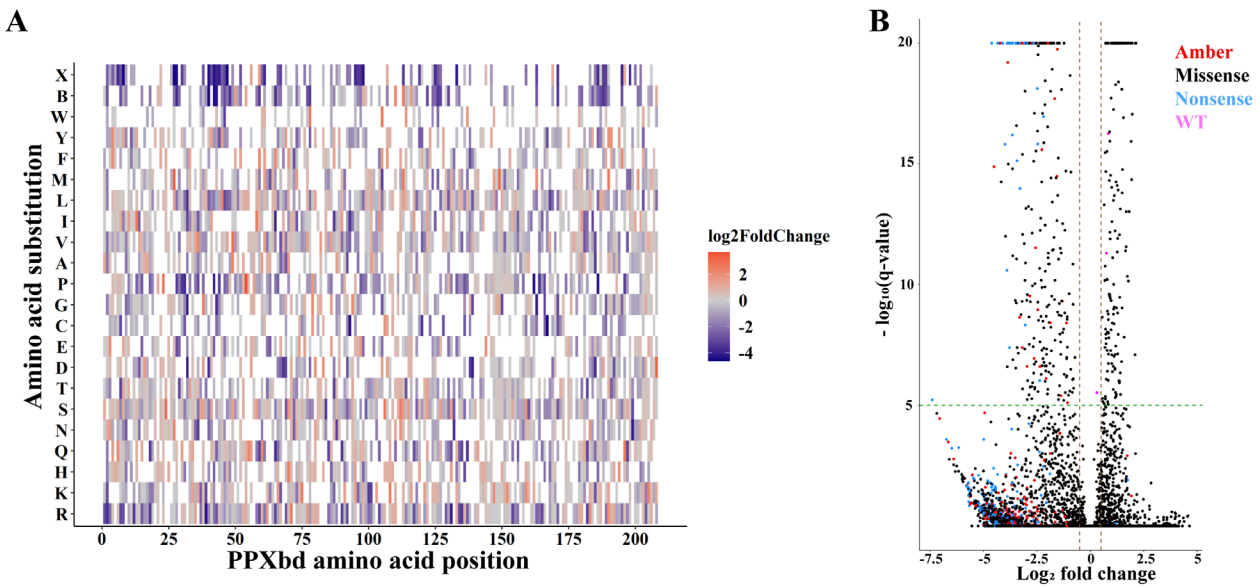

Supplementary figure 4.5 Competitive selection by high dose of heparin was performed using library B. 0.5 mL of 25 µM biotin-polyP$_{560}$ was added to each tube containing 30 µL of streptavidin coated Dynabeads. 5 x 10^9 phages mixed with 50 U/mL heparin were diluted in phage buffer II (see Method) and added into each tube. After 2-hour incubation, the unbound phages were washed off. The bound phages were cleaved overnight by enterokinase and eluted. DNA was extracted from eluted phages and the input library. The prepared amplicon sequencing library was submitted for HiSeq. The competitive selection NGS data was shown as heat map (A) and volcano plot (B). (A) Heat map indicating average Log_2 fold enrichment scores for PPXbd mutants selected for polyP binding with the competitions of 50 U/mL heparin. PPXbd amino acid positions were plotted on *x-axis* and the amino acid substitutions (X for ochre or opal stop whereas B for amber stop) were plotted on *y-axis*. Enriched mutations (log_2 fold change > 0) were indicated in red, while depleted mutations (log_2 fold change < 0) were indicated in blue. White indicates amino acid substitutions that were not present in the mutational library. (B) PPXbd wild type amplicon (●), mutant amplicon with missense (●), nonsense (●), or amber stop (●) mutation was plotted as individual dot on each panel, where the log_2 fold change values of the heparin competitive selection *versus* input library were plotted on the *x-axis* and the $–log_{10}$(q-value) of the positive selection were plotted on *y-axis*.

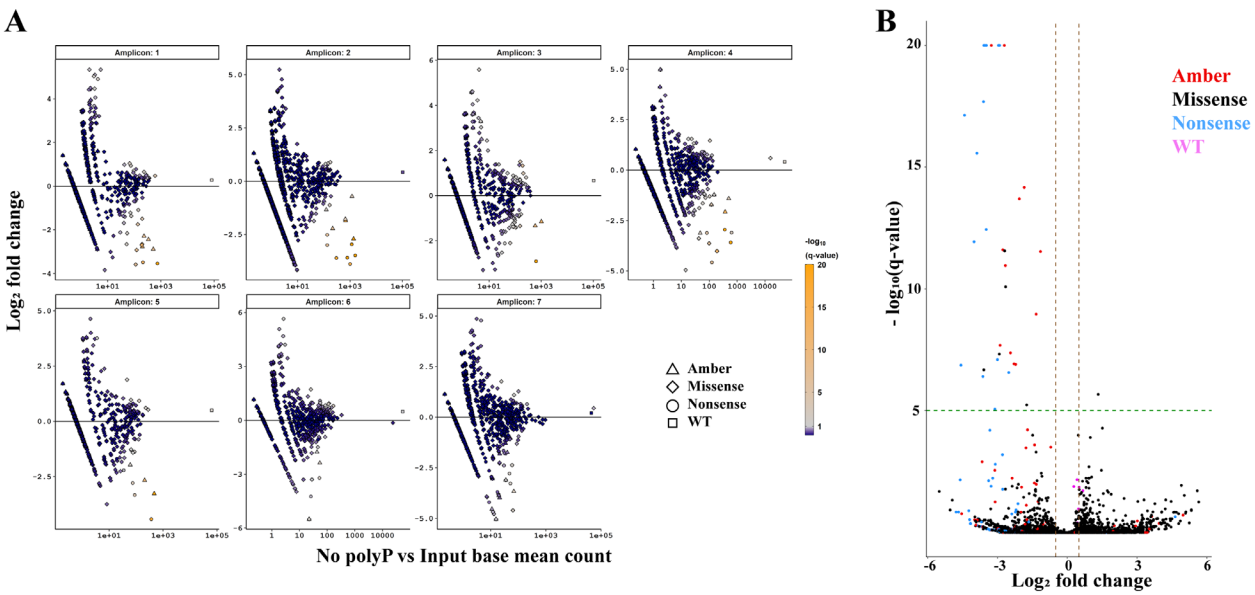

Supplementary figure 4.6 Negative selection without polyP was performed using library B. As a negative control, no biotin-polyP$_{560}$ was added to each tube containing 30 µL of streptavidin coated Dynabeads. 5 x 10^9 phages without any competitors were diluted in phage buffer II (see Method) and added into each tube. After 2-hour incubation, the unbound phages were washed off. The bound phages were cleaved overnight by enterokinase and eluted. DNA was extracted from eluted phages and the input library. The prepared amplicon sequencing library was submitted for HiSeq. The competitive selection NGS data was shown as MA plot (A) and volcano plot (B). (A) PPXbd wild type amplicon (□), or mutant amplicon with missense (◇), nonsense (○), or amber stop (△) mutation was plotted as individual dot on each panel, where the base mean counts of the input phage library were plotted on the *x-axes* and the log2 fold change values of the heparin competitive selection *versus* input library were plotted on *y-axes*. (B) PPXbd wild type amplicon (●), mutant amplicon with missense (●), nonsense (●), or amber stop (●) mutation was plotted as individual dot on each panel, where the $\log_2$ fold change values of the heparin competitive selection *versus* input library were plotted on the *x-axis* and the –$\log_{10}$(q-value) of the positive selection were plotted on *y-axis*.

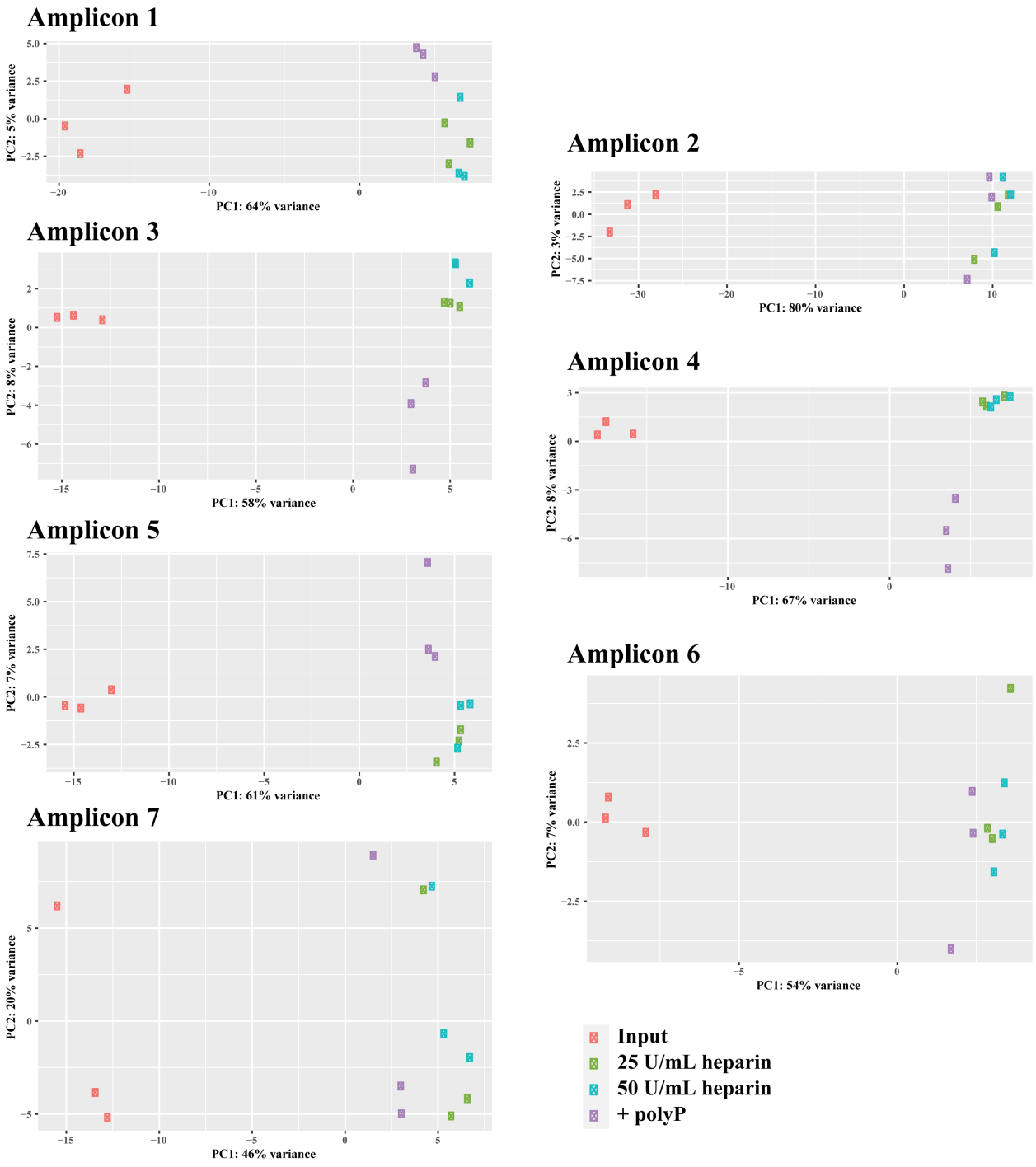

Supplementary figure 4.7 Principal component analysis revealed potential heparin interaction domains on PPXbd. Hiseq data from the competitive selection using phage library B were analyzed in R environment. The negative control group was removed and the rest of the groups were pooled together for DESeq2 analysis.[248] Principal component analysis was performed and data for individual amplicon from input library (☒), positive selection (☒), 25 U/mL heparin (☒) and 50 U/mL heparin (☒) competitive selection (each with biological triplicates) were plotted with PC1 variance on the *x-axes* and PC2 variance on the *y-axes*.

Supplementary table 4.1 *E. coli* PPXbd amino acid sequence.

MEGRFRHQDVRSRTASSLANQYHIDSEQARRVLDTTMQMYEQWREQQPKLAHPQLEALLRW AAMLHEVGLNINHSGLHRHSAYILQNSDLPGFNQEQQLMMATLVRYHRKAIKLDDLPRFTLF KKKQFLPLIQLLRLGVLLNNQRQATTTPPTLTLITDDSHWTLRFPHDWFSQNALVLLDLEKEQ EYWEGVAGWRLKIEEESTPEIAA*

Supplementary table 4.2 Primers for phage display library construction

Name	Sequence (5' – 3')
Phage library primer - fwd	ttctcggcccagccggccgg
Phage library primer - rev	gtccttgtagtcaccaccacctgcggcc
Mutation frequency PCR fwd	tgttctgctgttcctgctg
Mutation frequency PCR rev	cgtcatcgtccttgtagtcac

Supplementary table 4.3 Primers for NGS library preparation.

Name	Sequence (5' – 3')
Amplicon 1 fwd	NNNNNN-tcatgctgccggctttctc
Amplicon 1 rev	NNNNNN-gaacacgacgcgcttgct
Amplicon 2 fwd	NNNNNN-gaaccagtaccacatcgacagc
Amplicon 2 rev	NNNNNN-agcatcgccgcccaac
Amplicon 3 fwd	NNNNNN-acccgcagctggaagc
Amplicon 3 rev	NNNNNN-gctgttcttggttgaaacccg
Amplicon 4 fwd	NNNNNN-cgtcacagcgcgtacattc
Amplicon 4 rev	NNNNNN-cttaaacagggtgaaacgcgg
Amplicon 5 fwd	NNNNNN-cgttatcaccgtaaggcgatca
Amplicon 5 rev	NNNNNN-cggggtggtggtcgc
Amplicon 6 fwd	NNNNNN-ttctgctgaacaaccaacgtca
Amplicon 6 rev	NNNNNN-ccttctccagatccagcagc
Amplicon 7 fwd	NNNNNN-tagccagaacgcgctgg
Amplicon 7 rev	NNNNNN-ttgtagtcaccaccacctgc

Chapter 5 Generation and Characterization of a Transgenic Mouse Model with a Point Mutation Destroying the Active Site of Coagulation Factor XII

5.1 Introduction

FXII, as the key serine protease zymogen in the contact pathway and plays important roles in linking blood clotting and inflammation.[4,111,115] Similar to other serine protease zymogens in the clotting cascade, FXII contains a heavy chain responsible for surface binding and a light chain containing the protease domain, which consists of a catalytic triad (His, Asp and Ser).[53,63,253] The contact pathway is activated by exposure of blood to negatively charged molecules or suitable surfaces.[131] Upon activation, the serine protease FXIIa could further activate its substrate FXI and PK, generating FXIa and PKa.[60,135] PKa cleaves its substrate and cofactor HK to produce BK, which serves as an inflammatory mediator.[140] Dysregulation of BK generation may lead to life-threatening diseases or allergic reactions, such as hereditary angioedema[142] and anaphylactic shock.[254] On the other hand, the activated protease FXIa triggers the intrinsic pathway of coagulation. Some recent studies found associations between the FXII-dependent FXI activation with thrombosis.[42-45,171] Interestingly, FXII[39,40] or PK[41] deficient individuals or animal models do not have bleeding tendencies, implying that FXII did not participate in the normal hemostasis process. Therefore, targeting FXII holds promise for developing new anti-thrombotic drugs without interfering with hemostatic function. Apart from these functions, FXIIa is also part of the complement cascade,[60,255] and the fibrinolysis pathway.[256] There are multiple activators of FXII and the contact pathway, including polyP,[121,169] unfolded proteins,[128] neutrophil extracellular traps (NETs),[257] nucleic acids[117,128,187] and potentially β-amyloid.[258-260] Since more functions of FXII

and FXIIa has been discovered, generating a reliable FXII deficient mouse model would be helpful for scientists to study the FXII-related pathologic mechanisms *in vivo*.

One of the most widely used FXII deficient mouse models was generated by replacing exon 1 and exon 2 of the *F12* gene with the neomycin cassette.[261] Briefly, the mouse *F12* gene was disrupted in embryonic stem cells (ESC) by homologous recombination using a replacement-targeting vector containing pTKNeo and thymidine kinase expression cassettes. The correct ESC clone was injected into C57Bl/6J blastocysts to generated chimeric mice. Male chimeric mice transmitting the targeted mutation into the germ line were bred with female mice from C57Bl/6J or 129X1/SvJ strains to establish the FXII knock-out (KO) model. Similarly, another transgenic mouse model was generated by replacing exons 3-8 of the *F12* gene with NEO.[262] In both of these mouse models, the activated partial thromboplastin time (aPTT) of homozygous FXII deficient mice was markedly elongated compared to the heterozygous and wild-type litter mates. Interestingly, a recent study showed that FXII may play a more sophisticated role in vivo that has not been previously appreciated.[263] FXII zymogen was demonstrated to stimulate integrin expression on neutrophil surfaces, increase intracellular Ca^{2+} and promote extracellular DNA release. The sum of these activities contributed to neutrophil cell adhesion, migration, and release of neutrophil extracellular traps (NETs) in a process called NETosis. These activities were independent of FXIIa enzymatic activity and contact activation, implying a potential drawback of current FXII KO mouse models. Neutrophils not only participate in the inflammatory response, they interact with endothelial cells and platelets to play significant roles in the coagulation system.[264,265] Thus, depleting the entire FXII protein may alter neutrophil functions which may interfere with blood clotting and inflammation. In this study, we aimed to generate a new transgenic mouse strain where a point mutation will be introduced into the mouse *F12* gene to

inactivate its protease activity. The entire heavy chain of FXII was maintained while in the light chain, the Ser in the catalytic triad was mutated into Ala so that FXIIa would no longer be an active enzyme.

Instead of the conventional homologous recombination method to generate the genetically modified animal model, a genome editing tool that allows more precise modification of DNA sequence was chosen in this study to generate this transgenic mouse model. Zinc finger nucleases,[266] transcription activator-like effector nucleases (TALENs)[267] and clustered regularly interspaced short palindromic repeats (CRISPR)-associated (Cas) nucleases[268,269] are genome engineering tools for generating genetically modified animals via microinjection into fertilized eggs.[270] CRISPR/Cas9 has been widely used in gene editing in the past decade that allows precise editing at specific genomic loci.[271-273] In order to precisely control the point of mutation, a single-stranded oligodeoxynucleotide (ssODN) has been used as donor template in combination with the engineered nucleases while introduced into zygotes, since in mice, targeted knock-in (KI) with ssODN donors via homology-directed repair (HDR) has been reported to achieve high efficiency.[274,275]

5.2 Materials and methods

Ethics Statement

All microinjection, egg transplantation, breeding and experimental procedures using mice were approved by the Institutional Committee on the Use and Care of Animals for the University of Michigan (protocol number PRO00008681). Mice were housed in specific pathogen-free conditions with ad libitum access to food and water.

Materials

Cas9 mRNA was from PNABio (Thousand Oaks, CA), Ens-Cas9 Nuclease, T7 High Scribe, ApaI, NcoI, XbaI, Phusion polymerase and PCR cloning kit were from New England Biolabs (Ipswich, MA). KOD hot start polymerase and bovine hemoglobin were from Millipore Sigma (Burlington, MA). RNA clean up kit was from Zymo Research (Irvine, CA). DNA oligonucleotides used for gRNA synthesis, all primers, Invitrogen Maxiscript™ T7 kit, Phire Tissue Direct PCR Master Mix were from Thermo Fisher Scientific (Waltham, MA). ssODNs were from Integrated DNA Technologies IDT (Coralville, IA). HB101 Competent cells were from Molecular Innovations (Novi, MI). QIAquick PCR Purification kit was from Qiagen (Hilden, Germany). SYBR™ Safe DNA gel stain was from Invitrogen (Carlsbad, CA). Drabkin′s reagent was from RICCA Chemical Company (Arlington, TX). Owren-Koller buffer and the STA-PTTA (aPTT reagent) was from Diagnostica Stago, Inc (Parsippany, NJ). Human immunodepleted FXII deficient plasma was from Haematologic Technologies, Inc (Essex, Vermont). FXII KO mice were a generous gift from David Gailani's lab.

sgRNA design and synthesis

Murine *F12* genomic sequence was obtained from Ensembl.org (ENSMUSG00000021492). Several online sgRNA design tools were used to screen guide RNAs including Broad Institute, www.deskgen.com and http://crispor.tefor.net/. On-target and off-target scores were calculated using published methods.[276,277] The principle is to have maximum on-target score and minimum off-target sites, close to targeted nucleotides, ideally within 10 bp. Other considerations for choosing guides included targeted nucleotides serving as protospacer adjacent motif (PAM) or PAM proximal, which would prevent Cas9 cleavage after the desired point mutations were introduced. Target specific oligos and universal oligos (Supplementary table 5.1)

were assembled in a PCR reaction to generate the DNA templates for *in vitro* transcription of the sgRNA as previously described.[271]

ssODN design

We included two nucleotide mutations in the repaired template (Figure 5.1A). One T > G mutation was introduced in a TCC codon to create the S545A mutation, which "inactivated" the active site Ser545 in FXII. Another G > T mutation was also knocked into the following PAM region. This silent mutation did not change the translation of Gly546, but destroyed the PAM site. Since PAM site recognition is required for Cas9 to cleave the dsDNA, the strategy of including the silent mutation in the ssODN was to prevent further cleavage of the modified gene product by Cas9, improving the gene editing efficiency. In addition, the silent mutation also destroyed the original cleavage site (GGGCC'C) for the restriction enzyme, ApaI, which could be used for RFLP genotyping.

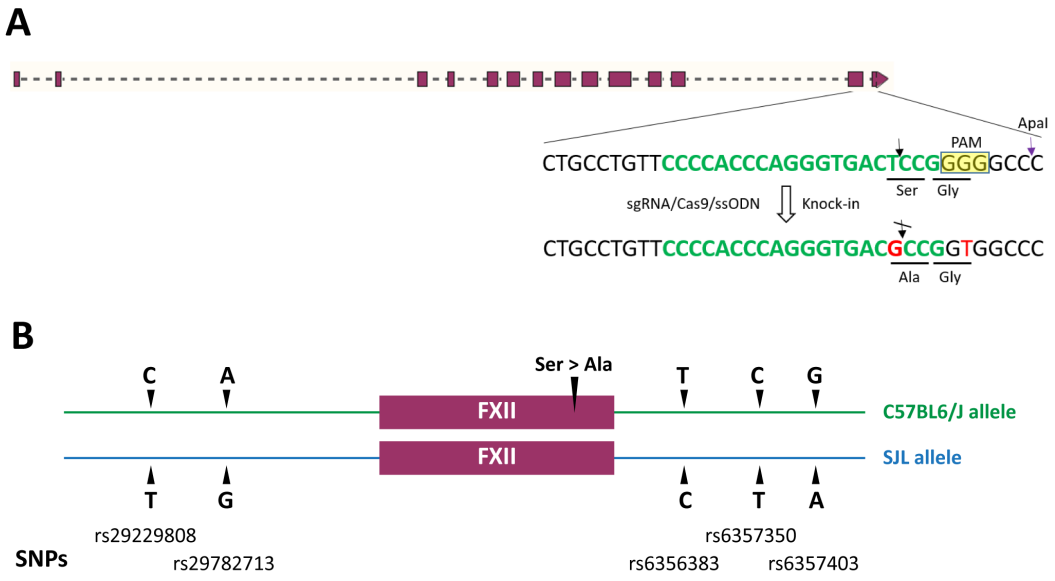

Figure 5.1 General scheme of generating FXII-S545A transgenic mouse model. (A) CRISPR/Cas was used in combination with a repair template (ssODN) for precise genetic modification. Located on the last exon of *F12* gene, the nucleotides TCC encode for the FXIIa active site Ser545. The designed sgRNA/Cas9 recognized the highlighted PAM sequence GGG after Ser545. In wild-type mice, the next amino acid residue after Ser545 should be Gly546. The presence of ssODN not only changed nucleotides TCC to GCC (S545A mutation), but also introduce a silence G > T mutation in the following PAM sequence. (B) An illustrative figure of SNPs distribution along the chromosomes in G0 founders were shown above. Two selected SNP loci were upstream of the *F12*

gene whereas three SNP loci were downstream of the *F12* gene. All five SNP loci contained different nucleotide sequences among C57BL6/J species and SJL species.

Repair template was designed to introduce desired point mutations in specific genomic locus. ssODN serving as repair template was chemically synthesized (Supplementary table 5.1). ssODN was complementary to the "no PAM" strand. ssODN contained asymmetric homology arms. A silent mutation was introduced to generate restriction enzyme cleavage site to ease genotyping of modified animals. Cleavage efficiency was measured in vitro using Cas9 protein according to the manufacture's instruction.

Microinjection

Zygote preparation and manipulation, microinjection and embryo transfer to pseudopregnant females followed standard methods.[278] To prepare microinjection solution, 100-200 ng/μL Cas9 nuclease, 50-100 ng/μL gRNA, and 100 ng/μL ssODN were mixed in TE buffer (20 mM Tris-HCl, 1 mM EDTA, pH7.4), incubated at room temperature for 10 min, and centrifuged at 13000 rpm for 5 min.[273] Supernatant was stored at - 80ºC or on ice for microinjection. Pronuclear alone or both pronuclear and cytoplasmic injected zygotes were transferred to pseudopregnant females at 2-cell stage. Microinjection was performed at the Transgenic Core of the University of Michigan. Mice were housed in ventilated racks with automatic watering and ventilated cages. Zygotes for microinjection were obtained by mating B6SJLF1 (Jackson Stock Number 100012) female mice with B6SJLF1 males. G0 founders were backcrossed with C57BL/6J (Jackson Stock Number 000664) mice to establish lines.

Genotyping of founder mice by deep sequencing

Since the G0 mice are all mosaics, the PCR products of the tail snip samples from selected G0 founders were submitted to GENEWIZ for next-generation sequencing to identify the founder mice that contain the correct mutations. The G0 founder mice containing the desired point

mutations were backcrossed with C57BL6/J mice for at least 7 generations to obtain the FXII-S545A transgenic strain with C57BL6/J background.

Due to the mixed genetic background of our founder mice (B6SJLF1), it was possible that the knock-in mutation was on either the SJL allele or C57BL6/J allele. If the S545A mutation was on the SJL allele, the transgenic strain would never be on a pure C57BL6/J background, since the flanking region of *F12* genome would remain on SJL background. In order to obtain the transgenic mouse line on a pure C57BL6/J background, several SNPs (rs29229808, rs29782713, rs6356383, rs6357350, rs6357403) upstream and downstream of the *F12* gene were selected for screening of G0 founders containing the S545A mutation on C57BL6/J allele (Figure 5.1B). The DNA of F1 pups from each G0 founder were extracted and each SNP region was amplified by PCR and sequenced.

Genotyping by PCR & restriction fragment length polymorphism (RFLP)

For G0 founder mice, F1, F2 and N2 pups, mouse tail tip biopsies were collected between 2-3 weeks of age by clean scissors and incubated in tissue lysis buffer (100 mM Tris, 5 mM EDTA, 200 mM NaCl, 0.2% SDS, pH8.0) with Proteinase K (0.4 mg/mL) at 55ºC overnight. Genomic DNA was isolated by isopropanol precipitation followed by washing with 70% ethanol. PCR primers were designed using Primer 3[279] and were listed in Table S1. PCR followed standard conditions. PCR products were digested using restriction enzyme ApaI and examined on 1-2% agarose gel. Those G0 founders' showing cleaved bands on the gel were sent for Sanger sequencing directly, or cloned into a vector using PCR cloning kit. 8-24 clones were screened and RFLP positive clones were sent for Sanger sequencing. For F1 or N2 progenies, PCR products were purified and submitted for Sanger sequencing. Sequencing alignments were performed using SnapGene® software (GSL Biotech).

For all the progenies of FXII-S545A mice, mouse tail tip biopsies or pulled hair containing follicles were collected by clean scissors or forceps, incubated in 20 μL sample dilution buffer supplemented with 0.5 μL DNA release additives (both in Phire Tissue Direct PCR Master Mix) at room temperature for 5-120 minutes. Samples were then boiled at 98ºC for 2-5 minutes to inactivate any nucleases released from tissue lysis. PCR followed by the instruction manual was conducted and products were digested using ApaI at room temperature before resolved on agarose gel. For FXII KO mice, a similar approach was used for sample preparation. PCR (primers[261] in Supplementary table 5.1) products were directly resolved on agarose gel without restriction digestion.

Background selection by single nucleotide polymorphisms (SNPs)

To ensure obtaining FXII-S545A mutant mice on a pure C57Bl6/J background after 10 rounds of backcrossing, the genetic background of F1 pups from each G0 founders were tested. 2-3 SNPs in Mouse Genome Informatics (MGI) that showed difference between C57Bl6/J and SJL strain were selected before and after FXII-S545A locus on mouse genome. These loci containing individual SNPs were amplified using PCR and sequenced (primers in Supplementary table 5.2).

Blood collection & plasma preparation

Based on previous studies, tail cut and heart puncture appeared to result in artificial coagulation activation due to tissue damage, and therefore *vena cava* puncture was recommended.[280] In this study, blood was draw from the caudal vena cava. Mice were anesthetized with an inhaled isoflurane-oxygen mixture and placed on a heated surgical tray. The abdominal cavity was opened, and blood was drawn from the caudal vena cava into a syringe containing 50 μL 3.1% sodium citrate. If more than 450 μL whole blood were drawn, extra citrate was then added to make a final concentration of 10% citrate v/v. Citrated blood (kept at 37°C for

no longer than 40 minutes) was centrifuged twice at 500 x g and once at 2000 x g to remove blood cells. Normal plasma samples were frozen at -80°C.

Tail bleeding assays

Mice were anesthetized with an inhaled isoflurane-oxygen mixture and placed on a heated surgical tray. The tail tip was immersed in a 15-mL plastic test tube filled with 37°C 0.9% saline. The distal 5 mm of tail was then transected with a razor blade and re-immersed in 37°C saline for 12.5 minutes. Bleeding time was measured with a stopwatch for the entire time frame, after which the blood samples were pelleted at 500*g* for 10 minutes at room temperature and stored at -80°C. The frozen blood pellet was resuspended in 2 mL Drabkin's Reagent and incubated at room temperature for 15 minutes with vortex. Amount of hemoglobin lost was quantified by comparing the absorbance of the samples at 540 nm to a standard curve of bovine hemoglobin in Drabkin's reagent.

Plasma clotting assays

Plasma clotting times were quantified at 37°C by using a STart4 coagulometer (Diagnostica Stago). 50 µL of plasma sample was pipetted into a prewarmed coagulometer cuvette with magnetic balls and incubated for 1 minute, after which 50 µL of prewarmed aPTT reagent was added and allowed to incubate for exactly 3 minutes at 37°C. Clotting was initiated by the addition of 50 µL of prewarmed 25 mM $CaCl_2$.

FXII activity tests

Pooled normal plasma from wild-type C57BL6/J mice were diluted with Owren-Koller buffer into 0.078%, 0.156%, 0.3125%, 0.625%, 1.25%, 2.5%, 5%, 10% and 20% v/v for use as standard samples. 15 µL of plasma samples from individual FXII-S545 mouse were diluted with 135 µL of Owren-Koller buffer. 50 µL of diluted plasma samples or standard samples were mixed

and prewarmed with 50 μL of human FXII deficient plasma before aPTT reagent was added. Plasma clotting times were then quantified.

$FeCl_3$-induced thrombosis in mouse carotid arteries

Mice were anesthetized by using an inhaled isoflurane-oxygen mixture and placed on a heated surgical tray. The left carotid artery was exposed via a midline cervical incision and blunt dissection, and blood flow was monitored with a Doppler vascular flow probe (Transonic 0.5PSB) connected to a perivascular flowmeter (Transonic TS420). To induce thrombosis, two 1 × 2-mm pieces of filter paper (Whatman GB003) saturated with freshly prepared 7.5% anhydrous $FeCl_3$ in saline were applied to the deep and superficial surfaces of the artery. After 5 minutes, the filter papers were removed and the vessel was irrigated with saline. Blood flow was monitored from $FeCl_3$ application for 30 minutes or until occlusion, defined as no detectable flow for 1 minute. Mice were then euthanized by cervical dislocation while still under anesthesia. Flow data were interpreted with LabScribe2 (iWorx Systems). Statistical analyses were performed by using GraphPad Prism 8. Unless otherwise noted, data throughout this study are reported as mean ± standard error of the mean.

5.3 Results

In this study, we used the CRISPR/Cas system in combination with an ssODN to precisely modify the *F12* gene at specific locations.

Selection of FXII-S545A G0 founder mice containing mutations on C57BL6/J allele

The chimeric G0 founders were backcrossed with wild-type C57BL6/J mice to produce F1 pups. Those who had germline transmission of the S545A mutation was selected by genotyping F1 pups. Out of all three G0 founders containing the correct mutation confirmed by deep sequencing, one did not have germline transmission of the mutant gene and one had the mutation

on the SJL allele. Only one had the mutation on C57BL6/J allele and had germline transmission, whom all the progeny mice were produced from and used in this study.

Genotype characterization of FXII-S545A mice

The F1 mice were intercrossed to produce F2 mice and backcrossed with wild-type C57BL6/J mice to produce N2 mice. F1, F2 and N2 FXII-S545A transgenic mice were genotyped by Sanger sequencing (Figure 5.2A). The three genotypes FXII-S545A$^{S/S}$, FXII-S545A$^{S/A}$, and FXII-S545A$^{A/A}$ showed distinctive peak patterns on the chromatograms. The sequencing result for both FXII-S545A$^{S/S}$ and FXII-S545A$^{A/A}$ mice showed clear single peaks at the mutant positions, although FXII-S545A$^{A/A}$ had a T > G mutation at Ser545 and the silent G > T mutation at the following PAM region. The sequencing result for the heterozygous FXII-S545A$^{S/A}$ mice showed overlapping peaks at these two positions, representing the wild-type allele and the mutant allele. This result demonstrated the linkage of these two mutations, suggesting that for mice containing the S545A mutation should also contain the silent mutation.

For the progeny mice that resulted from intercrossing or backcrossing N2 mice, genotyping was performed using RFLP by ApaI (Figure 5.2B). The PCR product from a wild-type *F12* gene would be cleaved by ApaI, generating 2 lower bands, but those from the S545A mutant *F12* genes would not be cleaved by ApaI, leaving an intact upper band. Therefore, the heterozygous FXII-S545A$^{S/A}$ mice showed all three bands. There were no observable defects or distinctive phenotypes among all three genotypes and the genotype ratio between wild-type, heterozygous and homozygous litter mates was roughly 1:2:1 (data not shown). In addition to the FXII-S545A mutant mice being generated in this study, the currently available FXII-KO mice were used as a positive control. Genotyping result of FXII-KO mice was consistent with previously published data (Figure 5.2C).[261]

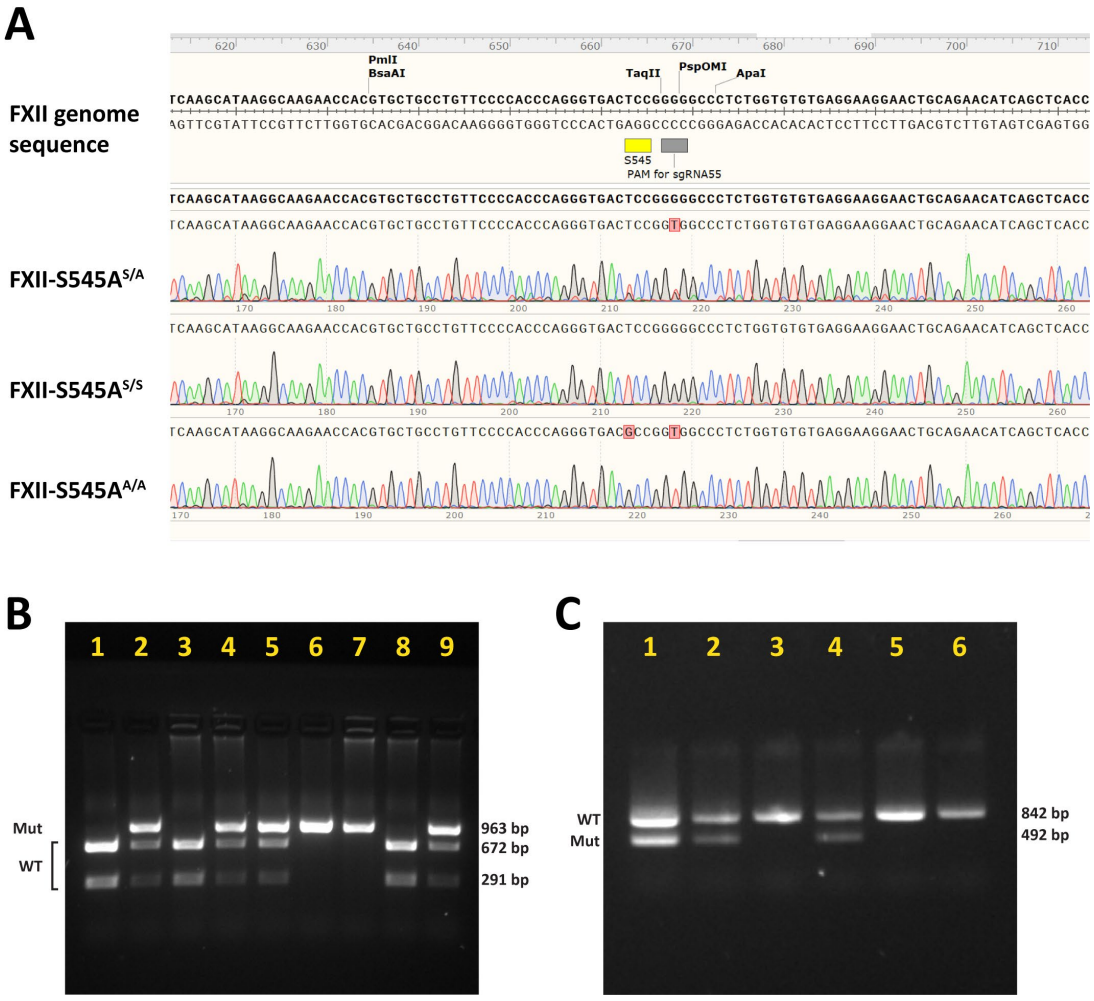

Figure 5.2 Genotype of FXII-S545A transgenic mice. (A) Sanger sequencing result distinguished different genotypes of FXII-S545A mice. Mice tail snips from all G0 founder mice, F1, F2 and N2 progenies were collected and DNA was extracted. FXII S545 region was amplified by PCR using standard protocol and submitted for Sanger sequencing. Sequences were aligned with wild-type *F12* genome DNA. Data were from representative FXII-S545A litter mates. (B) RFLP gel check confirmed genotypes of all progenies of the N2 generation mice. Mouse genomic DNA was extracted either from tail snips or from pulled hair. PCR products (963 bp) were digested by restriction enzyme ApaI. The wild-type *F12* gene will be cleaved into two fragments (672 bp and 291 bp) whereas the mutant gene will not be cleaved. Data were from representative FXII-S545A litter mates. (C) PCR gel check was used to confirm the genotypes of all FXII-KO mice. Mouse genomic DNA was extracted either from tail snips or from pulled hair. Three PCR primers were used and the PCR products from the wild-type *F12* gene showed a longer band (842 bp) whereas in the FXII-KO allele, PCR products showed a shorter band (492 bp). Data were from representative FXII-KO litter mates.

Loss of FXIIa enzymatic activity did not affect hemostatic function (tail bleeding)

FXII deficient humans do not show any increased bleeding tendency.[39,40] Previous studies using FXII-KO mice also indicated that there was no spontaneous or excessive injury-related bleeding.[45] Consistent with the result from previous studies, our FXII-S545A$^{A/A}$ mice did not show

prolonged bleeding time compared with FXII-S545A$^{S/A}$ and FXII-S545A$^{S/S}$ litter mates (Figure 5.3A). The amount of blood loss between all genotypes was not significantly different either (Figure 5.3B). The Spearman's correlation coefficient between bleeding time and total blood loss was calculated to be 0.52, indicating that there were no strong association between these two variables (Figure 5.3C). These results demonstrated that knocking out FXIIa enzymatic activities did not cause excessive injury-related bleeding.

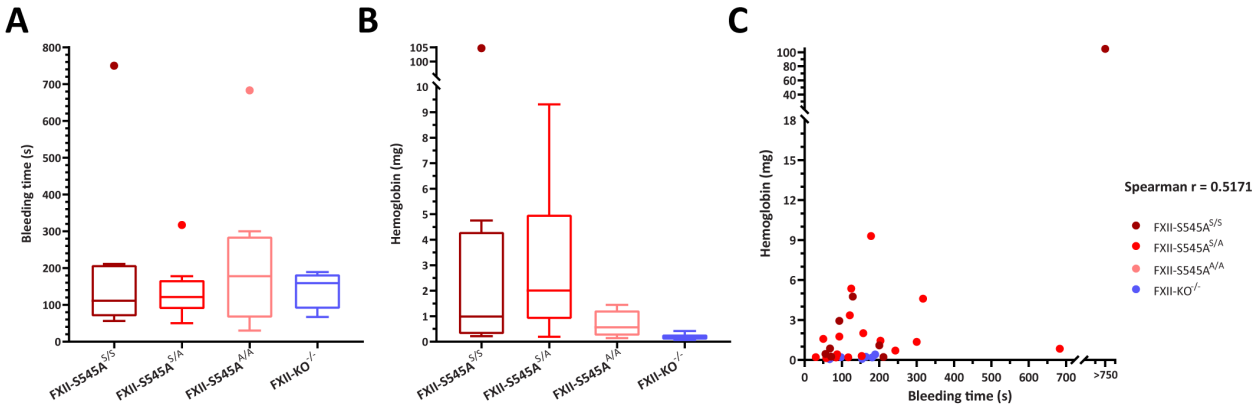

Figure 5.3 FXII-S545A mice did not show increased bleeding in the tail bleeding model. The FXII-S545A$^{S/S}$, FXII-S545A$^{S/A}$, FXII-S545A$^{A/A}$ litter mates and FXII-KO$^{-/-}$, which was included as a control, were anesthetized. The distal 5 mm of tails were then transected and immersed into prewarmed saline. (A) Bleeding time was measured in a 12.5-minute timeframe and plotted as a box-and-whisker plot ($n \geq 5$). Outliers were illustrated as individual dot. (B) Total blood loss was quantified as the amount of hemoglobin in the blood using Drabkin's reagent. The absorption data were interpreted using a bovine hemoglobin standard curve and plotted as a box-and-whisker plot ($n \geq 5$). Outlier was illustrated as individual dot. (C) For each individual mouse, the amount of blood loss expressed by the amount of hemoglobin in the blood was plotted on the *x-axis* and the bleeding time of each mouse was plotted on the *y-axis*. The Spearman's correlation coefficient r for all data points was calculated.

Loss of FXIIa enzymatic activity resulted in elongated clotting time and loss of FXII plasma activity

The aPTT coagulation assay was widely used in clinical diagnosis and FXII deficient individuals were discovered to have elongated aPTT clotting time.[281] We demonstrated that the prolonged clotting time was at least partially dependent on FXIIa enzymatic activity. FXII-S545A$^{S/S}$ mice had an average clotting time of 27.60 ± 0.70 seconds, FXII-S545A$^{S/A}$ mice had an average clotting time of 32.25 ± 1.39 seconds, whereas FXII-S545A$^{A/A}$ mice had a prolonged

average clotting time of 42.68 ± 1.085 seconds (Figure 5.4A). Using an aPTT assay based on human FXII-deficient plasma, it was determined that FXII-S545A$^{A/A}$ mice had a deficient FXII plasma activity (4.46 ± 0.75% of the FXII level of wild-type mice) as compared with FXII-S545A$^{S/A}$ and FXII-S545A$^{S/S}$ litter mates whose average FXII plasma activity were 35.62 ± 4.03% and 89.58 ± 10.48%, respectively (Figure 5.4B).

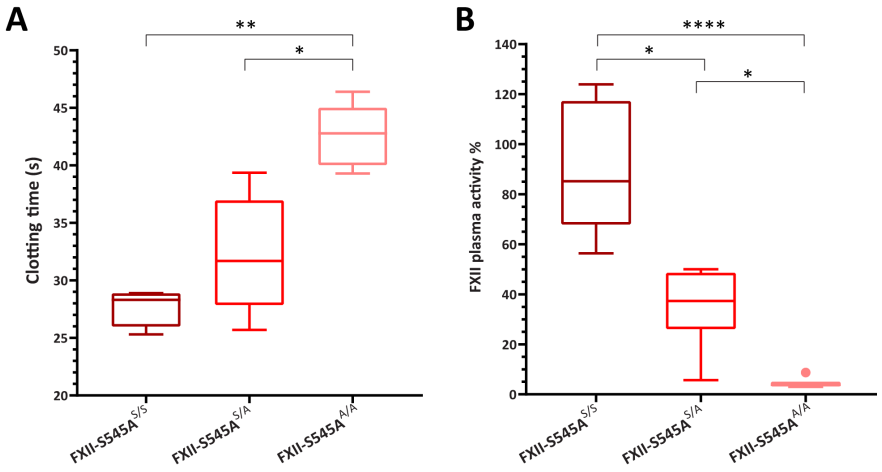

Figure 5.4 FXII-S545A mice showed elongated aPTT clotting time and depleted FXII plasma activity. The FXII-S545A$^{S/S}$, FXII-S545A$^{S/A}$, FXII-S545A$^{A/A}$ litter mates were anesthetized. Blood was collected from caudal vena cava and the plasma samples were prepared freshly. (A) APTT clotting assays were performed and the clotting times of each mouse were plotted as a box-and-whisker plot. (B) FXII plasma activity were quantified using human FXII depleted plasma and normalized to a standard curve generated by pooled normal plasma collected and prepared from wild-type C57BL6/J mice. Data were plotted as a box-and-whisker plot and an outlier was illustrated as individual dot. Data from both panels were analyzed by the non-parametric Kruskal–Wallis test followed by Dunn's multi comparisons test ($n \geq 5$). Statistical significance was indicated by Asterisk. Clotting assays were performed by Dr. Stephanie A Smith from Morrissey lab.

FXII-S545A mice demonstrated thromboprotective effect

A preliminary thrombosis experiment was conducted to test if this new transgenic mouse model that lacks FXIIa enzymatic activity would be protected from thrombosis. In the $FeCl_3$-induced carotid artery thrombosis model, none of the FXII-S545A$^{A/A}$ mice had occluded arteries over the 30-minute timeframe (Figure 5.5). Similar thromboprotective effect has been seen in FXII KO mice.[45] There was no significant difference between the clotting times of FXII-S545A$^{S/A}$ and

FXII-S545A$^{S/S}$ mice. These data suggested that the thrombus formation in the artificially induced thrombosis model was mediated by FXIIa enzymatic activity, rather than FXII zymogen.

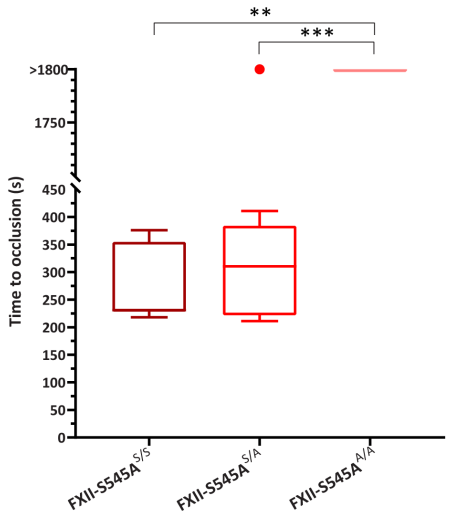

Figure 5.5 FXII-S545A transgenic mice demonstrated thromboprotective effect in a FeCl3-induced thrombosis model. The FXII-S545A$^{S/S}$, FXII-S545A$^{S/A}$, FXII-S545A$^{A/A}$ litter mates were anesthetized and 7.5% $FeCl_3$ solution was used to induce thrombosis in the carotid arteries of individual mouse. Blood flow was detected by a Doppler vascular flow probe and monitored for 30 minutes. Time to occlusion was plotted as a box-and-whisker plot. Data from both panels were analyzed by the non-parametric Kruskal–Wallis test followed by Dunn's multi comparisons test ($n \geq 2$). Statistical significance was indicated by Asterisk. Thrombosis experiments were performed by Dr. Stephanie A Smith from Morrissey lab.

5.4 Discussion

In this study, a new transgenic mouse model that lacks of FXIIa enzymatic activity was generated and briefly characterized. We demonstrated that FXII-S545A mice did not have increased injury-related bleeding tendency, but had a prolonged aPTT clotting time and loss of FXII plasma activity. We also found that the homozygous mice showed a thromboprotective effect when challenged by thrombosis induced reagent, $FeCl_3$. This new mouse model, upon further characterization, maybe used for future studies related to functions of FXIIa in blood clotting. We expect the new mouse model to be more suitable for FXIIa functionality studies compared with currently available FXII-KO mice, with less or no interference with neutrophil functions by maintaining the expression of intact FXII zymogen.

It was very interesting that the aPTT result from FXII-S545A$^{S/A}$ mice showed a different pattern as compared to FXII-KO$^{+/-}$ mice. In previous studies, the FXII-KO heterozygous mice showed a similar clotting time as compared with their wild-type litter mates.[261,262] However, the FXII-S545A$^{S/A}$ mice generally had clotting times in between FXII-S545A$^{A/A}$ and FXII-S545A$^{S/S}$ mice. It was possible that in the heterozygous mice, that “inactive” FXIIa will still bind to the negatively charged surface with FXI, though not being able to cleave FXI, which decreases the rate of FXI cleavage by the active FXIIa, and therefore decreased clotting. Alternatively, since FXII could undergo autoactivation (activation of zymogen FXII by FXIIa), the "inactive" FXIIa may also compete with FXI to bind with the active FXIIa on the surface without undergoing autoactivation. Despite being an artificial *in vitro* assay, the aPTT clotting time is widely used in diagnosing FXII deficiency in clinical studies. This result suggested that patients lacking the entire FXII protein *versus* those who lack functional FXIIa may have different aPTT clotting times.

Although we finished some early characterization, a wide range of experiments need to be conducted in the future. A recently published study indicated that PKa directly interacts with and activates FIX, resulting in thrombin generation and fibrin formation independent of FXI.[282] This finding challenged the classical “waterfall” coagulation cascade,[5,6] suggesting that there may be additional protease reactions that bypass the activation of FXI by FXIIa. The interaction between FXII, PK and FXI is complicated, as both autoactivation and reciprocal activations are involved. For future studies, additional thrombosis experiments will be conducted to thoroughly investigate the role of FXII, PK and FXI in blood clotting.

In addition, neutrophil functionality tests would be of interest to compare the difference between this new mouse model with the traditional FXII-KO mouse model. As FXII serves as a

crosstalk between coagulation and inflammation, it will be interesting to compare the survival rate of both mouse models when challenged with lipopolysaccharide (LPS).

5.5 Supplementary tables

Supplementary table 5.1 Primers used for generation and characterization of transgenic mice. * T7 promoter, T7 polymerase binding site, target sequence and tracr RNA sequence were assembled by DNA oligos 1-5. The Ser545 residue was encoded by highlighted TCC.

Name	Sequence (5' – 3')
DNA template for sgRNA synthesis	GAAATTAATACGACTCACTATAGCCCACCCAGGGTGACTCCG GTTTTAGAGCTAGAAATAGCAAGTTAAAATAAGGCTAGTCCGTTA TCAACTTGAAAAAGTGGCACCGAGTCGGTGCTTTT
Oligo 1 (universal T7)	GAAATTAATACGACTCACTATA
Oligo 2 (target specific)	CGACTCACTATAGCCCACCCAGGGTGACTCCG
Oligo 3 (target specific)	TCTAGCTCTAAAACCGGAGTCACCCTGGGTGGG
Oligo 4 (universal tracr RNA)	AAAAGCACCGACTCGGTGCCACTTTTTCAAGTTGATAACGGACTA GCCTTATTTTAACTTGCTATTTCTAGCTCTAAAAC
Oligo 5 (universal tracr RNA)	AAAAGCACCGACTCGGTGCC
ssODN (repair template)	CAAGCATAAGGCAAGAACCACGTGCTGCCTGTTCCCCACCCAGGG TGACGCCGGTGGCCCTCTGGTGTGTGAGGAAGGAACTGCAGAACA TCAGCTCACCCTGCGCGGAGTCATCAGCTGGGGCTC
FXII-S545A genotyping PCR forward primer	CTTCTGGAGGCATCTCTTCG
FXII-S545A genotyping PCR reverse primer	CTGAGGAACGTTTTCAAAGCAC
FXII-S545A genotyping PCR sequencing primer	TTGCAGGGGCTGAAGAATAC
FXII-KO genotyping PCR primer 1	GGCCTCTTGTATTGACTGATGA
FXII-KO genotyping PCR primer 2	AACTGCCATCATAACGTTAGCC
FXII-KO genotyping PCR primer 3	GCAGAGGTTACGGCAGTTTGTCTCTCC

Supplementary table 5.2 Primers used for SNP-containing regions PCR.

SNP ID	PCR Primers	Sequence (5' – 3')
rs29229808	Forward and sequencing	GACCTGGATACCTTGACTCAG
	Reverse	GTGCCTACATTTGAGTGCTTC
rs29782713	Forward and sequencing	TATGGGGCTGGGAATATAACG
	Reverse	ACAATTTTCAGTTGGTGACAGG
rs6356383	Forward and sequencing	AAGCGGAGAAGTTCCCTTTG
	Reverse	AAGACTGCAGCCAAATTTCTG
rs6357350	Forward and sequencing	TCAAACCTCTCATCCTTCGC
rs6357403	Reverse	CAGAGCTGGTTGGTCCTAAG

Bibliography

1. Colman RW. Are hemostasis and thrombosis two sides of the same coin? *J Exp Med*. 2006; 203: 493-495.

2. Gale AJ. Continuing education course #2: current understanding of hemostasis. *Toxicol Pathol*. 2011; 39: 273-280.

3. Mackman N. Triggers, targets and treatments for thrombosis. *Nature*. 2008; 451: 914-918.

4. Didiasova M, Wujak L, Schaefer L, Wygrecka M. Factor XII in coagulation, inflammation and beyond. *Cell Signal*. 2018; 51: 257-265.

5. Davie EW, Ratnoff OD. Waterfall Sequence for Intrinsic Blood Clotting. *Science*. 1964; 145: 1310-1312.

6. Macfarlane RG. An Enzyme Cascade in the Blood Clotting Mechanism, and Its Function as a Biochemical Amplifier. *Nature*. 1964; 202: 498-499.

7. Davie EW. A brief historical review of the waterfall/cascade of blood coagulation. *J Biol Chem*. 2003; 278: 50819-50832.

8. McMichael M. New models of hemostasis. *Top Companion Anim Med*. 2012; 27: 40-45.

9. Nemerson Y, Pitlick FA. Purification and characterization of the protein component of tissue factor. *Biochemistry*. 1970; 9: 5100-5105.

10. Osterud B, Berre A, Otnaess AB, Bjorklid E, Prydz H. Activation of the coagulation factor VII by tissue thromboplastin and calcium. *Biochemistry*. 1972; 11: 2853-2857.

11. Fujikawa K, Coan MH, Legaz ME, Davie EW. The mechanism of activation of bovine factor X (Stuart factor) by intrinsic and extrinsic pathways. *Biochemistry*. 1974; 13: 5290-5299.

12. Rapaport SI, Schiffman S, Patch MJ, Ames SB. The importance of activation of antihemophilic globulin and proaccelerin by traces of thrombin in the generation of intrinsic prothrombinase activity. *Blood*. 1963; 21: 221-236.

13. Eaton D, Rodriguez H, Vehar GA. Proteolytic processing of human factor VIII. Correlation of specific cleavages by thrombin, factor Xa, and activated protein C with activation and inactivation of factor VIII coagulant activity. *Biochemistry*. 1986; 25: 505-512.

14. Nesheim ME, Mann KG. Thrombin-catalyzed activation of single chain bovine factor V. *J Biol Chem*. 1979; 254: 1326-1334.

15. Adams RL, Bird RJ. Review article: Coagulation cascade and therapeutics update: relevance to nephrology. Part 1: Overview of coagulation, thrombophilias and history of anticoagulants. *Nephrology (Carlton)*. 2009; 14: 462-470.

16. Wolberg AS, Campbell RA. Thrombin generation, fibrin clot formation and hemostasis. *Transfus Apher Sci*. 2008; 38: 15-23.

17. Mackman N, Tilley RE, Key NS. Role of the extrinsic pathway of blood coagulation in hemostasis and thrombosis. *Arterioscler Thromb Vasc Biol*. 2007; 27: 1687-1693.

18. McVey JH. The role of the tissue factor pathway in haemostasis and beyond. *Curr Opin Hematol*. 2016; 23: 453-461.

19. Carmeliet P, Mackman N, Moons L, et al. Role of tissue factor in embryonic blood vessel development. *Nature*. 1996; 383: 73-75.

20. Rauch U, Nemerson Y. Circulating tissue factor and thrombosis. *Curr Opin Hematol*. 2000; 7: 273-277.

21. Muller YA, Ultsch MH, Kelley RF, de Vos AM. Structure of the extracellular domain of human tissue factor: location of the factor VIIa binding site. *Biochemistry*. 1994; 33: 10864-10870.

22. Fleck RA, Rao LV, Rapaport SI, Varki N. Localization of human tissue factor antigen by immunostaining with monospecific, polyclonal anti-human tissue factor antibody. *Thromb Res*. 1990; 59: 421-437.

23. Eisenreich A, Rauch U. Regulation and differential role of the tissue factor isoforms in cardiovascular biology. *Trends Cardiovasc Med*. 2010; 20: 199-203.

24. Goldin-Lang P, Tran QV, Fichtner I, et al. Tissue factor expression pattern in human non-small cell lung cancer tissues indicate increased blood thrombogenicity and tumor metastasis. *Oncol Rep*. 2008; 20: 123-128.

25. Eisenreich A, Zakrzewicz A, Huber K, et al. Regulation of pro-angiogenic tissue factor expression in hypoxia-induced human lung cancer cells. *Oncol Rep*. 2013; 30: 462-470.

26. Boltzen U, Eisenreich A, Antoniak S, et al. Alternatively spliced tissue factor and full-length tissue factor protect cardiomyocytes against TNF-alpha-induced apoptosis. *J Mol Cell Cardiol*. 2012; 52: 1056-1065.

27. Szotowski B, Goldin-Lang P, Antoniak S, et al. Alterations in myocardial tissue factor expression and cellular localization in dilated cardiomyopathy. *J Am Coll Cardiol*. 2005; 45: 1081-1089.

28. Smith SA, Travers RJ, Morrissey JH. How it all starts: Initiation of the clotting cascade. *Crit Rev Biochem Mol Biol*. 2015; 50: 326-336.

29. Nemerson Y, Repke D. Tissue factor accelerates the activation of coagulation factor VII: the role of a bifunctional coagulation cofactor. *Thromb Res*. 1985; 40: 351-358.

30. Rao LV, Rapaport SI. Activation of factor VII bound to tissue factor: a key early step in the tissue factor pathway of blood coagulation. *Proc Natl Acad Sci U S A*. 1988; 85: 6687-6691.

31. Radcliffe R, Nemerson Y. Activation and control of factor VII by activated factor X and thrombin. Isolation and characterization of a single chain form of factor VII. *J Biol Chem*. 1975; 250: 388-395.

32. Kisiel W, Fujikawa K, Davie EW. Activation of bovine factor VII (proconvertin) by factor XIIa (activated Hageman factor). *Biochemistry*. 1977; 16: 4189-4194.

33. Masys DR, Bajaj SP, Rapaport SI. Activation of human factor VII by activated factors IX and X. *Blood*. 1982; 60: 1143-1150.

34. Tsujioka H, Suehiro A, Kakishita E. Activation of coagulation factor VII by tissue-type plasminogen activator. *Am J Hematol*. 1999; 61: 34-39.

35. Yamamoto M, Nakagaki T, Kisiel W. Tissue factor-dependent autoactivation of human blood coagulation factor VII. *J Biol Chem*. 1992; 267: 19089-19094.

36. Mariani G, Bernardi F. Factor VII Deficiency. *Semin Thromb Hemost*. 2009; 35: 400-406.

37. Komiyama Y, Pedersen AH, Kisiel W. Proteolytic activation of human factors IX and X by recombinant human factor VIIa: effects of calcium, phospholipids, and tissue factor. *Biochemistry*. 1990; 29: 9418-9425.

38. Nemerson Y, Gentry R. An ordered addition, essential activation model of the tissue factor pathway of coagulation: evidence for a conformational cage. *Biochemistry*. 1986; 25: 4020-4033.

39. Ratnoff OD, Colopy JE. A familial hemorrhagic trait associated with a deficiency of a clot-promoting fraction of plasma. *J Clin Invest*. 1955; 34: 602-613.

40. Lämmle B, Wuillemin WA, Huber I, et al. Thromboembolism and bleeding tendency in congenital factor XII deficiency--a study on 74 subjects from 14 Swiss families. *Thromb Haemost*. 1991; 65: 117-121.

41. Kokoye Y, Ivanov I, Cheng Q, et al. A comparison of the effects of factor XII deficiency and prekallikrein deficiency on thrombus formation. *Thromb Res*. 2016; 140: 118-124.

42. Kleinschnitz C, Stoll G, Bendszus M, et al. Targeting coagulation factor XII provides protection from pathological thrombosis in cerebral ischemia without interfering with hemostasis. *J Exp Med*. 2006; 203: 513-518.

43. Matafonov A, Leung PY, Gailani AE, et al. Factor XII inhibition reduces thrombus formation in a primate thrombosis model. *Blood*. 2014; 123: 1739-1746.

44. Cheng Q, Tucker EI, Pine MS, et al. A role for factor XIIa-mediated factor XI activation in thrombus formation in vivo. *Blood*. 2010; 116: 3981-3989.

45. Renné T, Pozgajová M, Grüner S, et al. Defective thrombus formation in mice lacking coagulation factor XII. *J Exp Med*. 2005; 202: 271-281.

46. Reddigari SR, Shibayama Y, Brunnee T, Kaplan AP. Human Hageman factor (factor XII) and high molecular weight kininogen compete for the same binding site on human umbilical vein endothelial cells. *J Biol Chem*. 1993; 268: 11982-11987.

47. Cool DE, MacGillivray RT. Characterization of the human blood coagulation factor XII gene. Intron/exon gene organization and analysis of the 5'-flanking region. *J Biol Chem*. 1987; 262: 13662-13673.

48. Stavrou E, Schmaier AH. Factor XII: what does it contribute to our understanding of the physiology and pathophysiology of hemostasis & thrombosis. *Thromb Res*. 2010; 125: 210-215.

49. Clarke BJ, Cote HC, Cool DE, et al. Mapping of a putative surface-binding site of human coagulation factor XII. *J Biol Chem*. 1989; 264: 11497-11502.

50. Pixley RA, Stumpo LG, Birkmeyer K, Silver L, Colman RW. A monoclonal antibody recognizing an icosapeptide sequence in the heavy chain of human factor XII inhibits surface-catalyzed activation. *J Biol Chem*. 1987; 262: 10140-10145.

51. Cool DE, Edgell CJ, Louie GV, Zoller MJ, Brayer GD, MacGillivray RT. Characterization of human blood coagulation factor XII cDNA. Prediction of the primary structure of factor XII and the tertiary structure of beta-factor XIIa. *J Biol Chem*. 1985; 260: 13666-13676.

52. Citarella F, te Velthuis H, Helmer-Citterich M, Hack CE. Identification of a putative binding site for negatively charged surfaces in the fibronectin type II domain of human factor XII--an immunochemical and homology modeling approach. *Thromb Haemost*. 2000; 84: 1057-1065.

53. Citarella F, Ravon DM, Pascucci B, Felici A, Fantoni A, Hack CE. Structure/function analysis of human factor XII using recombinant deletion mutants. Evidence for an additional region involved in the binding to negatively charged surfaces. *Eur J Biochem*. 1996; 238: 240-249.

54. McMullen BA, Fujikawa K. Amino acid sequence of the heavy chain of human alpha-factor XIIa (activated Hageman factor). *J Biol Chem*. 1985; 260: 5328-5341.

55. Cochrane CG, Revak SD, Wuepper KD. Activation of Hageman factor in solid and fluid phases. A critical role of kallikrein. *J Exp Med*. 1973; 138: 1564-1583.

56. Røjkjaer R, Schousboe I. The surface-dependent autoactivation mechanism of factor XII. *Eur J Biochem*. 1997; 243: 160-166.

57. Samuel M, Pixley RA, Villanueva MA, Colman RW, Villanueva GB. Human factor XII (Hageman factor) autoactivation by dextran sulfate. Circular dichroism, fluorescence, and ultraviolet difference spectroscopic studies. *J Biol Chem*. 1992; 267: 19691-19697.

58. Ewald GA, Eisenberg PR. Plasmin-mediated activation of contact system in response to pharmacological thrombolysis. *Circulation*. 1995; 91: 28-36.

59. Revak SD, Cochrane CG, Bouma BN, Griffin JH. Surface and fluid phase activities of two forms of activated Hageman factor produced during contact activation of plasma. *J Exp Med*. 1978; 147: 719-729.

60. Long AT, Kenne E, Jung R, Fuchs TA, Renné T. Contact system revisited: an interface between inflammation, coagulation, and innate immunity. *J Thromb Haemost*. 2016; 14: 427-437.

61. Braat EA, Dooijewaard G, Rijken DC. Fibrinolytic properties of activated FXII. *Eur J Biochem*. 1999; 263: 904-911.

62. Muller F, Renne T. Novel roles for factor XII-driven plasma contact activation system. *Curr Opin Hematol*. 2008; 15: 516-521.

63. Dementiev A, Silva A, Yee C, et al. Structures of human plasma beta-factor XIIa cocrystallized with potent inhibitors. *Blood Adv*. 2018; 2: 549-558.

64. Dunn JT, Silverberg M, Kaplan AP. The cleavage and formation of activated human Hageman factor by autodigestion and by kallikrein. *J Biol Chem*. 1982; 257: 1779-1784.

65. Mandle RJ, Colman RW, Kaplan AP. Identification of prekallikrein and high-molecular-weight kininogen as a complex in human plasma. *Proc Natl Acad Sci U S A*. 1976; 73: 4179-4183.

66. Wuepper KD, Cochrane CG. Plasma prekallikrein: isolation, characterization, and mechanism of activation. *J Exp Med*. 1972; 135: 1-20.

67. Hooley E, McEwan PA, Emsley J. Molecular modeling of the prekallikrein structure provides insights into high-molecular-weight kininogen binding and zymogen activation. *J Thromb Haemost*. 2007; 5: 2461-2466.

68. Emsley J, McEwan PA, Gailani D. Structure and function of factor XI. *Blood*. 2010; 115: 2569-2577.

69. Li C, Voos KM, Pathak M, et al. Plasma kallikrein structure reveals apple domain disc rotated conformation compared to factor XI. *J Thromb Haemost*. 2019; 17: 759-770.

70. Koumandou VL, Scorilas A. Evolution of the plasma and tissue kallikreins, and their alternative splicing isoforms. *PLoS One*. 2013; 8: e68074.

71. Colman RW, Schmaier AH. Contact system: a vascular biology modulator with anticoagulant, profibrinolytic, antiadhesive, and proinflammatory attributes. *Blood*. 1997; 90: 3819-3843.

72. Griffin JH, Cochrane CG. Mechanisms for the involvement of high molecular weight kininogen in surface-dependent reactions of Hageman factor. *Proc Natl Acad Sci U S A*. 1976; 73: 2554-2558.

73. Scott CF, Silver LD, Schapira M, Colman RW. Cleavage of human high molecular weight kininogen markedly enhances its coagulant activity. Evidence that this molecule exists as a procofactor. *J Clin Invest*. 1984; 73: 954-962.

74. Bernardo MM, Day DE, Halvorson HR, Olson ST, Shore JD. Surface-independent acceleration of factor XII activation by zinc ions. II. Direct binding and fluorescence studies. *J Biol Chem*. 1993; 268: 12477-12483.

75. Vu TT, Fredenburgh JC, Weitz JI. Zinc: An important cofactor in haemostasis and thrombosis. *Thromb Haemost*. 2013; 109: 421-430.

76. Herwald H, Morgelin M, Svensson HG, Sjöbring U. Zinc-dependent conformational changes in domain D5 of high molecular mass kininogen modulate contact activation. *Eur J Biochem*. 2001; 268: 396-404.

77. DeLa Cadena RA, Colman RW. The sequence HGLGHGHEQQHGLGHGH in the light chain of high molecular weight kininogen serves as a primary structural feature for zinc-dependent binding to an anionic surface. *Protein Sci*. 1992; 1: 151-160.

78. Hasan AA, Cines DB, Herwald H, Schmaier AH, Muller-Esterl W. Mapping the cell binding site on high molecular weight kininogen domain 5. *J Biol Chem*. 1995; 270: 19256-19261.

79. Gailani D, Sun MF, Sun Y. A comparison of murine and human factor XI. *Blood*. 1997; 90: 1055-1064.

80. Thompson RE, Mandle R, Jr., Kaplan AP. Studies of binding of prekallikrein and Factor XI to high molecular weight kininogen and its light chain. *Proc Natl Acad Sci U S A*. 1979; 76: 4862-4866.

81. Thompson RE, Mandle R, Jr., Kaplan AP. Association of factor XI and high molecular weight kininogen in human plasma. *J Clin Invest*. 1977; 60: 1376-1380.

82. Renne T, Gailani D, Meijers JC, Muller-Esterl W. Characterization of the H-kininogen-binding site on factor XI: a comparison of factor XI and plasma prekallikrein. *J Biol Chem*. 2002; 277: 4892-4899.

83. Papagrigoriou E, McEwan PA, Walsh PN, Emsley J. Crystal structure of the factor XI zymogen reveals a pathway for transactivation. *Nat Struct Mol Biol*. 2006; 13: 557-558.

84. Geng Y, Verhamme IM, Smith SA, et al. Factor XI anion-binding sites are required for productive interactions with polyphosphate. *J Thromb Haemost*. 2013; 11: 2020-2028.

85. Mohammed BM, Matafonov A, Ivanov I, et al. An update on factor XI structure and function. *Thromb Res*. 2018; 161: 94-105.

86. Wu Y. Contact pathway of coagulation and inflammation. *Thrombosis Journal*. 2015; 13: 17.

87. Puy C, Rigg RA, McCarty OJ. The hemostatic role of factor XI. *Thromb Res*. 2016; 141 Suppl 2: S8-S11.

88. Naito K, Fujikawa K. Activation of human blood coagulation factor XI independent of factor XII. Factor XI is activated by thrombin and factor XIa in the presence of negatively charged surfaces. *J Biol Chem*. 1991; 266: 7353-7358.

89. Matafonov A, Sarilla S, Sun MF, et al. Activation of factor XI by products of prothrombin activation. *Blood*. 2011; 118: 437-445.

90. Di Scipio RG, Kurachi K, Davie EW. Activation of human factor IX (Christmas factor). *J Clin Invest*. 1978; 61: 1528-1538.

91. Taran LD. Factor IX of the blood coagulation system: a review. *Biochemistry (Mosc)*. 1997; 62: 685-693.

92. Fahs SA, Hille MT, Shi Q, Weiler H, Montgomery RR. A conditional knockout mouse model reveals endothelial cells as the principal and possibly exclusive source of plasma factor VIII. *Blood*. 2014; 123: 3706-3713.

93. Everett LA, Cleuren AC, Khoriaty RN, Ginsburg D. Murine coagulation factor VIII is synthesized in endothelial cells. *Blood*. 2014; 123: 3697-3705.

94. Orlova NA, Kovnir SV, Vorobiev, II, Gabibov AG, Vorobiev AI. Blood Clotting Factor VIII: From Evolution to Therapy. *Acta Naturae*. 2013; 5: 19-39.

95. Chaudhry R, Usama SM, Babiker HM. Physiology, Coagulation Pathways. StatPearls. Treasure Island (FL); 2020.

96. Duga S, Asselta R, Tenchini ML. Coagulation factor V. *Int J Biochem Cell Biol*. 2004; 36: 1393-1399.

97. Mann KG, Kalafatis M. Factor V: a combination of Dr Jekyll and Mr Hyde. *Blood*. 2003; 101: 20-30.

98. Nicolaes GA, Dahlback B. Factor V and thrombotic disease: description of a janus-faced protein. *Arterioscler Thromb Vasc Biol*. 2002; 22: 530-538.

99. Di Cera E. Thrombin. *Mol Aspects Med*. 2008; 29: 203-254.

100. Mosesson MW. Fibrinogen and fibrin structure and functions. *J Thromb Haemost*. 2005; 3: 1894-1904.

101. Peters R, Harris T. Advances and innovations in haemophilia treatment. *Nat Rev Drug Discov*. 2018; 17: 493-508.

102. High KA. Antithrombin III, protein C, and protein S. Naturally occurring anticoagulant proteins. *Arch Pathol Lab Med*. 1988; 112: 28-36.

103. C1 esterase inhibitor (human). *P T*. 2010; 35: 2-3.

104. Cesarman-Maus G, Hajjar KA. Molecular mechanisms of fibrinolysis. *Br J Haematol*. 2005; 129: 307-321.

105. Srivastava A, Brewer AK, Mauser-Bunschoten EP, et al. Guidelines for the management of hemophilia. *Haemophilia*. 2013; 19: e1-47.

106. Sharma R, Flood VH. Advances in the diagnosis and treatment of Von Willebrand disease. *Blood*. 2017; 130: 2386-2391.

107. Sadler JE. Biochemistry and genetics of von Willebrand factor. *Annu Rev Biochem*. 1998; 67: 395-424.

108. Peyvandi F, Garagiola I, Biguzzi E. Advances in the treatment of bleeding disorders. *J Thromb Haemost*. 2016; 14: 2095-2106.

109. Coughlin SR. Protease-activated receptors in hemostasis, thrombosis and vascular biology. *J Thromb Haemost*. 2005; 3: 1800-1814.

110. Mackman N. Role of tissue factor in hemostasis, thrombosis, and vascular development. *Arterioscler Thromb Vasc Biol*. 2004; 24: 1015-1022.

111. Woodruff RS, Sullenger B, Becker RC. The many faces of the contact pathway and their role in thrombosis. *J Thromb Thrombolysis*. 2011; 32: 9-20.

112. Denis CV, Wagner DD. Platelet adhesion receptors and their ligands in mouse models of thrombosis. *Arterioscler Thromb Vasc Biol*. 2007; 27: 728-739.

113. Shantsila E, Lip GY. The role of monocytes in thrombotic disorders. Insights from tissue factor, monocyte-platelet aggregates and novel mechanisms. *Thromb Haemost*. 2009; 102: 916-924.

114. Mackman N. New insights into the mechanisms of venous thrombosis. *J Clin Invest*. 2012; 122: 2331-2336.

115. Schmaier AH. The contact activation and kallikrein/kinin systems: pathophysiologic and physiologic activities. *J Thromb Haemost*. 2016; 14: 28-39.

116. Foley JH, Conway EM. Cross talk pathways between coagulation and inflammation. *Circulation Research*. 2016; 118: 1392-1408.

117. Gajsiewicz JM, Smith SA, Morrissey JH. Polyphosphate and RNA differentially modulate the contact pathway of blood clotting. *J Biol Chem*. 2017; 292: 1808-1814.

118. Smith SA, Gajsiewicz JM, Morrissey JH. Ability of polyphosphate and nucleic acids to trigger blood clotting: Some observations and caveats. *Frontiers in Medicine*. 2018; 5: 107.

119. Wang Y, Ivanov I, Smith SA, Gailani D, Morrissey JH. Polyphosphate, Zn(2+) and high molecular weight kininogen modulate individual reactions of the contact pathway of blood clotting. *J Thromb Haemost*. 2019.

120. Müller F, Mutch NJ, Schenk WA, et al. Platelet polyphosphates are proinflammatory and procoagulant mediators in vivo. *Cell*. 2009; 139: 1143-1156.

121. Ivanov I, Matafonov A, Sun MF, et al. Proteolytic properties of single-chain factor XII: a mechanism for triggering contact activation. *Blood*. 2017; 129: 1527-1537.

122. Engel R, Brain CM, Paget J, Lionikiene AS, Mutch NJ. Single-chain factor XII exhibits activity when complexed to polyphosphate. *J Thromb Haemost*. 2014; 12: 1513-1522.

123. Ivanov I, Shakhawat R, Sun MF, et al. Nucleic acids as cofactors for factor XI and prekallikrein activation: Different roles for high-molecular-weight kininogen. *Thromb Haemost*. 2017; 117: 671-681.

124. Zhu S, Diamond SL. Contact activation of blood coagulation on a defined kaolin/collagen surface in a microfluidic assay. *Thromb Res*. 2014; 134: 1335-1343.

125. Gould TJ, Vu TT, Swystun LL, et al. Neutrophil extracellular traps promote thrombin generation through platelet-dependent and platelet-independent mechanisms. *Arteriosclerosis, Thrombosis, and Vascular Biology*. 2014; 34: 1977-1984.

126. Oehmcke S, Mörgelin M, Herwald H. Activation of the human contact system on neutrophil extracellular traps. *J Innate Immun*. 2009; 1: 225-230.

127. Fuchs TA, Brill A, Duerschmied D, et al. Extracellular DNA traps promote thrombosis. *Proc Natl Acad Sci U S A*. 2010; 107: 15880-15885.

128. Maas C, Govers-Riemslag JW, Bouma B, et al. Misfolded proteins activate factor XII in humans, leading to kallikrein formation without initiating coagulation. *J Clin Invest*. 2008; 118: 3208-3218.

129. Joseph K, Shibayama Y, Ghebrehiwet B, Kaplan AP. Factor XII-dependent contact activation on endothelial cells and binding proteins gC1qR and cytokeratin 1. *Thromb Haemost*. 2001; 85: 119-124.

130. Shariat-Madar Z, Mahdi F, Schmaier AH. Identification and characterization of prolylcarboxypeptidase as an endothelial cell prekallikrein activator. *J Biol Chem*. 2002; 277: 17962-17969.

131. Griffin JH. Role of surface in surface-dependent activation of Hageman factor (blood coagulation factor XII). *Proc Natl Acad Sci U S A*. 1978; 75: 1998-2002.

132. Tans G, Rosing J, Berrettini M, Lämmle B, Griffin JH. Autoactivation of human plasma prekallikrein. *J Biol Chem*. 1987; 262: 11308-11314.

133. Schmaier AH. Assembly, activation, and physiologic influence of the plasma kallikrein/kinin system. *Int Immunopharmacol*. 2008; 8: 161-165.

134. Shariat-Madar Z, Mahdi F, Schmaier AH. Recombinant prolylcarboxypeptidase activates plasma prekallikrein. *Blood*. 2004; 103: 4554-4561.

135. Bouma BN, Griffin JH. Human blood coagulation factor XI. Purification, properties, and mechanism of activation by activated factor XII. *J Biol Chem*. 1977; 252: 6432-6437.

136. Doggen CJ, Rosendaal FR, Meijers JC. Levels of intrinsic coagulation factors and the risk of myocardial infarction among men: Opposite and synergistic effects of factors XI and XII. *Blood*. 2006; 108: 4045-4051.

137. Merlo C, Wuillemin WA, Redondo M, et al. Elevated levels of plasma prekallikrein, high molecular weight kininogen and factor XI in coronary heart disease. *Atherosclerosis*. 2002; 161: 261-267.

138. Xu Y, Cai TQ, Castriota G, et al. Factor XIIa inhibition by Infestin-4: in vitro mode of action and in vivo antithrombotic benefit. *Thromb Haemost*. 2014; 111: 694-704.

139. Schulze-Topphoff U, Prat A, Bader M, Zipp F, Aktas O. Roles of the kallikrein/kinin system in the adaptive immune system. *Int Immunopharmacol*. 2008; 8: 155-160.

140. Golias C, Charalabopoulos A, Stagikas D, Charalabopoulos K, Batistatou A. The kinin system--bradykinin: biological effects and clinical implications. Multiple role of the kinin system--bradykinin. *Hippokratia*. 2007; 11: 124-128.

141. Weidmann H, Heikaus L, Long AT, Naudin C, Schluter H, Renne T. The plasma contact system, a protease cascade at the nexus of inflammation, coagulation and immunity. *Biochim Biophys Acta Mol Cell Res*. 2017; 1864: 2118-2127.

142. Bjorkqvist J, Sala-Cunill A, Renne T. Hereditary angioedema: a bradykinin-mediated swelling disorder. *Thromb Haemost*. 2013; 109: 368-374.

143. Singer M, Deutschman CS, Seymour CW, et al. The Third International Consensus Definitions for Sepsis and Septic Shock (Sepsis-3). *JAMA*. 2016; 315: 801-810.

144. Pixley RA, De La Cadena R, Page JD, et al. The contact system contributes to hypotension but not disseminated intravascular coagulation in lethal bacteremia. In vivo use of a monoclonal anti-factor XII antibody to block contact activation in baboons. *J Clin Invest*. 1993; 91: 61-68.

145. Jansen PM, Pixley RA, Brouwer M, et al. Inhibition of factor XII in septic baboons attenuates the activation of complement and fibrinolytic systems and reduces the release of interleukin-6 and neutrophil elastase. *Blood*. 1996; 87: 2337-2344.

146. Mitchell JL, Lionikiene AS, Georgiev G, et al. Polyphosphate colocalizes with factor XII on platelet-bound fibrin and augments its plasminogen activator activity. *Blood*. 2016; 128: 2834-2845.

147. Kaplan AP, Austen KF. A prealbumin activator of prekallikrein. II. Derivation of activators of prekallikrein from active Hageman factor by digestion with plasmin. *J Exp Med*. 1971; 133: 696-712.

148. Kleniewski J, Blankenship DT, Cardin AD, Donaldson V. Mechanism of enhanced kinin release from high molecular weight kininogen by plasma kallikrein after its exposure to plasmin. *J Lab Clin Med*. 1992; 120: 129-139.

149. Morrissey JH, Choi SH, Smith SA. Polyphosphate: an ancient molecule that links platelets, coagulation, and inflammation. *Blood*. 2012; 119: 5972-5979.

150. Kornberg A, Rao NN, Ault-Riché D. Inorganic polyphosphate: a molecule of many functions. *Annu Rev Biochem*. 1999; 68: 89-125.

151. Docampo R, Moreno SN. Acidocalcisomes. *Cell Calcium*. 2011; 50: 113-119.

152. Rao NN, Gomez-Garcia MR, Kornberg A. Inorganic polyphosphate: essential for growth and survival. *Annu Rev Biochem*. 2009; 78: 605-647.

153. Rao NN, Kornberg A. Inorganic polyphosphate supports resistance and survival of stationary-phase Escherichia coli. *J Bacteriol*. 1996; 178: 1394-1400.

154. Kumble KD, Kornberg A. Inorganic polyphosphate in mammalian cells and tissues. *J Biol Chem*. 1995; 270: 5818-5822.

155. Zakharian E, Thyagarajan B, French RJ, Pavlov E, Rohacs T. Inorganic polyphosphate modulates TRPM8 channels. *PLoS One*. 2009; 4: e5404.

156. Kim D, Cavanaugh EJ. Requirement of a soluble intracellular factor for activation of transient receptor potential A1 by pungent chemicals: role of inorganic polyphosphates. *J Neurosci*. 2007; 27: 6500-6509.

157. Wang L, Fraley CD, Faridi J, Kornberg A, Roth RA. Inorganic polyphosphate stimulates mammalian TOR, a kinase involved in the proliferation of mammary cancer cells. *Proc Natl Acad Sci U S A*. 2003; 100: 11249-11254.

158. Holmstrom KM, Marina N, Baev AY, Wood NW, Gourine AV, Abramov AY. Signalling properties of inorganic polyphosphate in the mammalian brain. *Nat Commun*. 2013; 4: 1362.

159. Seidlmayer LK, Gomez-Garcia MR, Blatter LA, Pavlov E, Dedkova EN. Inorganic polyphosphate is a potent activator of the mitochondrial permeability transition pore in cardiac myocytes. *J Gen Physiol*. 2012; 139: 321-331.

160. Jimenez-Nunez MD, Moreno-Sanchez D, Hernandez-Ruiz L, et al. Myeloma cells contain high levels of inorganic polyphosphate which is associated with nucleolar transcription. *Haematologica*. 2012; 97: 1264-1271.

161. Bentley-DeSousa A, Holinier C, Moteshareie H, et al. A Screen for Candidate Targets of Lysine Polyphosphorylation Uncovers a Conserved Network Implicated in Ribosome Biogenesis. *Cell Rep*. 2018; 22: 3427-3439.

162. Kawano MM. Inorganic polyphosphate induces apoptosis specifically in human plasma cells. *Haematologica*. 2006; 91: 1154A.

163. Smith SA, Choi SH, Davis-Harrison R, et al. Polyphosphate exerts differential effects on blood clotting, depending on polymer size. *Blood*. 2010; 116: 4353-4359.

164. Omelon S, Georgiou J, Henneman ZJ, et al. Control of vertebrate skeletal mineralization by polyphosphates. *PLoS One*. 2009; 4: e5634.

165. Xie L, Jakob U. Inorganic polyphosphate, a multifunctional polyanionic protein scaffold. *J Biol Chem*. 2019; 294: 2180-2190.

166. Ruiz FA, Lea CR, Oldfield E, Docampo R. Human platelet dense granules contain polyphosphate and are similar to acidocalcisomes of bacteria and unicellular eukaryotes. *J Biol Chem*. 2004; 279: 44250-44257.

167. Moreno-Sanchez D, Hernandez-Ruiz L, Ruiz FA, Docampo R. Polyphosphate is a novel pro-inflammatory regulator of mast cells and is located in acidocalcisomes. *J Biol Chem*. 2012; 287: 28435-28444.

168. Verhoef JJ, Barendrecht AD, Nickel KF, et al. Polyphosphate nanoparticles on the platelet surface trigger contact system activation. *Blood*. 2017; 129: 1707-1717.

169. Wang Y, Ivanov I, Smith SA, Gailani D, Morrissey JH. Polyphosphate, Zn(2+) and high molecular weight kininogen modulate individual reactions of the contact pathway of blood clotting. *J Thromb Haemost*. 2019; 17: 2131-2140.

170. Schmaier AH. The contact activation and kallikrein/kinin systems: pathophysiologic and physiologic activities. *J Thromb Haemost*. 2016; 14: 28-39.

171. Revenko AS, Gao D, Crosby JR, et al. Selective depletion of plasma prekallikrein or coagulation factor XII inhibits thrombosis in mice without increased risk of bleeding. *Blood*. 2011; 118: 5302-5311.

172. Brown MR, Kornberg A. Inorganic polyphosphate in the origin and survival of species. *Proc Natl Acad Sci U S A*. 2004; 101: 16085-16087.

173. Morrissey JH. Polyphosphate: a link between platelets, coagulation and inflammation. *Int J Hematol*. 2012; 95: 346-352.

174. Smith SA, Baker CJ, Gajsiewicz JM, Morrissey JH. Silica particles contribute to the procoagulant activity of DNA and polyphosphate isolated using commercial kits. *Blood*. 2017; 130: 88-91.

175. Smith SA, Morrissey JH. Sensitive fluorescence detection of polyphosphate in polyacrylamide gels using 4',6-diamidino-2-phenylindol. *Electrophoresis*. 2007; 28: 3461-3465.

176. Levison PR, Tomalin G. Studies on the temperature-dependent autoinhibition of human plasma kallikrein I. *Biochem J*. 1982; 205: 529-534.

177. Chung DW, Fujikawa K, McMullen BA, Davie EW. Human plasma prekallikrein, a zymogen to a serine protease that contains four tandem repeats. *Biochemistry*. 1986; 25: 2410-2417.

178. Wallisch M, Tucker EI, Lorentz CU, et al. The anti-factor XII antibody AB052 is antithrombotic without hemostatic impairment in a primate model of extracorporeal membrane oxygenation. *Blood*. 2017; 130: 236.

179. Brown MR, Kornberg A. The long and short of it – polyphosphate, PPK and bacterial survival. *Trends Biochem Sci*. 2008; 33: 284-290.

180. Wu JW, Wu Y, Wang ZX. Kinetic analysis of a simplified scheme of autocatalytic zymogen activation. *Eur J Biochem*. 2001; 268: 1547-1553.

181. Hojima Y, Pierce JV, Pisano JJ. Plant inhibitors of serine proteinases: Hageman factor fragment, kallikreins, plasmin, thrombin, factor Xa, trypsin, and chymotrypsin. *Thromb Res*. 1980; 20: 163-171.

182. Chong GL, Reeck GR. Interaction of trypsin, beta-factor XIIa, and plasma kallikrein with a trypsin inhibitor isolated from barley seeds: a comparison with the corn inhibitor of activated Hageman factor. *Thromb Res*. 1987; 48: 211-221.

183. Smith SA, Mutch NJ, Baskar D, Rohloff P, Docampo R, Morrissey JH. Polyphosphate modulates blood coagulation and fibrinolysis. *Proc Natl Acad Sci U S A*. 2006; 103: 903-908.

184. Caen J, Wu Q. Hageman factor, platelets and polyphosphates: early history and recent connection. *J Thromb Haemost*. 2010; 8: 1670-1674.

185. Erickson HP. Size and shape of protein molecules at the nanometer level determined by sedimentation, gel filtration, and electron microscopy. *Biol Proced Online*. 2009; 11: 32-51.

186. Bolesch DG, Keasling JD. Polyphosphate binding and chain length recognition of *Escherichia coli* exopolyphosphatase. *J Biol Chem*. 2000; 275: 33814-33819.

187. Gansler J, Jaax M, Leiting S, et al. Structural requirements for the procoagulant activity of nucleic acids. *PLoS One*. 2012; 7: e50399.

188. Kleniewski J. Plasma high molecular weight kininogen concentration in health and in chosen impairments of haemostasis. Evidence that plasmin uncovers a new antigenic site in high molecular weight kininogen. *Thromb Haemost*. 1979; 42: 1046-1055.

189. Moreno-Sanchez D, Hernandez-Ruiz L, Ruiz FA, Docampo R. Polyphosphate is a novel pro-inflammatory regulator of mast cells and is located in acidocalcisomes. *J Biol Chem*. 2012; 287: 28435-28444.

190. Marx G, Korner G, Mou X, Gorodetsky R. Packaging zinc, fibrinogen, and factor XIII in platelet a-granules. *J Cell Physiol*. 1993; 156: 437-442.

191. Schmaier AH. Plasma prekallikrein: Its role in hereditary angioedema and health and disease. *Frontiers in Medicine*. 2018; 5: 3.

192. Shariat-Madar Z, Mahdi F, Schmaier AH. Recombinant prolylcarboxypeptidase activates plasma prekallikrein. *Blood*. 2004; 103: 4554-4561.

193. Moreira CR, Schmaier AH, Mahdi F, da MG, Nader HB, Shariat-Madar Z. Identification of prolylcarboxypeptidase as the cell matrix-associated prekallikrein activator. *FEBS Lett*. 2002; 523: 167-170.

194. Reddigari SR, Shibayama Y, Brunnee T, Kaplan AP. Human Hageman factor (factor XII) and high molecular weight kininogen compete for the same binding site on human umbilical vein endothelial cells. *J Biol Chem*. 1993; 268: 11982-11987.

195. Choi SH, Smith SA, Morrissey JH. Polyphosphate is a cofactor for the activation of factor XI by thrombin. *Blood*. 2011; 118: 6963-6970.

196. Geng Y, Verhamme IM, Smith SB, et al. The dimeric structure of factor XI and zymogen activation. *Blood*. 2013; 121: 3962-3969.

197. Kunapuli SP, DeLa Cadena RA, Colman RW. Deletion mutagenesis of high molecular weight kininogen light chain. Identification of two anionic surface binding subdomains. *J Biol Chem*. 1993; 268: 2486-2492.

198. Akiyama M, Crooke E, Kornberg A. An exopolyphosphatase of Escherichia coli. The enzyme and its ppx gene in a polyphosphate operon. *J Biol Chem*. 1993; 268: 633-639.

199. Lonetti A, Szijgyarto Z, Bosch D, Loss O, Azevedo C, Saiardi A. Identification of an evolutionarily conserved family of inorganic polyphosphate endopolyphosphatases. *J Biol Chem*. 2011; 286: 31966-31974.

200. Shiba T, Nishimura D, Kawazoe Y, et al. Modulation of mitogenic activity of fibroblast growth factors by inorganic polyphosphate. *J Biol Chem*. 2003; 278: 26788-26792.

201. Hernandez-Ruiz L, González-García I, Castro C, Brieva JA, Ruiz FA. Inorganic polyphosphate and specific induction of apoptosis in human plasma cells. *Haematologica*. 2006; 91: 1180-1186.

202. Gray MJ, Jakob U. Oxidative stress protection by polyphosphate--new roles for an old player. *Curr Opin Microbiol*. 2015; 24: 1-6.

203. Kumar A, Gangaiah D, Torrelles JB, Rajashekara G. Polyphosphate and associated enzymes as global regulators of stress response and virulence in Campylobacter jejuni. *World J Gastroenterol*. 2016; 22: 7402-7414.

204. Cowling RT, Birnboim HC. Incorporation of [32P] orthophosphate into inorganic polyphosphates by human granulocytes and other human cell types. *J Biol Chem*. 1994; 269: 9480-9485.

205. Pisoni RL, Lindley ER. Incorporation of [32P] orthophosphate into long chains of inorganic polyphosphate within lysosomes of human fibroblasts. *J Biol Chem*. 1992; 267: 3626-3631.

206. Griffin JB, Davidian NM, Penniall R. Studies of phosphorus metabolism by isolated nuclei VII. Identification of polyphosphate as a product. *J Biol Chem*. 1965; 240: 4427-4434.

207. Lynn WS, Brown RH. Synthesis of polyphosphate by rat liver mitochondria. *Biochemical and biophysical research communications*. 1963; 11: 367-371.

208. Smith SA, Choi SH, Collins JN, Travers RJ, Cooley BC, Morrissey JH. Inhibition of polyphosphate as a novel strategy for preventing thrombosis and inflammation. *Blood, The Journal of the American Society of Hematology*. 2012; 120: 5103-5110.

209. Han KY, Hong BS, Yoon YJ, et al. Polyphosphate blocks tumour metastasis via anti-angiogenic activity. *Biochem J*. 2007; 406: 49-55.

210. Kawazoe Y, Shiba T, Nakamura R, et al. Induction of calcification in MC3T3-E1 cells by inorganic polyphosphate. *J Dent Res*. 2004; 83: 613-618.

211. Schroder H, Kurz L, Muller W, Lorenz B. Polyphosphate in bone. *BIOCHEMISTRY C/C OF BIOKHIMIIA*. 2000; 65: 296-303.

212. Zhang C-m, Yamaguchi K, So M, et al. Possible mechanisms of polyphosphate-induced amyloid fibril formation of β2-microglobulin. *Proceedings of the National Academy of Sciences*. 2019; 116: 12833-12838.

213. Tammenkoski M, Koivula K, Cusanelli E, et al. Human metastasis regulator protein H-prune is a short-chain exopolyphosphatase. *Biochemistry*. 2008; 47: 9707-9713.

214. Allan RA, Miller JJ. Influence of S-adenosylmethionine on DAPI-induced fluorescence of polyphosphate in the yeast vacuole. *Can J Microbiol*. 1980; 26: 912-920.

215. Tijssen JP, Beekes HW, Van Steveninck J. Localization of polyphosphates in Saccharomyces fragilis, as revealed by 4',6-diamidino-2-phenylindole fluorescence. *Biochim Biophys Acta*. 1982; 721: 394-398.

216. Schlagenhauf A, Pohl S, Haidl H, Leschnik B, Gallistl S, Muntean W. Non-enzymatic quantification of polyphosphate levels in platelet lysates and releasates. *J Pharm Biomed Anal*. 2016; 131: 1-5.

217. Du Y, Han Z, Wang X, Wan C. [A fluorometric method for direct detection of inorganic polyphosphate in enterohemorrhagic Escherichia coli O157:H7]. *Nan Fang Yi Ke Da Xue Xue Bao*. 2019; 39: 344-350.

218. Li L, Khong ML, Lui ELH, et al. Long-chain polyphosphate in osteoblast matrix vesicles: Enrichment and inhibition of mineralization. *Biochim Biophys Acta Gen Subj*. 2019; 1863: 199-209.

219. Gomes FM, Ramos IB, Wendt C, et al. New insights into the in situ microscopic visualization and quantification of inorganic polyphosphate stores by 4',6-diamidino-2-phenylindole (DAPI)-staining. *Eur J Histochem*. 2013; 57: e34.

220. Voronkov A, Sinetova M. Polyphosphate accumulation dynamics in a population of Synechocystis sp. PCC 6803 cells under phosphate overplus. *Protoplasma*. 2019; 256: 1153-1164.

221. Martin P, Van Mooy BA. Fluorometric quantification of polyphosphate in environmental plankton samples: extraction protocols, matrix effects, and nucleic acid interference. *Appl Environ Microbiol*. 2013; 79: 273-281.

222. Kolozsvari B, Parisi F, Saiardi A. Inositol phosphates induce DAPI fluorescence shift. *Biochem J*. 2014; 460: 377-385.

223. Ohtomo R, Sekiguchi Y, Mimura T, Saito M, Ezawa T. Quantification of polyphosphate: different sensitivities to short-chain polyphosphate using enzymatic and colorimetric methods as revealed by ion chromatography. *Anal Biochem*. 2004; 328: 139-146.

224. Angelova PR, Agrawalla BK, Elustondo PA, et al. In situ investigation of mammalian inorganic polyphosphate localization using novel selective fluorescent probes JC-D7 and JC-D8. *ACS Chem Biol*. 2014; 9: 2101-2110.

225. Rangarajan ES, Nadeau G, Li Y, et al. The structure of the exopolyphosphatase (PPX) from Escherichia coli O157:H7 suggests a binding mode for long polyphosphate chains. *J Mol Biol*. 2006; 359: 1249-1260.

226. Lorenzo-Orts L, Hohmann U, Zhu J, Hothorn M. Molecular characterization of CHAD domains as inorganic polyphosphate-binding modules. *Life Sci Alliance*. 2019; 2.

227. Martinez J, Truffault V, Hothorn M. Structural Determinants for Substrate Binding and Catalysis in Triphosphate Tunnel Metalloenzymes. *J Biol Chem*. 2015; 290: 23348-23360.

228. Saito K, Ohtomo R, Kuga-Uetake Y, Aono T, Saito M. Direct labeling of polyphosphate at the ultrastructural level in Saccharomyces cerevisiae by using the affinity of the polyphosphate binding domain of Escherichia coli exopolyphosphatase. *Appl Environ Microbiol*. 2005; 71: 5692-5701.

229. Werner TP, Amrhein N, Freimoser FM. Specific localization of inorganic polyphosphate (poly P) in fungal cell walls by selective extraction and immunohistochemistry. *Fungal Genet Biol*. 2007; 44: 845-852.

230. Werner TP, Amrhein N, Freimoser FM. Inorganic polyphosphate occurs in the cell wall of Chlamydomonas reinhardtii and accumulates during cytokinesis. *BMC Plant Biol*. 2007; 7: 51.

231. Labberton L, Kenne E, Long AT, et al. Neutralizing blood-borne polyphosphate in vivo provides safe thromboprotection. *Nat Commun*. 2016; 7: 12616.

232. Bolesch DG, Keasling JD. Polyphosphate binding and chain length recognition of Escherichia coli exopolyphosphatase. *J Biol Chem*. 2000; 275: 33814-33819.

233. Zhu S, Travers RJ, Morrissey JH, Diamond SL. FXIa and platelet polyphosphate as therapeutic targets during human blood clotting on collagen/tissue factor surfaces under flow. *Blood*. 2015; 126: 1494-1502.

234. Smith SA, Choi SH, Collins JN, Travers RJ, Cooley BC, Morrissey JH. Inhibition of polyphosphate as a novel strategy for preventing thrombosis and inflammation. *Blood*. 2012; 120: 5103-5110.

235. Zilberman-Rudenko J, Reitsma SE, Puy C, et al. Factor XII Activation Promotes Platelet Consumption in the Presence of Bacterial-Type Long-Chain Polyphosphate In Vitro and In Vivo. *Arterioscler Thromb Vasc Biol*. 2018; 38: 1748-1760.

236. Puy C, Tucker EI, Ivanov IS, et al. Platelet-Derived Short-Chain Polyphosphates Enhance the Inactivation of Tissue Factor Pathway Inhibitor by Activated Coagulation Factor XI. *PLoS One*. 2016; 11: e0165172.

237. Alvarado J, Ghosh A, Janovitz T, Jauregui A, Hasson MS, Sanders DA. Origin of exopolyphosphatase processivity: Fusion of an ASKHA phosphotransferase and a cyclic nucleotide phosphodiesterase homolog. *Structure*. 2006; 14: 1263-1272.

238. Boetsch C, Aguayo-Villegas DR, Gonzalez-Nilo FD, Lisa AT, Beassoni PR. Putative binding mode of Escherichia coli exopolyphosphatase and polyphosphates based on a hybrid in silico/biochemical approach. *Arch Biochem Biophys*. 2016; 606: 64-72.

239. Thonnard-Neumann E. Studies of Basophils. The Effects of Exogenous Heparin Upon the Number and Morphology of Basophils. *Acta Haematol*. 1964; 31: 24-35.

240. Linhardt RJ, Ampofo SA, Fareed J, Hoppensteadt D, Mulliken JB, Folkman J. Isolation and characterization of human heparin. *Biochemistry*. 1992; 31: 12441-12445.

241. Guilarte M, Sala-Cunill A, Luengo O, Labrador-Horrillo M, Cardona V. The Mast Cell, Contact, and Coagulation System Connection in Anaphylaxis. *Front Immunol*. 2017; 8: 846.

242. Levin EG, Santell L. Conversion of the active to latent plasminogen activator inhibitor from human endothelial cells. *Blood*. 1987; 70: 1090-1098.

243. Kretz CA, Tomberg K, Van Esbroeck A, Yee A, Ginsburg D. High throughput protease profiling comprehensively defines active site specificity for thrombin and ADAMTS13. *Sci Rep*. 2018; 8: 2788.

244. Yee A, Tan FL, Ginsburg D. Functional display of platelet-binding VWF fragments on filamentous bacteriophage. *PLoS One*. 2013; 8: e73518.

245. Baker CJ, Smith SA, Morrissey JH. Diversification of polyphosphate end-labeling via bridging molecules. *PLoS One*. 2020; 15: e0237849.

246. Kretz CA, Dai M, Soylemez O, et al. Massively parallel enzyme kinetics reveals the substrate recognition landscape of the metalloprotease ADAMTS13. *Proc Natl Acad Sci U S A*. 2015; 112: 9328-9333.

247. CF B, DR B, GJ S. Phage Display: A laboratory manual: Cold Spring Harbor Laboratory Press; 2001.

248. Love MI, Huber W, Anders S. Moderated estimation of fold change and dispersion for RNA-seq data with DESeq2. *Genome Biol*. 2014; 15: 550.

249. Capila I, Linhardt RJ. Heparin-protein interactions. *Angew Chem Int Ed Engl*. 2002; 41: 391-412.

250. Gandhi NS, Mancera RL. The structure of glycosaminoglycans and their interactions with proteins. *Chem Biol Drug Des*. 2008; 72: 455-482.

251. Sprague BL, Muller F, Pego RL, Bungay PM, Stavreva DA, McNally JG. Analysis of binding at a single spatially localized cluster of binding sites by fluorescence recovery after photobleaching. *Biophys J*. 2006; 91: 1169-1191.

252. Amarasinghe SL, Su S, Dong X, Zappia L, Ritchie ME, Gouil Q. Opportunities and challenges in long-read sequencing data analysis. *Genome Biol*. 2020; 21: 30.

253. Renné T, Schmaier AH, Nickel KF, Blombäck M, Maas C. In vivo roles of factor XII. *Blood*. 2012; 120: 4296-4303.

254. Kaplan AP. Kinins, airway obstruction, and anaphylaxis. *Chem Immunol Allergy*. 2010; 95: 67-84.

255. Renne T, Stavrou EX. Roles of Factor XII in Innate Immunity. *Front Immunol*. 2019; 10: 2011.

256. Konings J, Hoving LR, Ariëns RS, et al. The role of activated coagulation factor XII in overall clot stability and fibrinolysis. *Thromb Res*. 2015; 136: 474-480.

257. Englert H, Rangaswamy C, Deppermann C, et al. Defective NETs Clearance contributes to sustained FXII Activation in COVID-19-associated Pulmonary Thrombo-Inflammation. *bioRxiv*. 2020: 2020.2012.2029.424644.

258. Zamolodchikov D, Chen Z-L, Conti BA, Renné T, Strickland S. Activation of the factor XII-driven contact system in Alzheimer's disease patient and mouse model plasma. *Proc Natl Acad Sci U S A*. 2015; 112: 4068-4073.

259. Bergamaschini L, Parnetti L, Pareyson D, Canziani S, Cugno M, Agostoni A. Activation of the contact system in cerebrospinal fluid of patients with Alzheimer disease. *Alzheimer Dis Assoc Disord*. 1998; 12: 102-108.

260. Zamolodchikov D, Renné T, Strickland S. The Alzheimer's disease peptide beta-amyloid promotes thrombin generation through activation of coagulation factor XII. *J Thromb Haemost*. 2016; 14: 995-1007.

261. Pauer HU, Renne T, Hemmerlein B, et al. Targeted deletion of murine coagulation factor XII gene-a model for contact phase activation in vivo. *Thromb Haemost*. 2004; 92: 503-508.

262. Iwaki T, Castellino FJ. Plasma levels of bradykinin are suppressed in factor XII-deficient mice. *Thromb Haemost*. 2006; 95: 1003-1010.

263. Stavrou EX, Fang C, Bane KL, et al. Factor XII and uPAR upregulate neutrophil functions to influence wound healing. *J Clin Invest*. 2018; 128: 944-959.

264. Cohen WM, Wu HF, Featherstone GL, Jenzano JW, Lundblad RL. Linkage between blood coagulation and inflammation: stimulation of neutrophil tissue kallikrein by thrombin. *Biochem Biophys Res Commun*. 1991; 176: 315-320.

265. Iba T, Levy JH. Inflammation and thrombosis: roles of neutrophils, platelets and endothelial cells and their interactions in thrombus formation during sepsis. *J Thromb Haemost*. 2018; 16: 231-241.

266. Mashimo T. Gene targeting technologies in rats: zinc finger nucleases, transcription activator-like effector nucleases, and clustered regularly interspaced short palindromic repeats. *Dev Growth Differ*. 2014; 56: 46-52.

267. Carroll D. Genome engineering with targetable nucleases. *Annu Rev Biochem*. 2014; 83: 409-439.

268. de la Fuente-Nunez C, Lu TK. CRISPR-Cas9 technology: applications in genome engineering, development of sequence-specific antimicrobials, and future prospects. *Integr Biol (Camb)*. 2017; 9: 109-122.

269. Hsu PD, Lander ES, Zhang F. Development and applications of CRISPR-Cas9 for genome engineering. *Cell*. 2014; 157: 1262-1278.

270. Kim H, Kim JS. A guide to genome engineering with programmable nucleases. *Nat Rev Genet*. 2014; 15: 321-334.

271. Liu Y, Saunders TL, Sisson T, Blackburn R, Ginsberg DS, Day D. Optimizing CRISPR/Cas9 System to Precisely Model Plasminogen Activator Inhibitor-1 Point Mutations in Mice. *bioRxiv*. 2018: 254805.

272. Yoshimi K, Kunihiro Y, Kaneko T, Nagahora H, Voigt B, Mashimo T. ssODN-mediated knock-in with CRISPR-Cas for large genomic regions in zygotes. *Nat Commun*. 2016; 7: 10431.

273. Qin W, Kutny PM, Maser RS, et al. Generating Mouse Models Using CRISPR-Cas9-Mediated Genome Editing. *Curr Protoc Mouse Biol*. 2016; 6: 39-66.

274. Wang H, Yang H, Shivalila CS, et al. One-step generation of mice carrying mutations in multiple genes by CRISPR/Cas-mediated genome engineering. *Cell*. 2013; 153: 910-918.

275. Yang H, Wang H, Shivalila CS, Cheng AW, Shi L, Jaenisch R. One-step generation of mice carrying reporter and conditional alleles by CRISPR/Cas-mediated genome engineering. *Cell*. 2013; 154: 1370-1379.

276. Doench JG, Fusi N, Sullender M, et al. Optimized sgRNA design to maximize activity and minimize off-target effects of CRISPR-Cas9. *Nat Biotechnol*. 2016; 34: 184-191.

277. Hsu PD, Scott DA, Weinstein JA, et al. DNA targeting specificity of RNA-guided Cas9 nucleases. *Nat Biotechnol*. 2013; 31: 827-832.

278. Ittner LM, Gotz J. Pronuclear injection for the production of transgenic mice. *Nat Protoc*. 2007; 2: 1206-1215.

279. Untergasser A, Cutcutache I, Koressaar T, et al. Primer3--new capabilities and interfaces. *Nucleic Acids Res*. 2012; 40: e115.

280. Unruh M, Grunow A, Gottstein C. Systemic coagulation parameters in mice after treatment with vascular targeting agents. *Thromb J*. 2005; 3: 21.

281. Ratnoff OD, Margolius A, Jr. Hageman trait: an asymptomatic disorder of blood coagulation. *Trans Assoc Am Physicians*. 1955; 68: 149-154.

282. Kearney KJ, Butler J, Posada OM, et al. Kallikrein directly interacts with and activates Factor IX, resulting in thrombin generation and fibrin formation independent of Factor XI. *Proc Natl Acad Sci U S A*. 2021; 118.